Layered Double Hydroxides: Structure, Synthesis and Catalytic Applications

Hannah Elizabeth Griffiths (née Cross)

A thesis submitted to the University of Huddersfield
in partial fulfilment of the requirements for
the degree of Doctor of Philosophy

May 2012

The Department of Chemical and Biological Sciences
University of Huddersfield
Queensgate
Huddersfield HD1 3DH

Copyright Statement

i. The author of this thesis (including any appendices and/or schedules to this thesis) owns any copyright in it (the "Copyright") and she has given The University of Huddersfield has the right to use such Copyright for any administrative, promotional, educational and/or teaching purposes.

ii. Copies of this thesis, either in full or in extracts, may be made only in accordance with the regulations of the University Library. Details of these regulations may be obtained from the Librarian. This page must form part of any such copies made.

iii. The ownership of any patents, designs, trademarks and any and all other intellectual property rights except for the Copyright (the "Intellectual Property Rights") and any reproductions of copyright works, for example graphs and tables ("Reproductions"), which may be described in this thesis, may not be owned by the author and may be owned by third parties. Such Intellectual Property Rights and Reproductions cannot and must not be made available for use without the prior written permission of the owner(s) of the relevant Intellectual Property Rights and/or Reproductions.

Publications

1. Microwave calcination of Cu/Mg/Al hydrotalcite catalyst precursor, H. E. Cross, G. M. B. Parkes, D. R. Brown, *Applied Catalysis A: General*, In Press, (2012).

2. Entrained sodium in mixed metal oxides derived from layered double hydroxides, H. E. Cross, D. R. Brown, *Catalysis Communications*, 12 (2010) 243-245.

3. On the interplay between lateral interactions, hydrophobicity and acid strength on catalytic activity of nanoporous sulfonic acid silicas. J-P. Dacquin, H. E. Cross, D. R. Brown, T. Duren, J. Williams, A. F. Lee, K. Wilson, *Green Chemistry*, 12 (2010) 1383-1391.

4. A new and simple method for the synthesis of highly functionalised pyrrolizidines, indolizidines and pyrroloazepines. P. A. O'Gorman, T. Chen, H. E. Cross, S. Naeem, A. Pitard, M. Qamar, K. Hemming, *Tetrahedron Letters*, 49 (2008) 6316-6319.

5. Enhanced Acidic and Catalytic Properties of Polystyrene Sulfonic Acid Resins, D. R. Brown, H. E. Cross, P. F. Siril. "Recent advances in Ion-Exchange", Proceedings of IEX 2008 Eds; M. Cox, *Society of Chemical Industry*, (2008) 435-442.

6. New polystyrene sulfonic acid resin catalysts with enhanced acidic and catalytic properties, P. F. Siril, H. E. Cross, D. R. Brown, *Journal of Molecular Catalysis A*, 179 (2007) 63-68.

<u>Acknowledgments</u>

I would like to thank my supervisor, Professor Robert Brown for all his guidance, not just throughout my PhD but from day one of beginning my undergraduate degree. Many thanks go to Dr Elizabeth Dawson, Dr Gareth Parkes and Dr Howard Williams for their help, discussions and invaluable expertise gifted to me during the past four years.

I would like to acknowledge my parents for their continued support. I would like to thank my husband, Morgan, for his belief in everything I try to succeed in – this thesis would not have been completed without you.

Finally, to my Grandfather, Henry Edward Cross, to whom I am dedicating this thesis - I would not have achieved my goals without your encouragement, I want to take this opportunity to thank you.

__Abstract__

The objective of the work studied here was to relate the structure of the conventional Layered Double Hydroxide (LDH), hydrotalcite and several transition metal doped hydrotalcites to their function once calcined into catalysts for use in the production of biodiesel.

Attention was paid to the preparation of the LDHs. Three preparative methods were investigated, using sodium hydroxide and carbonate, using ammonia, and using urea as precipitating agents. The properties of the resultant LDHs and those of the mixed oxides produced on calcination were shown to be relatively independent of the synthesis method. The importance of ensuring that sodium salts were removed from the catalyst precursors before use, when using the first synthetic method, was shown. Evidence was provided which showed the significant effect on activity of the calcined catalysts when sodium was present. The importance of thorough washing of the LDH precipitates was clearly demonstrated.

The calcination process was also studied and materials were subjected to two methods of calcination, "feedback-controlled" microwave heating and conventional heating in a furnace. This method of controlled microwave calcination may offer promise in the production of optimised mixed metal oxide and other catalysts.

A copper-substituted hydrotalcite was subjected to calcination under feedback-controlled microwave heating, in which microwave power is continuously modulated to generate a defined sample temperature programme or constant sample temperature. The results showed that microwave calcination resulted in enhanced crystallinity of the resultant oxides and spinel phase formed at high temperature. In addition, an additional phase, Cu_2MgO_3, was detected following microwave calcination, which was not formed at any temperature (up to 1000 ^{o}C) under conventional heating. The concentrations and strengths of surface basic sites were significantly higher for materials calcined using microwaves than using conventional heating. Catalytic activities in the base-catalysed transesterification of tributyrin with methanol were also higher. Microwave calcination under feedback-control, while allowing control of material bulk temperature during calcination and preventing major

temperature excursions, may allow quite large but highly localised temperature variation, for instance as water is released during dehydroxylation, which are beneficial in developing surface defects and surface basicity.

Other LDHs were studied incorporating the transition metals, cobalt, nickel and iron. All three showed some activity but basicity appeared to be enhanced by doping hydrotalcite with copper (II) and cobalt (II) particularly. Whether this is because of the presence of these ions on the catalyst surface and their behaviour as Lewis bases, or whether their presence leads to surface defect sites that show electron donating abilities, is not clear.

The effect of microwave calcination on these other substituted LDHs seems to be variable and not always as pronounced as it is with the copper containing LDH. It seems likely that the extent to which microwaves are effective depends on their capacity to couple with the metals in the structures and the fact that this varies between metals perhaps explains why the different LDHs show different behaviours.

Although not the most active material, perhaps the most interesting material formed upon calcination was the mixed oxides of $Mg_{5.82}Al_{1.12}Fe_{0.88}(CO_3)(OH)_{16}.4H_2O$, possessing both acidic and basic sites. All other LDHs studied possessed basic sites only. This could be very useful for the production of biodiesel from waste oil containing free fatty acids (FFAs) which require the presence of an acid catalyst for pre-esterification of these free acids.

Table of Contents

Chapter 1

Introduction

Chapter 1

Introduction

Layered double hydroxides (LDHs) are precursors to mixed metal oxide catalysts and exhibit properties that make them useful for many applications as, for example, ion-exchangers, additives in polymers, anion adsorbants and biosensors [1-3]. In this thesis catalytic applications of oxides formed from the calcination of several different LDH-based have been studied, with specific focus on the base-catalysed transesterification reaction for the production of biodiesel.

1.1 – Catalysis

A catalyst is a substance that increases the rate of a reaction by lowering the activation energy or providing an alternative reaction route. This substance does not undergo any chemical change and can be regenerated at the end of the reaction. In reality, regeneration of a catalyst is often not simple, more so when the catalyst is in the same phase as the reactants and products. Many homogeneous catalysts used in liquid phase reactions are difficult to remove after reactions and are often waste products of the reaction. The use of these catalysts has been driven by their affordability and high activity. The requirement for 'greener' catalysts has recently increased, typically meaning solid catalysts that can be easily separated from the reaction mixture, as replacements for homogeneous catalysts [4]. However, there are many difficulties to overcome, with activities of the most active solid catalysts being relatively low.

There are many attributes of a catalyst that may seem 'green' when directly comparing one to another but care must be taken in labelling a catalyst in this fashion. For example, the use of a solid catalyst that can be filtered off at the end of a liquid phase reaction and used again may seem a green option. However, many solid catalysts require the use of homogeneous catalysts and reagents in their synthesis and high calcination temperatures are often required to activate solid catalysts before a reaction, both of which factors detract from their environmental attractiveness. This thesis attempts to address some of the problems associated

with the production of 'green' solid catalysts as replacements for liquid phase homogeneous catalysts. It is important to note that, although solid heterogeneous catalysts are generally less active than their homogenous counterparts, sometimes they can be tuned to provide better product selectivity, offsetting, at least in part, their disadvantages based on activity.

The main objective in the development of green catalysts is to reduce waste. A summary of the general attributes of solid catalysts for liquid phase reactions compared to homogeneous catalysts is shown in Figure 1.1.

HOMOGENEOUS CATALYST	HETEROGENEOUS CATALYST
1. **Relatively high activity (often as much as 3,000 times more active than heterogeneous catalysts [4])**	1. Relatively low activity
2. **Often difficult to separate from products**	2. Easier separation, usually by filtration or simply settling
3. **Generally low selectivity**	3. Frequently more selective towards reaction products
4. **Relatively low cost**	4. Generally more expensive
5. **Large quantities of waste (usually liquid) associated with their separation/disposal**	5. Less waste because separation is easier

Figure 1.1 – Comparisons between heterogeneous and homogeneous catalysts.

1.2 – Basic catalysts

Solid base catalysts can exhibit Brønsted and/or Lewis basicity. A Brønsted base is defined as a proton acceptor and a Lewis base is defined as an electron donor. Solid base catalysts can frequently be tuned through synthesis to exhibit one or the other. Catalysis by a Brønsted base site usually proceeds by a proton being removed from the reactant. Lewis base sites donate electrons to the reactant.

Solid base catalysts have not been studied as much as solid acid catalysts although the clay-type laminar solid base catalysts, which include LDHs, of which the mineral hydrotalcite is the most common, have received significant attention [5]. There are many types of solid bases suitable for use as catalysts. These include thermally stable metal oxides and supported metal oxides as well as supported organic bases where functional groups are grafted onto high surface area supports. These last types can potentially deliver super-basicities (e.g. supported polyguanidines) but often suffer from poor thermal stability and problems of leaching of the functional groups into the reaction mixture [6].

Many single solid oxides have been suggested as suitable replacements for homogenous base catalysts [7-9]. The basic strength of the Group II metal oxides follows the order: BaO>SrO>CaO>MgO, after high temperature treatment [10]. Of Group I metal oxides only Li_2O is really a viable solid base catalyst but it is not generally used as a single oxide catalyst because of the high cost of synthesis. It is, however, sometimes doped into Group II metal oxides, for instance MgO, to significant effect [11,12]. Other Group I oxides are potentially strong but are generally too reactive to handle.

Layered double hydroxides (LDHs) are precursors to mixed oxides. Single oxides are not usually as catalytically active as mixed oxides, partly because mixed oxides tend to exhibit more surface defects which can impart basicity. Mixed oxides are studied in this thesis and, in general, exist as either crystalline materials with surface areas below 100 $m^2\,g^{-1}$ or as a mixture of amorphous and crystalline materials, with surface areas of typically 200-500 $m^2\,g^{-1}$. Basicity and sometimes acidity can be tuned through metal type and valency, and composition [13].

Basic catalytic activity of metal oxides is generally associated with surface sites where oxide ions are electron rich. Surface oxides, including those at defect sites, are co-ordinately unsaturated and it is this feature that results in strong basicity. Surface metal ions and oxide ions would, in an inert atmosphere, be acidic and basic respectively, being electron deficient and electron rich. However they are easily stabilised and deactivated by water and CO_2 from the atmosphere. If these metal oxides are to be highly active catalysts, they have to be activated at high temperatures and prevented from adsorbing water and CO_2.

1.3 – Layered Double Hydroxides

The first discovered layered double hydroxide was the mineral Hydrotalcite $Mg_6Al_2(CO_3)(OH)_{16} \cdot 4(H_2O)$, Figure 1.2. Hydrotalcite bears its name for its water content (hydro) and also its resemblance to talc (talc-ite). The structure and properties were not fully characterised until the 1960s when Allmann and Taylor determined the structure by powder X-ray diffraction [15,16].

Figure 1.2 – Naturally occurring hydrotalcite, from Sweden [17].

The important point about layered hydrotalcite-type mixed metal hydroxides as catalyst precursors is that, on calcination, they yield intimate mixtures of the oxides of the metals. These materials tend to have relatively high surface areas and, as stated above, they frequently show catalytic activity, particularly as solid bases [18].

1.3.1 – Structure

LDHs, of which hydrotalcite is the most commonly known, are lamellar hydroxides, with the general formula $M_{(1-x)}M_x(OH)_2]^{x+}(CO_3)_{x/n}^{2-}$, (Figure 1.3). LDHs consist of a divalent and a trivalent metal ion and adopt the layered brucite structure with metal ions octahedrally coordinated to hydroxide ions, with exchangeable anions, usually carbonate, in the interlayer regions to balance the lattice positive charge associated with the trivalent ions. Hydrotalcite contains magnesium (II) and aluminium (III) ions usually in a molar ratio of about three to one. It occurs widely in nature and can be synthesised easily, if necessary with other metal ions isomorphously substituted for magnesium and/or aluminium. Many of the transition metals can be built into the structure. It should be noted that more than one additional tri or divalent cation can be substituted in the same compound. For example, LDHs can be prepared with nickel (II) and magnesium, and aluminium and iron (III), in the same lattice [19].
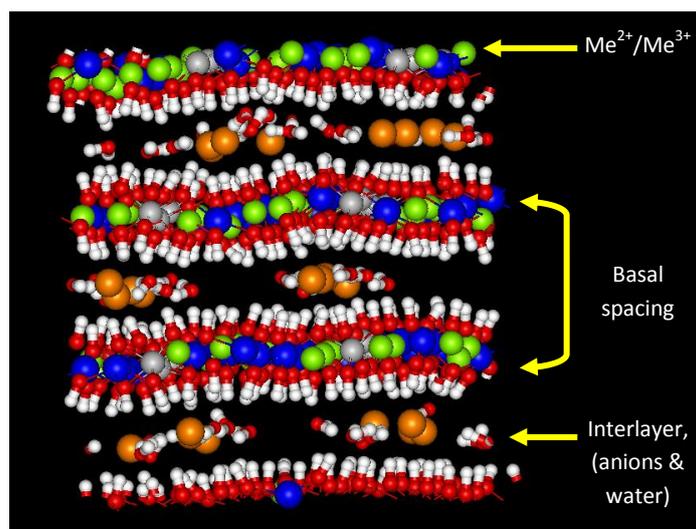
Figure 1.3 – Structure of a layered double hydroxide (cations not to size).
Blue/green/silver balls represent metal cations. Red and white balls represent hydroxyl ions. Orange, white and red balls represent carbonate anions.

Because of the relatively weakly held anions (usually carbonate) in the interlayer region, LDHs generally possess anion exchange properties. The advantage of LDHs over other anion-exchangers is the large storage capacity between the brucite layers. Anions of choice can also be incorporated during the initial synthesis (precipitation) stage.

1.3.2 – Synthesis

LDHs can be synthesised easily in the laboratory by co-precipitation from solution of the corresponding metal nitrates [20]. The most common method of precipitation is by the use of sodium hydroxide and sodium carbonate, to form a carbonate interlayer. Mixed oxides are formed when LDHs are calcined at temperatures above 500 °C [18].

The M^{2+}/M^{3+} ratio can be controlled outside the traditional hydrotalcite value of 3/1. It has been well documented, however, that the most crystalline LDH materials sit in the M^{2+}/M^{3+} range of $2.5 \leq x \leq 5$ [21-23]. There are reports of synthetic LDHs with M^{2+}/M^{3+} ratio outside this range but questions have arisen over the LDH phase purity [24,25]. The crystallinity of synthetic LDHs is affected by the precipitation method [26,27] and can be improved by ageing the aqueous suspension of the precipitate [28,29].

Co-precipitation is often performed by the slow addition of metal nitrate solutions to a solution of hydroxide and carbonate. Because addition is slow, the time taken to precipitate the LDH can be as much as an hour or more, during which the ageing time for the precipitate is unbalanced. Valim et al showed that the crystallite size distribution is wider when there is no additional ageing step [30]. Pinnavia et al compared the ageing step with the level of crystallinity of hydrotalcite and found there was an enhancement in crystallinity [31] with increased ageing time. There was no correlation, however, between base catalytic activity and improved crystallinity.

Co-precipitation of the metal hydroxides can be induced using ammonia instead of sodium/potassium hydroxide. Another alternative method is to use a solution of urea, which gradually hydrolyses to release hydroxide ions and gives very finely controlled precipitation. This process starts at low pH and increases gradually to pH 7.6.

However, the relatively gradual way in which the pH increases with urea hydrolysis is not always advantageous. For example, most divalent cation nitrates will precipitate as hydroxides quite readily using urea but trivalent cations, with the exception of aluminium, will not. So, attempts at the incorporation of some cations into the LDH structure using urea will not always be successful. Whichever method of precipitation is used, normal practice is to stir the solution vigorously (1200 rpm), to reduce concentration gradients and local differences in hydroxide ion concentration [32].

$$CO(NH_2)_2 + 3H_2O \rightarrow CO_2 + 2NH_4^+ + 2OH^-$$

Equation 1.1

1.3.3 – Metals ions in LDHs

The radii of transition metal cations in divalent and trivalent oxidation states govern the prospect of their being successfully incorporated into the brucite-like lattice [33]. Ionic radii of some cations are shown in Figure 1.4. It is clear from Figure 1.4 why, for instance, Zn^{2+} and Co^{2+} can be used in place of Mg^{2+} in hydrotalcite and why La^{2+} and Be^{2+} cannot.

Ion	Ionic radius (Å)
Mg^{2+}	0.72
Zn^{2+}	0.74
Fe^{2+}	0.78
Co^{2+}	0.75
Ni^{2+}	0.69
Cu^{2+}	0.73
Be^{2+}	0.45
La^{2+}	1.03
Cr^{3+}	0.62
Fe^{3+}	0.65
Al^{3+}	0.54

Figure 1.4 – Ionic radii of M^{2+} and M^{3+} cations [34].

1.3.4 – Calcination of LDHs

On calcination, layered hydrotalcite-type compounds dehydrate and then dehydroxylate to yield mixtures of oxides of the metals they contain. The calcination of these materials has been studied in detail [35-38]. For the most widely studied hydrotalcite mineral, $Mg_6Al_2(CO_3)(OH)_{16}.4H_2O$, progressive temperature increase results in the loss of physically bound water and water in the interlayer regions, followed by desorption of water coordinating any exchangeable negative ions. If carbonate anions are present, they decompose above 300 ^{o}C. The last major process is the dehydroxylation of the crystalline matrix to generate the oxides at around 500 ^{o}C. This is characterised by broad lines in the powder X-ray diffraction pattern associated with the oxide of the most/more abundant metal in the precursor, indicative of very small crystallites of the oxide. Raising the temperature beyond 500 °C is known to induce gradual sintering of the oxides and formation of spinel phases [39].

The calcination of LDHs generally provides mixed metal oxides that are more catalytically active than the parent LDHs [40], with activity being dependant on calcination temperature [41]. Generally calcined LDHs exhibit strong base sites but it is also documented that Al^{3+} Lewis acid sites can exist following calcination at very high temperatures (ca. 1000 °C) [42].

1.3.4 – LDHs as solid base catalysts

In general, solid bases are less easy to describe and define than solid acids. In solid acids the active sites may be Brønsted acid sites with ionisable hydrogen, or well defined electron deficient Lewis acid sites. In solid bases it is usually more difficult to identify distinct active basic sites. It is also significant that IUPAC describes a superacid as a medium that has acidity greater than that of pure sulfuric acid. A superbase, in contrast, has only a limited definition, being identified as a medium having "very high basicity" [43].

Describing the "strength" of solid acids and bases is more difficult than describing the strength of liquid acids and bases. There are a number of ways of measuring and classifying solid base strengths. The methods for expressing acid and base strength are not as clear cut as the pH scale used for dilute aqueous solutions of acids or bases. The Hammett function (H) is frequently used and this is essentially an extension of the pH scale to allow acid/base strength to be quantified in the absence of the solvent water. Hammett acidity/basicity is usually determined using specific Hammett indicators which change the colour of the solution at particular values of H. These can be used in titrations (in aprotic solvents) and the measure of acidity or basicity is given by the colour of the indicator on adsorption on the solid. Disadvantages of using Hammett indicators are that the colour observed is often difficult to identify. Another disadvantage is that the indicators used for this type of analysis are quite large molecules, creating problems in accessing all of the sites within the solid sample.

The other technique to be discussed is temperature programmed desorption (TPD), where the sample is subjected to a gas adsorbate (such as SO_2 in the case of a solid

base and NH_3 for a solid acid) and then heated to remove the adsorbate. The temperature(s) at which the adsorbate is desorbed from the sample is an indication of the strength of base or acid sites. Disadvantages of this technique are that it is limited to thermally stable materials. A third method, as used in the work described here, is calorimetric adsorption of an acidic probe gas (for a solid base) [44]. This technique is well established and has been used widely to study basic sites, relating the amount of an acidic probe gas adsorbed and the enthalpy of adsorption to the concentration and the strength of the surface basic sites. Some of the more widely used solid acid and bases are shown in Figure 1.5 in terms of their relative acid and base strengths.

Strength of sites		Material (BASIC)	Material (ACIDIC)
Very strong	—		SO_4/ZrO_2
			SO_4/Nb_2O_5
			$HSbF_6$
			TaF_5/AlF_3
		Li-MgO	
Strong	—	CaO	Heteropolyacids
		Hydrotalcite	Zeolite *β*
Medium	—	ZnO	
		La_2O_3	
		Nd_2O_3	Ion-exchange resins
		ZrO_2	
Weak	—	Ga_2O_3	ZrO_2
		Al_2O_3	Al_2O_3
		TiO_2	SiO_2, Nb_2O_5

Figure 1.5 – Relative orders of acid or base strengths based on adsorption of acidic/basic probe gases [44-49].

Studies into hydrotalcite-type materials have been extensive and optimum compositions for ultimate catalytic performance have been deduced for many different types of LDHs. The structure of the conventional LDH, hydrotalcite, is well defined [50]. Subtle changes in composition have been shown to make major differences to catalytic properties [51].

Oxides made from LDHs have been studied as catalysts in many reactions, including condensation, alkylation and Michael addition reactions [52-55]. Hydrotalcite has been synthesised with partial replacement of Mg with Ni, Cu and Co cations and Al with Fe for use in hydrogenation/oxidation reactions [56].

LDHs without any calcination have also been used as catalysts [57]. In addition, calcined LDHs that have been rehydrated have also been used as basic catalysts [58]. After calcination of an LDH to a mixed oxide, the mixed oxide can be placed in water and the LDH partially reforms. This process is called the "memory effect" [59]. It is known that the interlayer anion is replaced with Brønsted OH^- groups and it is this that promotes the basicity of the rehydrated compound. Base catalytic activity is apparent in the rehydrated LDH (because of OH^- groups) but it is not generally as high as for the oxides from which they are made [60,61].

LDH derived catalysts for use in biodiesel production

1.4 – Biodiesel

There is almost certainly a direct link between CO_2 emissions from the combustion of fossil fuels and global warming [62]. The United Nations Framework Convention on Climate Change, (UNFCCC) was formed over a decade ago to recognise and address the problem of global temperature rises, and the UNFCC acknowledged the contribution of emissions from the combustion of fossil fuels [63].

Escalating prices for petroleum throughout the world, as well as serious environmental concerns, have stimulated the need for alternative renewable fuels. An alternative to petroleum diesel is renewable biodiesel, believed by some to be carbon neutral [64]. No modification of diesel engines is needed to use this fuel.

The first diesel engine was created over 100 years ago by Rudolf Diesel and it was Diesel who first successfully used vegetable oils, specifically peanut oil, as a fuel for

the diesel engine, in 1893 [65]. However, it was over 40 years later that the process for transforming vegetable oil to the less viscous fuel we now call biodiesel was patented, by Chavanne of the University of Brussels [66].

Today, there are financial incentives offered by the EU for production of biofuels, and in the UK tax relief for the first 2,500 litres of biodiesel produced is currently in place [67]. A target of 10% the worlds transport fuels to be biofuels by 2020 has been set [68].

Biodiesel can be produced from vegetable oils by a reforming process which simply converts the triglycerides to smaller molecules [69]. The more common approach however is to carry out base-catalysed transesterification with methanol. This is a relatively simple process to operate, on both small and large scales. However, the economics are marginal and the fuel versus food debate adds controversy [70]. In addition, the most commonly used catalysts, homogeneous sodium and potassium hydroxides, are corrosive and are relatively difficult to remove from the product. Improvements in the technology to produce biodiesel are needed if its manufacture is to be viable. This work focuses on replacing these liquid phase base catalysts with solid base catalysts.

Solid catalysts would be easily separated from the products of transesterification and may even be re-usable. Their use would remove the need for extensive washing of the fuel which is required when homogeneous catalysts are used. If their activity could be increased to levels at least approaching those of homogeneous caustic conditions, they would carry with them cost savings for biodiesel synthesis [71,72].

1.4.1 – Transesterification of triglycerides

Biodiesel is synthesised by the transesterification of triglycerides, using an alcohol (usually methanol) in excess and a base catalyst, producing the methyl ester which is the major component of the fuel. Typically, the reaction is operated at 65 $^\circ$C with a 6:1 stoichiometric ratio of methanol to triglyceride, Figure 1.6. In fact, the reaction proceeds by conversion of the triglyceride to di-glyceride then mono-glyceride and then glycerol, with methyl ester produced at each step.
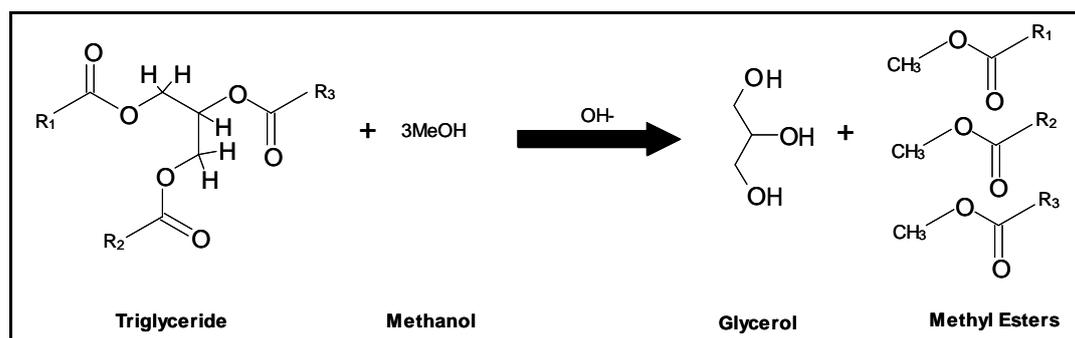
Figure 1.6 – Transesterification of triglycerides.

The by-product of the transesterification reaction is glycerol. It is essential to remove the glycerol from the biodiesel as small amounts can deposit inside diesel engines reducing performance and efficiency [73]. This is relatively easy because the glycerol is immiscible with the methyl ester. As stated above, the most common catalysts for this process are sodium and potassium hydroxides. These catalysts are inexpensive and their use is driven by the very fact that they are highly active, at least an order of magnitude more active that the best current solid catalysts [74]. However, liquid catalysts exhibit major disadvantages in that the fuel has to be extensively washed to remove them after the reaction, generating large quantities of liquid waste.

During the transesterification reaction of vegetable oil and alcohol, there are difficulties that arise from the miscibility of reactants, Figure 1.7. Methanol and vegetable oils are largely immiscible, meaning that whatever catalyst is used, the initial reaction rate is always low. As the oil is converted to methyl esters the mixture becomes fully miscible and the reaction rate increases. The immiscibility of reactants at the beginning of the reaction is a particular problem when using a solid catalyst. Clearly, the agitation rates used in the early stages are crucial to controlling the diffusion rates of reactants. This fact means that simple experimental comparisons of solid catalysts are difficult using vegetable oil/methanol mixtures. Many workers use a model, relatively small, triglyceride, glyceryl tributyrate (tributyrin), which is miscible with alcohol, to overcome this in work comparing solid catalysts [75].
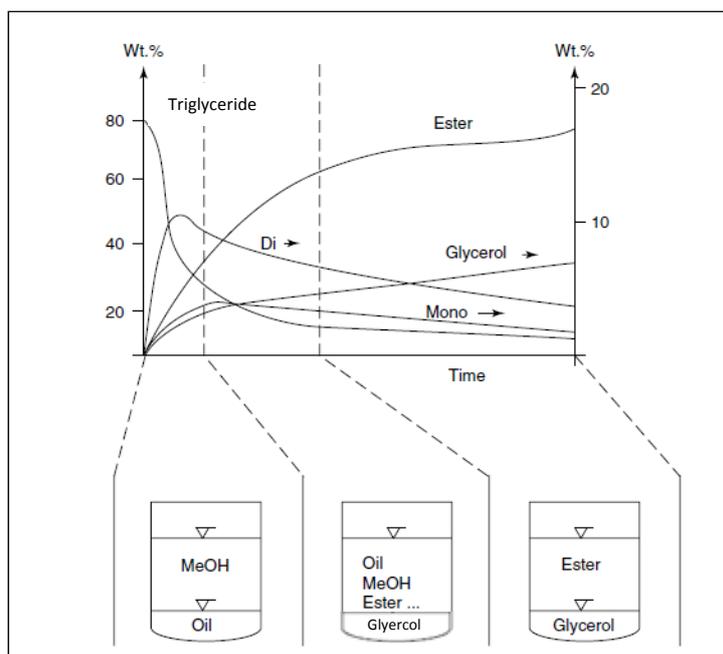
Figure 1.7 – Miscibility of reactants and products during transesterification [76].

It is worth mentioning that in addition to the conventional method of transesterification of triglycerides with alcohol using a catalyst, there have been other methods used to reduce the amount of waste. The reaction can be carried out without a catalyst using supercritical methanol. Under these conditions, free fatty acids, as well as triglycerides, are converted to the methyl esters. Reaction times are very low. However it is not very economical, requiring temperatures in the region of 400 °C and pressures of 100-250 Bar [77].

1.4.2 – Sourcing the oils

Much debate still exists about the harvesting of crops for use as the raw material (vegetable oil) needed for biodiesel. Issues arise from the amount of land required to grow crops needed for biodiesel and the effect of this on food production. In contrast, there is a belief that in some parts of the world, for example Brazil, much of the land which could be used for 'fuel' crops would not be suitable for 'food' crops

[78]. The use of this normally derelict land would produce income for the land owners. In addition, this boost in economy would play a part in rural development.

The duty levied on biodiesel in the UK, after the first 2,500 litres, does not currently make the total price of production of biodiesel from refined vegetable oils significantly lower than that of petroleum diesel [79]. Therefore, at this time, the only viable option is to use waste oil, often used cooking oil. Waste oil requires the same treatment as that needed to transesterify virgin oil but it sometimes contains high concentrations of free fatty acid which require an additional step to process, in which the acids are esterified with methanol under acid catalysis.

Lack of uniformity of waste oils can also be a problem. A research group in the USA collected waste oils from 15 different restaurants and found that the viscosity and the acid value varied a great deal [80]. This can produce substantially different fuel properties. The viscosity of the fuel, as an example, can affect the start-up of an engine in cooler climates.

1.4.3 – Metal oxide catalysts for biodiesel synthesis

Alkaline earth oxides show potential as catalysts for use as a base in transesterification reactions. These single oxides have been studied extensively [81,82]. Doping these oxides can result in even higher activities and one example is CaO, tested in a transesterification reaction [81]. When the oxide was doped with small amounts of lithium, there was a vast enhancement of activity. The amount doped on to the CaO was found to be crucial and activity decreased at loading of more than 2 % w/w Li. Measurements using Hammett indicators showed that the incorporation of lithium increased the basic strength of CaO but surprisingly there was no direct dependence of base strength on lithium loading, and so a relatively poor correlation between base strength and catalytic activity was found in this series of catalysts.

Other alkaline earth oxides have shown high activity. For example, the single metal oxide, SrO was evaluated for the transesterification of soybean oil [82]. The precursor to the metal oxide was $SrCO_3$ and it was calcined 1200 °C for 5 hours prior

to the reaction. Only a slight reduction in activity was observed after reusing the catalyst ten times.

1.5 – Objectives

1.5.1 – Overall objective

To understand the relationship between the structure of layered double hydroxides (or layered mixed hydroxide) and their basic and catalytic properties, and so to optimise their properties for use in biodiesel synthesis.

1.5.2 – Specific objectives

1. To prepare layered double hydroxides or layered mixed hydroxides with a range of metals and a range of compositions.
2. To characterise the materials and products of calcination in terms of physical and chemical properties, basicities and catalytic activities.
3. To compare the effect of calcination of these materials using conventional and microwave heating (under feedback control).
4. To evaluate calorimetric adsorption techniques as reliable methods for characterising surface basicity and/or acidity.

References

[1]   S. Abello, F. Medina, D. Tichit, J. Perez-Ramirez, Y. Cesteros, P. Salagre, *Chem. Commun.,* 11 (2005) 1453-1455.

[2]   C. Forano, W. Fernando, K. Gundappa, *Int. J. Environ. Sci. Tech.*, 1 (2004) 425-458.

[3]   S. Morandi, F. Prinetto, M. Di Martino, G. Ghiotti, O. Lorret, D. Tichit, C. Malagù, B. Vendemiati, M. C. Carotta, *Sensor. Actuat. B-Chem.,* 118 (2006) 215-220.

[4]   R. A. Sheldon, I. W. C. E. Arends, U. Hanefeld, *Introduction: Green Chemistry and Catalysis*, Wiley-VCH Verlag GmbH & Co. KGaA, (2007).

[5]   K. Tanabe, W. F. Holderich, *Appl. Catal. A-Gen*, 181 (1999) 399-434.

[6]   U. Schuchardt, R. M. Vargas, G. Gelbard, *Appl. Catal. A-Gen*, 109 (1996) 37-44.

[7]   M. C. G. Albuquerque, D. C. S. Azevedo, C. L. Cavalcante Jr, J. Santamaría-González, J. M. Mérida-Robles, R. Moreno-Tost, E. Rodríguez-Castellón, A. Jiménez-López, P. Maireles-Torres, *J. Mol. Catal. A-Chem.,* 300 (2009) 19-24.

[8]   T. F. Dossin, M.-F. Reyniers, G. B. Marin, *App. Catal. B: Environ.*, 62 (2006) 35-45.

[9]   G. Zhao, J. Shi, G. Liu, Y. Liu, Z. Wang, W. Zhang,, M. Jia, *J. Mol. Catal. A-Chem.,* 327 (2010) 32-37.

[10]   G. Thornton, Angew. Chem.-Eng. Edit., 48 (2009) 3902-3903.

[11]   X. K. Zhang, A. B. Walters, M. A. Vannice, *J. Catal.*, 146 (1994) 568-578.

[12]   J. A. Cortes-Concepcion, F. Patcas, M. D. Amiridis, *Appl. Catal. A: Gen.*, 386 (2010) 1-8.

[13]   J. S. Valente, J. Hernandez-Cortez, M. S. Cantu, G. Ferrat, E. López-Salinas, *Catal. Today.,* 150 (2010) 340-345.

[14]   F. Cavani, F. Trifirò, A. Vaccari, *Catal. Today.*, 11 (1991) 173-301.

[15]   R. Allmann, H. Lohse, E. Hellner, *Die Kristallstruktur des Koenenits: Z. Kristallogr.,* 126 (1968) 7-22.

[16]   H. F. W. Taylor, *Crystal Min. Mag.,* 39 (1973) 377-389.

[17]   MineralData,[Webpage],[cited 10/03/2010]
http://webmineral.com/specimens/picshow.php?id=1937

[18]   J. S. Valente, H. Pfeiffer, E. Lima, J. Prince, J. Flores, *J. Catal.*, 279 (2011) 196-204.

[19]   G. Carja, R. Nakamura, T. Aida, H. Niiyama, *J. Catal.*, 218 (2003) 104-110.

[20]   D. Seebach, B. Seuring, H. O. Kalinowski, W. Lubosch,B. Renger, *Angew. Chem-Eng Edit.,* 16 (1977) 264-265.

[21]   S. K. Sharma, P. A. Parikh, R. V. Jasra, *J Mol Catal. A-Chem.,* 317 (2010) 27-33.

[22]   A. de Roy, C. Forano, J.P. Besse In: V. Rives, Editor, *Layered Double Hydroxides*, Nova Science Publisher, Inc, New York, (2001) 1.

[23]   M. A. Aramendía, V. Borau, C. Jiménez, J. M. Marinas, J. R. Ruiz, F. J. Urbano, *J. Solid State Chem.*, 168 (2002) 156-161.

[24]   J. J. Bravo-Suárez, E. A. Páez-Mozo, S. Ted Oyama, *Micropor. Mesopor. Mat.,* 67 (2004) 1-17.

[25]   A. M. Fogg, V. M. Green, H. G. Harvey, D. O'Hare, *Adv. Mat.*, 11 (1999) 1466-1469.

[26]   A. Corma, V. Fornés, R. M. Martín-Aranda, F. Rey, *J. Catal.,*134 (1992) 58-65.

[27]   W. Meng, F. Li, D. G. Evans, X. Duan, *Mater. Chem. Phys.* 86 (2004) 1-4.

[28]   F. Basile, P. Benito, G. Fornasari, A. Vaccari., *Appl. Clay Sci*, 48 (2010) 250-259.

[29]   F. Cavani, F. Trifirò, A. Vaccari, *Catal. Today*, 11 (1991) 173-301.

[30]   Y. Zhao, F. Li, R. Zhang, D. G. Evans, X. Duan, *Chem. Mater.*, 14 (2002) 4286-4291.

[31]   E. L. Crepaldi, J. B. Valim, *Quim. Nova.,* 21 (1998) 300-311.

[32]   S. K. Yun, T. J. Pinnavaia, *Chem. Mater.,* 7 (1995) 348-354.

[33]   J. S. Valente, J. Hernandez-Cortez, M. S. Cantu, G. Ferrat, E. López-Salinas, *Catal.Today*, 150 (2010) 340-345.

[34]   R. Shannon, *Acta. Crystallogr. Sect. A.*, 32 (1976) 751-767.

[35]   M. L. Occelli, J. P. Olivier, A. Auroux, M. Kalwei, H. Eckert, *Chem. Mater.*, 15 (2003) 4231-4238.

[36]   V. Rives, *Mater. Chem. Phys.*, 75 (2002) 19-25.

[37]   M. R. Pérez, C. Barriga, J. M. Fernández, V. Rives, M. A. Ulibarri, *J. Solid State Chem.*, 180 (2007) 3434-3442.

[38]   T. Kameda, Y. Fubasami, N. Uchiyama, T. Yoshioka, *Thermochimica Acta.* 499 (2010) 106-110.

[39]   Y. Liu, E. Lotero, J. G. Goodwin Jr, X. Mo, *Appl. Catal. A-Gen*, 331 (2007) 138-148.

[40]   N. Tahir, Z. Abdelssadek, D. Halliche, A. Saadi, O. Cherifi, K. Bachari, P. M. Antoine Gédéon, B. Florence, *Stud. Surf. Sci. Catal.*, (2008) 1287-1290.

[41]   C. Qi, J. C. Amphlet, B. A. Peppley, *Appl. Catal. A-Gen.*, 302 (2006) 237-243.

[42]   A. Tada, *Mater. Chem. Phys.* 17 (1987) 145-159.

[43]   IUPAC, [http://goldbook.iupac.org/S06135.html], [cited 08/09/2010].

[44]   J. C. Vartuli, J. G. Santiesteban, P. Traverso, N. Cardona-Martinéz, C. D. Chang, S. A. Stevenson, *J. Catal.*, 187 (1999) 131-138.

[45]   A. L. Petre, A. Auroux, P. Gélin, M. Caldararu, N. I. Ionescu, *Thermochimica Acta.,* 379 (2001) 177-185.

[46]   H. Zhao, S. Bennici, J. Cai, J. Shen, A. Auroux, *J. Catal.*, 274 (2010) 259-272.

[47]   H. Onoda, T. Ohta, J. Tamaki, K. Kojima, H. Nariai, *Mater. Chem. Phys.,* 96 (2006) 163-169.

[48]   S. Ardizzone, C. L. Bianchi, *Appl. Surf. Sci.,* 152 (1999) 63-69.

[49]   P. F. Siril, A. D. Davison, J. K. Randhawa, D. R. Brown, *J Mol. Catal. A-Chem.,* 267 (2007) 72-78.

[50]   W. T. Reichle, *Solid State Ionics.,* 22 (1986) 135-141.

[51]   D. G. Cantrell, L. J. Gillie, A. F. Lee, K. Wilson, *Appl. Catal. A-Gen.*, 287 (2005) 183-190.

[52]   A. I. Tsyganok, M. Inaba, T. Tsunoda, K. Uchida, K. Suzuki, K. Takehira, T. Hayakawa, *Appl. Catal. A-Gen.*, 292 **(**2005) 328-343.

[53]   Z. Lü, F. Zhang, X. Lei, L. Yang, S. Xu, X. Duan, *Chem. Eng. Sci.,* 63 (2008) 4055-4062.

[54]   H. A. Prescott, Z. J. Li, E. Kemnitz, A. Trunschke, J. Deutsch, H. Lieske, A. Auroux, *J. Catal.,* 234 (2005) 119-130.

[55]   S. Velu, C. S. Swamy, *Appl. Catal. A-Gen.*, 162 (1997) 81-91.

[56]   I.-C. Marcu, D. Tichit, F. Fajula, N. Tanchoux, *Catal. Today.,* 147 (2009) 231-238.

[57]   L. Dussault, J. C. Dupin, E. Dumitriu, A. Auroux, C. Guimon, *Thermochimica Acta.,* 434 (2005) 93-99.

[58]   I. Kirm, F. Medina, X. Rodríguez, Y. Cesteros, P. Salagre, J. Sueiras, *Appl. Catal. A-Gen.*, 272 (2004) 175-185.

[59]   F. Wong, R. G. Buchheit, *Prog. Org. Coat.*, 51 (2004) 91-102.

[60]   K. L. Erickson, T. E. Bostrom, R. L. Frost, *Mater. Lett.,* 59 (2005) 226-229.

[61]   B. M. Choudary, M. Lakshmi Kantam, C. R. Venkat Reddy, K. Koteswara Rao, F. Figueras, *J Mol Catal. A-Chem.,* 146 (1999) 279-284.

[62]   M. J. Climent, A. Corma, S. Iborra, A. Velty, *J. Catal.,* 221 (2004) 474-482.

[63]   U.S. Geological Survey. 2009. *2007 Minerals Yearbook - Cement* H.G. van Oss (Ed.), U.S. Department of the Interior, U.S. Geological Survey, Reston, Virginia.

[64]   UNFCCC, [http://unfccc.int/ghg_data/ghg_data_non_unfccc/items/3170.php], [cited 21/02/2011].

[65]   S. V. Ranganathan, S. L. Narasimhan, K. Muthukumar, *Bioresour. Technol.*, 99 (2008), 3975-3981.

[66]   R. Diesel, *Springer*, Die Entstehung des dieselmotors verlag von ulius, Berlin (1913).

[67]   HMRC, [http://customs.hmrc.gov.uk/channelsPortalWebApp/channelsPortalWebApp.portal?_nfpb=true&_pageLabel=pageVAT_ShowContent&id=HMCE_CL_000205&propertyType=document], [cited 21/02/2011].

[68]   C. G. Chavanne, *Belgian Patent*, Procede de transformation d'huiles vegetales en vue de leur utilisation comme carburants., (1937) 422, 877.

[69]   M. Slinn, K. Kendall, C. Mallon, J. Andrews, *Bioresour. Technol.,* 99 (2008) 5851-5858.

[70]   J. Janaun, N. Ellis, *Renewable Sustainable Energy Rev.*, 14 (2010) 1312-1320.

[71]   J. Lee, Shiro Saka, Bioresour. *Technol.,* 101 (2010) 7191-7200.

[72]   X. Deng, Z. Fang, Y. Liu, C. Yu, *Energy.,* 36 (2011) 777-784.

[73]   P. S. Bindraban, E. H. Bulte, S. G. Conijn, *Agric. Syst.*, 101 (2009) 197-199.

[74]   D. Tomes, P. Lakshmanan.   Biofuels - Global Impact on Renewable Energy, Production Agriculture, Technological Advancements., 1 (2010) 311.

[75]   W. Xie, X. Huan, H. Li, *Bioresour. Technol.*, 98 (2007) 936-939.

[76]   D. G. Cantrell, L. J. Gillie, A. F. Lee, K. Wilson, *Appl. Catal. A-Gen.*, 287 (2005) 183-190.

[77]   R. Schlögl, M. Che, O. Clause, C. Marcilly, C. Louis, H. Knöinger, E. Teglauer, W. Keim, B. Drieben-Hölscher, J. W. Geus, A. J. van Dillen, J. Barbier, *Preparation of Solid Catalysts,* Wiley-VCH Verlag GmbH. (2008).

[78]   D. Y. C. Leung, X. Wu, M. K. H. Leung, *Appl. Energy.*, 87 (2010) 1083-1095.

[79]   M. M. Gui, K. T. Lee, S. Bhatia, *Energy.,* 33 (2008) 1646-1653.

[80]   A. Kumar Tiwari, A. Kumar, H. Raheman, *Biomass Bioenergy.,* 31 (2007) 569-575.

[81]   R. S. Watkins, A. F. Lee, K. Wilson, *Green Chem.,* 6 (2004) 335-340.

[82]   X. Liu, H. He, Y. Wang, S. Zhu, *Catal. Commun.*, 8 (2007) 1107-1111.

Chapter 2

Experimental and Instrumental Techniques: Background Theory and Practical Applications

Chapter 2

Background Theory

The catalysts and catalyst precursors studied in this thesis were characterised using a number of techniques. Powder X-ray diffraction (p-XRD) was used to confirm crystal structures. Adsorption microcalorimetry was used to determine the number and strength of surface basic and, in one case, acid sites. Scanning electron microscopy-energy dispersive spectroscopy (SEM-EDS) was used to study the elemental compositions. Nitrogen adsorption measurements were performed to determine porosities and surface areas. Gas chromatography (GC) was used to monitor reaction rates by quantitative analysis of reactants and products in a transesterification reaction.

2.1 – Test Reaction and Reaction Mechanism

The transesterification of a triglyceride reaction was chosen for catalytic testing and this reaction can be seen in Figure 2.1.
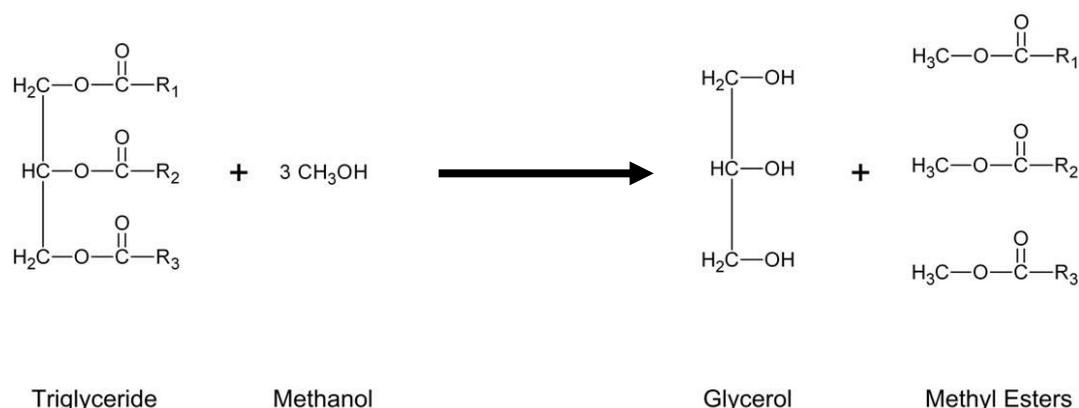
Figure 2.1 – Transesterification of a triglyceride.

The mechanism of this reaction when base catalysed can be seen in Figure 2.2. The initial stage of the reaction proceeds by the OH^- (catalyst) deprotonating the

methanol, resulting in the formation of an alkoxide and protonated base (1).   The alkoxide attacks the carbonyl species on the triglyceride, resulting in an intermediate (2) by which the alkyl ester and the corresponding anion of the diglyceride are formed (3). The diglyceride then deprotonates the base (catalyst), which is now free again to deprotonate the methanol and restart the cycle of ester formation (4).   It is by this mechanism that the mono- and di- glycerides are able to form the alkyl esters and glycerol.

$$ROH \; + \; B \; \rightleftharpoons \; RO^- \; + \; BH^+ \tag{1}$$
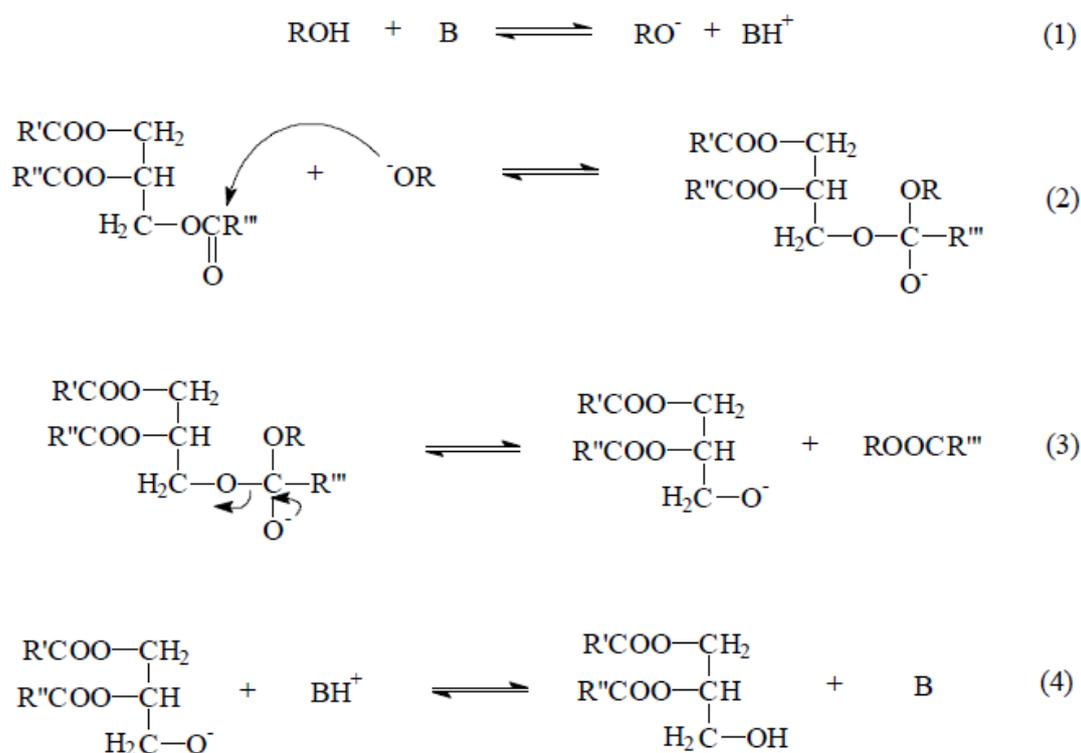
Figure 2.2 – Mechanism of the base-catalysed transesterification of a triglyceride. (B=Base).

A model reaction for the transesterification of triglycerides and alcohol to biodiesel was chosen between tributyrin (glyceryl tributyrate) and methanol.   The transesterification reaction of tributyrin with methanol consists of three consecutive reactions. Cantrell *et al* [1] have shown that the reaction initially proceeds via the formation of the diglyceride and the ester, (methyl butanoate), after which monoglyceride and then glycerol are formed.   For the first reaction the rate of

removal of tributyrin (this is what we have measured) is assumed to be first order in tributyrin. The reaction rate using 'real' vegetable oils and methanol is often difficult to measure reliably because of mass transfer limitations resulting from the two reactants being immiscible [2-6].   However, this complication is removed with tributyrin which is miscible in methanol. Because of this, reaction rates in this thesis are calculated for conversion of tributyrin for the initial stage of the reaction.

2.2 – Powder X-Ray Diffraction (p-XRD)

Powder X-Ray Diffraction (p-XRD) has been used to characterise all samples in this thesis. p-XRD was discovered in 1912 by Laue, Friederich and Knipping and later developed by W. H. Bragg and W. L. Bragg [7].

A monochromatic beam of x-rays can be diffracted by atoms in a crystal. The angle at which intense reflections are detected is governed by interferences between x-ray beams reflected by adjacent planes of atoms in the crystal. From these angles, the spacing between the various planes of atoms can be determined. Diffraction patterns (intensity of reflections vs. 2θ, where θ is both the incident and reflected angle between the x-ray beam and the planes of the atoms) recorded for individual crystalline materials can be interpreted in terms of the crystal structure of the material.

Reflected x-rays from a set of planes interfere constructively when the Bragg condition is met, (Equation 2.1 and Figure 2.3), where d is the spacing between the planes, θ the angle between both incident and reflected beams and the plane, and n is an integer, the order of reflection. There are many sets of planes of atoms in a crystal that give rise to diffraction. Each set of planes is defined by Miller indices, h, k and l. These relate how planes intersect the three axes, x, y and z relative to the dimensions of the crystal unit cell. Diffraction patterns recorded from powdered (polycrystalline) samples contain less information than those collected from single crystals but sometimes give information on specific lattice spacings which help characterise the powdered material. Powder XRD patterns are routinely used to fingerprint crystal structures.

$$n\lambda = 2d_{hkl}\sin\theta$$

Equation 2.1
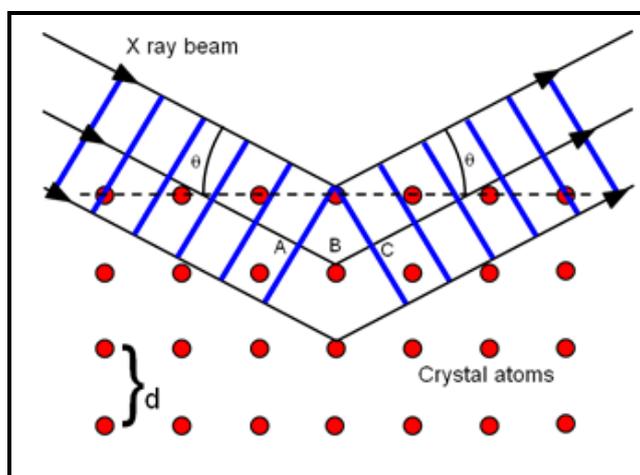
Figure 2.3 – Powder X-ray diffraction, lattice planes [8].

The p-XRD pattern of a typical layered double hydroxide (LDH) is quite characteristic and can be seen in Figure 2.4. The intense reflections labelled 003 (third order reflection from the 001 planes) can be used to calculate d_{001} which depends directly on the interlayer spacing and hence the nature of the exchangeable anion and the extent of solvation of the material. Another reflection that can be used quantitatively is that from the 110 planes since d_{110} depends on the nature of metal ions in the LDH lattice. Changes in d_{110} can be used to confirm the extent to which "new" metal ions are isomorphously substituted.
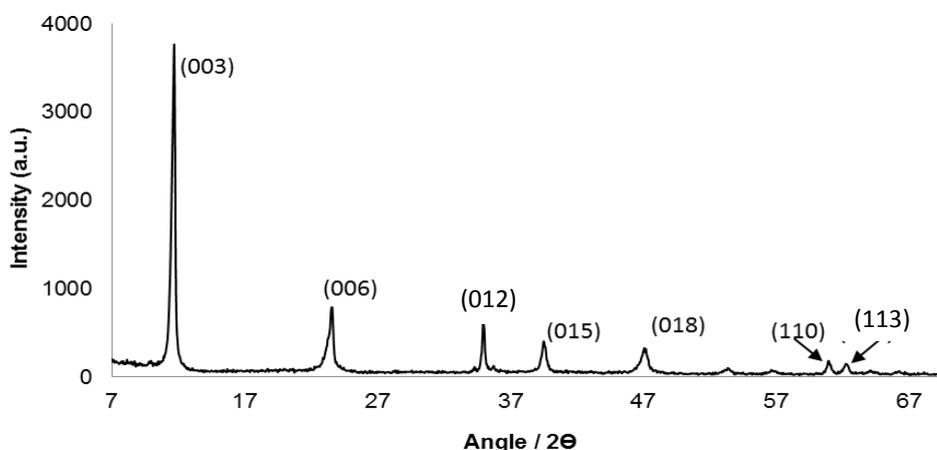
Figure 2.4 – Powder X-ray diffraction pattern typical of hydrotalcite.

The resolution of the diffraction pattern, or sharpness of lines in the pattern of intensity versus 2 θ, depends on the number of aligned planes contributing to the reflections. The Scherrer equation can be used to calculate the average dimensions of the crystallites (along the axis perpendicular to the planes causing the reflections) from the width of a diffraction peak at half height, where L is the crystallite size, β is the line width, θ is the diffraction angle and K is a constant 'normally equal to about one'.

$$L = \frac{K\lambda}{\beta cos\theta}$$

Equation 2.2

2.3 – Nitrogen Adsorption

By using the adsorption of an inert gas onto a solid surface we can calculate the surface area of the solid. Typically, nitrogen is used as an adsorbate, and an adsorption isotherm is generated by measuring the amount of nitrogen adsorbed by a solid as a function of the pressure of nitrogen in equilibrium with the solid. The pressure is conventionally expressed as P/P_0 where P is the pressure of nitrogen and P_0 is the saturated vapour pressure at the adsoprtion temperature. Adsorption isotherms are normally reported over P/P_0 range of zero to 1.0. With nitrogen, adsorption isotherms are usually collected at 77 K when the saturated vapour pressure P_0 is 1.0 atmosphere.

Adsorption of a gas onto a solid can be either via van der Waals (physical) or covalent (chemical) interactions.   There are six identified types of adsorption isotherm that are classified in terms of the nature (porosity) of the adsorbent (Figure 2.5).
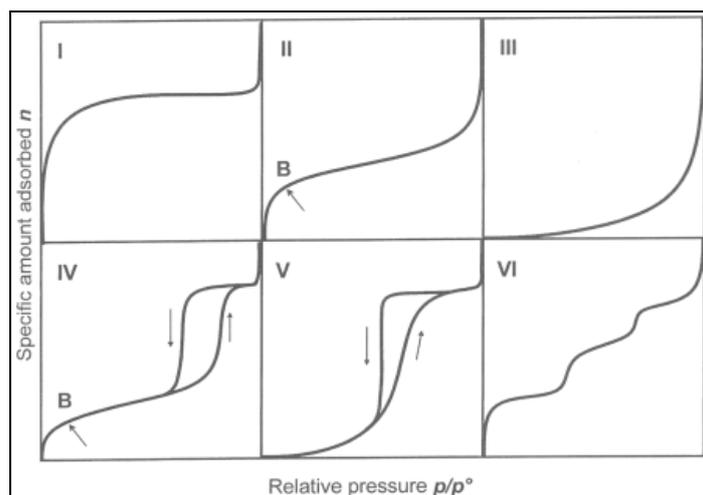
Figure 2.5 - IUPAC classification of isotherms [9].

Type I isotherms are apparent when a monolayer forms on the surface. It is typically observed for microporous adsorbants (where pore widths do not exceed 2 nm). The adsorption takes place at relatively low pressure and the isotherm flattens off when a monolayer of adsorbate forms, only rising again when P/Po approaches 1.0 and condensation occurs. Type II isotherms are typical of non-porous (or macroporous) solids for which multilayer adsorption occurs. Type III isotherms do not show any point at which a monolayer is formed. These are seen when the heat of adsorption is less than that of liquefaction. This type of isotherm is very uncommon. The type IV isotherm is characteristic of mesoporous solids (pores widths 2 nm – 50 nm). Hysteresis loops are apparent because the capillary condensation that occurs in mesoporous solids is not replicated at the same pressures during the desorption process. Pores appear to fill at higher pressure during adsorption and then at lower pressure during desorption. Type IV isotherms are initially similar to type I isotherms as a monolayer is formed but gradually multilayer formation can be seen as the pores fill up. Type V isotherms are not common and are obtained when there is very little interaction between the adsorbent and the adsorbate. Type VI isotherms are also uncommon because the sites involved are usually non-uniform in size and energetics. The steps that are seen in this isotherm show that there are groups of different sized pores.

2.3.1 – Adsorption Isotherm Models

The simplest model for the adsorption process of gas molecules onto a surface was derived by Langmuir in 1918 [10]. This model assumes the following:

1. Adsorption cannot form more than one molecular layer on the surface.
2. All adsorption sites are uniform and equivalent.
3. The probability of a site adsorbing a molecule is the same, irrespective of whether the adjacent sites are vacant or not.
4. Every adsorption site can accommodate only one molecule of adsorbate.
5. Molecules of the adsorbate do not interact with one another.
6. Equilibrium is achieved between the rate at which species adsorb and desorb from the surface. Hence, adsorption is a dynamic process.

The Langmuir isotherm equation can be derived by looking at the processes of adsorption and desorption of a gas on a uniform solid surface. At equilibrium, the rate of adsorption is equal to the rate of desorption.

The rate of adsorption of gas A on the surface is proportional to the pressure of gas and the concentration of vacant sites, expressed as the fraction of sites on the surface that are available for adsorption (when θ = the fraction of surface sites occupied by gas A), (Equation 2.3).

$$rate_{ads} = k_{ads}\, P_A (1 - \theta)$$

Equation 2.3

The rate of desorption of gas A is proportional to the concentration of sites occupied by gas A on the surface, expressed as the fractional coverage of gas A on the surface ө, (Equation 2.4).

$$rate_{des} = k_{des}\theta$$

Equation 2.4

At equilibrium:

$$k_{ads}\,P_A(1-\theta) = k_{des}\theta$$

Equation 2.5

Therefore:

$$\frac{k_{des}}{k_{ads}} = \frac{P_A(1-\theta)}{\theta}$$

Equation 2.6

If "b" is defined as k_{ads}/k_{des} then from Equation 2.6 it can be shown that:

$$\theta = \frac{bP}{1+bP}$$

Equation 2.7

Now, $\theta = \dfrac{V}{Vm}$, where V is the volume of gas A (at STP) adsorbed at equilibrium and

V_m is the volume of gas required to complete a monolayer of A on the surface of the adsorbent, so:

$$\frac{V}{V_m} = \frac{bP}{1+bP}$$

Equation 2.8

We can rearrange this equation:

$$\frac{P}{V} = \frac{1}{bV_m} + \frac{P}{V_m}$$

Equation 2.9

Therefore, if Langmuir's model isotherm is obeyed, a plot of P/V against P over the equilibrium pressure range studied will give a straight line. The intercept will be equal to $1/bV_m$ and the gradient of $1/V_m$. If the surface area occupied by one molecule of the adsorbate is known then the volume V_m can be used to calculate the surface area of the solid. The value of b gives an indication of the "strength" of the adsorption of gas A on the surface.

If V_m is the volume of gas at STP required to form a monolayer on the sample used (of known weight), N_A is Avogadro's number and σ is the cross-sectional area of one molecule of adsorbant, in this case N_2 (16.2 Å), the surface area of the surface sample (S) is given by:

$$S = \frac{101325}{8.314 \times 298} V_m \times N_A \times \sigma$$

Equation 2.10

The assumptions made by Langmuir are not appropriate for many porous materials and there have been several attempts to develop a model that does not rely so heavily on them, one of which is the BET (Braunauer, Emmett and Teller) model [6].

The BET equation is based on the Langmuir model but with the following additional assumptions:

1. The adsorbate may form more than a single layer on the surface.

2. The initial monolayer heat of adsorption has a specific value. The heat of adsorption of the second and subsequent layers of adsorbed gas molecules is equal to the heat of condensation of the gas.

3. Interactions between the vapour and surface only correspond to adsorption and desorption.

4. Adsorbed molecules are not free to migrate from one layer to another.

The BET equation is:

$$\frac{P}{V(P_o - P)} = \frac{1}{V_m c} + \frac{(c-1)}{V_m c} \cdot \frac{P}{P_o}$$

Equation 2.11

P is the equilibrium pressure of the adsorbate and P_0 is the saturated vapour pressure. V is the volume of gas adsorbed at P/P_0. V_m is the volume of gas adsorbed to form a monolayer and the constant c is associated with the net heat of adsorption. A straight line, usually between P/P_0 values of 0.05-0.35, is obtained by plotting:

$$\frac{P}{V(P_o - P)} \quad \text{vs.} \quad \frac{P}{P_o}$$

Equation 2.12

The intercept, $\frac{1}{V_m c}$ and the slope, $\frac{(c-1)}{V_m c}$ can be used to calculate V_m and then the surface area of the solid can be calculated as before.

$$V_m = \frac{1}{slope + intercept}$$

Equation 2.13

An example of a nitrogen adsorption/desorption isotherm of a transition metal doped hydrotalcite, typical of a layered double hydroxide, can be seen in Figure 2.6 – a type IV isotherm. The surface area is normally calculated using the desorption isotherm.
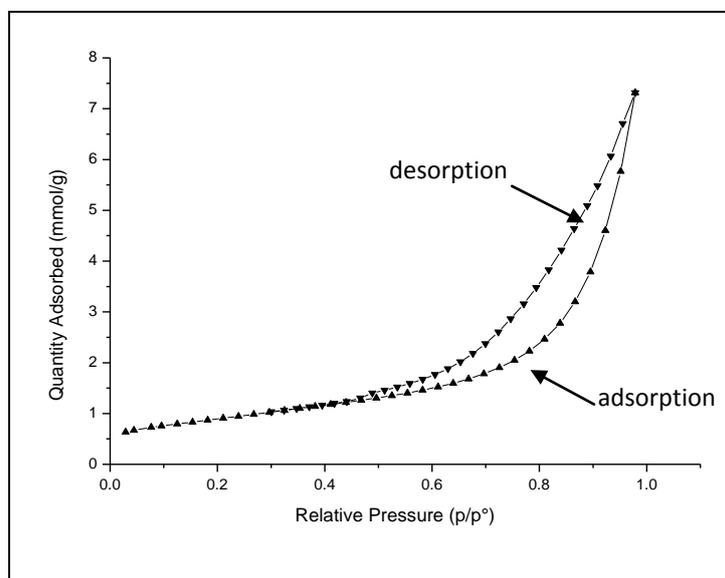
Figure 2.6 – Nitrogen adsorption isotherm typical of that of an LDH.

2.3.1.1 – Adsorption in Pores

In this thesis the BJH (Barrett, Joyner and Halenda) method is used to calculate the pore size distribution of porous solid samples [11].   This method is used conventionally to analyse mesoporous materials and is based on the Kelvin equation. There are assumptions made, which are:

- The pores are of a uniform shape.
- All pores are in the mesoporous range (pore widths between 2 nm and 50 nm).

The presence of pores in an adsorbent solid can affect the shape of an adsorption/desorption isotherm because the equilibrium vapour pressure above condensed liquid in a (cylindrical) pore, in which the surface of the liquid is curved, is lower than that above a liquid with a flat surface.

The Kelvin equation relates the equilibrium vapour pressure of a liquid in a small cylindrical pore where the surface of the liquid takes up a regular curvature. The Kelvin equation describes the dependence of the equilibrium vapour pressure of a liquid in the pore on the radius of the pore, r, and the contact angle, θ. Because the equilibrium vapour pressure above a curved surface is lower than above a flat surface, vapour condenses in pores at lower P/P_0 values than on a flat surface, with narrow pores filling at lower pressures than wide pores. From the pressure at which condensation occurs, the radius of the pores can be calculated. The Kelvin equation is given below. In the equation, P/P_0 is the relative vapour pressure at which condensation occurs in pores of radius r with contact angle of the condensed liquid with the pore walls θ. (θ is assumed to be zero for pores in the size range studied here). Other constants are γ, the surface tension of the condensed liquid, V_{molar}, the molar volume of the liquid, R and T.

$$\ln \frac{P}{P^o} = \frac{-2.\gamma.V_{molar}}{r.R.T}.\cos\theta$$

Equation 2.14

An example of the calculation of pore radius using nitrogen at 77K is given below (Equation 2.15):

$$r = -\frac{2.(8.85.10^{-3}).(3.467.10^{-5})}{(8.314).(77.3).ln(\frac{P}{P^o})}$$
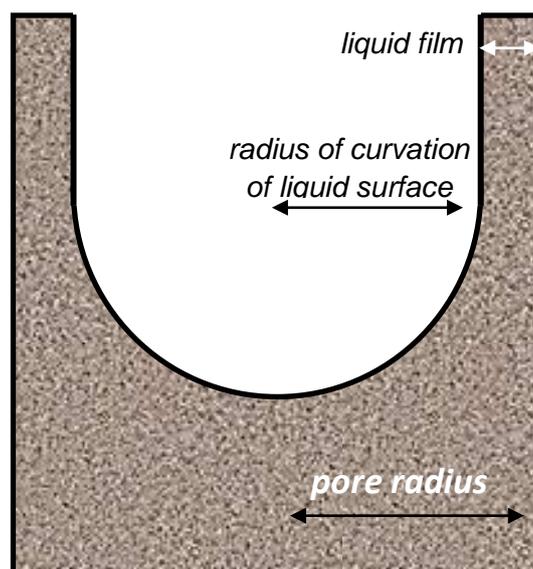
Equation 2.15

Figure 2.7 – Cylindrical pores for calculation of pore size/pore size distribution using the BJH method.

The BJH method involves a correction of the pore radius (Figure 2.7) given by the Kelvin equation to allow for a film of condensed vapour on the pore walls which means that the pore radius is slightly larger than the radius of curvature of the meniscus. Data shown in this thesis is BJH corrected pore diameter.

2.4 – Adsorption Calorimetry

Adsorption calorimetry is a technique which measures the amount of heat given out when a gas molecule adsorbs on the surface of a solid adsorbent. Catalysts can be characterised using adsorption calorimetry with suitable probe adsorbate compounds, where enthalpies of adsorption can be linked to the "strength" of active sites.

The adsorption of a probe acid or base gas onto an adsorbent surface is via either a physical or chemical interaction. A physical interaction (physisorption) between a gas and adsorbate is generally reversible and is usually through van der Waals forces of attraction. In calorimetric terms, the enthalpy of this adsorption is usually

<90 kJ mol^{-1} for the relatively polar and reactive gases used in this thesis [12].
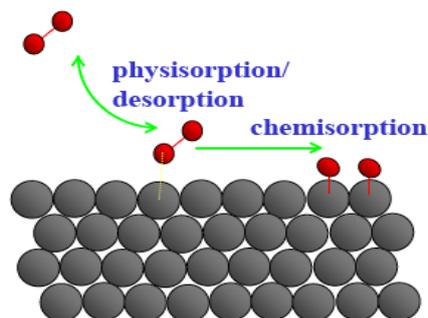
Figure 2.8 – Irreversible chemisorption and reversible physisorption [13].

A chemical interaction (chemisorption) involves the gas attaching to the surface and forming a chemical bond (Figure 2.8). Usually, chemisorption is restricted to monolayer formation because of the nature of the interaction.

In adsorption calorimetry it is necessary to relate the amount of gas adsorbed in an experiment to the amount of heat released in the adsorption process. The latter is measured calorimetrically. There are a number of ways of introducing and measuring the probe gas on a solid surface. The amount of gas adsorbed as a function of the equilibrium pressure of gas above the sample can be measured using a volumetric system of gas burette linked directly to the calorimeter cell holding the adsorbent. Another way of monitoring adsorbed gas is by using a gravimetric method, monitoring increases/decreases in mass before and after adsorption/desorption.

A flowing system can also be used where a probe gas is introduced to a carrier gas flow over the solid, monitoring the concentration of probe gas downstream of the sample by a mass spectrometer. The flow system largely removes ambiguity about whether the adsorption is reversible or irreversible because only irreversible adsorbed gas contributes to the measurement. A comparison between a volumetric system and a flow system has been carried out using CO_2 as the gas probe [14].

Figure 2.9 shows a typical heat signal recorded by a differential heat flow calorimeter in a flow adsorption calorimetry system. A series of pulses of probe gas is passed over the sample and the size of the heat signal (heat flow vs. time) is a measure of the extent and strength of adsorption, and the shape gives information on the rate at which adsorption occurs. Irreversible adsorption in the early stages is replaced by reversible adsorption, often a few pulses.
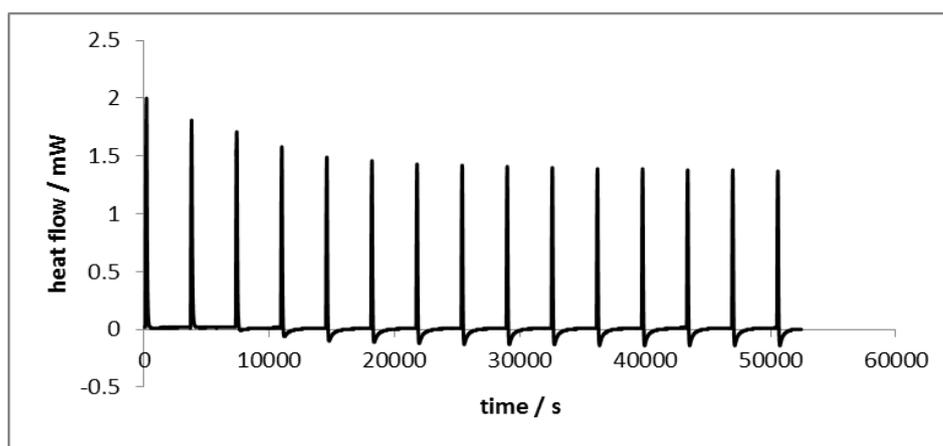
Figure 2.9 - Adsorption calorimetry: a typical heat signal recorded by a differential calorimeter as a series of pulses of probe gas is passed over the sample.

2.4.1 – Measuring the Heat of Adsorption

When heat, q, is added to a system at constant pressure then the enthalpy change in the system is equal to q:

$$\Delta H_{sys} = q$$

Equation 2.17

A calorimeter records the heat released **by** the system:

$$\Delta H_{sys} = -q_{calorimeter}$$

Equation 2.18

The change in enthalpy of a system is equal to the change in the internal energy of the system, corrected for any pressure/volume work that the system may do. As such it broadly reflects the formation and the breaking of bonds, the former resulting in negative values of ΔH (exothermic processes) and the latter positive values (endothermic processes).

This can be explained in more detail. In this thesis, calorimetry measurements are analysed using the measured heat of adsorption given by the heat evolved during the interaction between a gas and a clean surface on a solid. The heat evolved can infer much information about the bonding that has occurred between the two species. For a closed system, where the Calvert calorimeter was used attached to a glass volumetric system, the adsorption process can be discussed as q^{diff}. For an open system, the adsorption process is defined in this thesis as $\Delta H^{\circ}ads$. The reasoning for this is outlined below;

Using the first law of thermodynamics we can denote that the change in internal energy can be written as;

$$\Delta U = q + w$$

Equation 2.19

The change in energy is defined as the heat, (q), and work, (w), of a system. Work can be seen to be either work done by the system or work done on the system. If there is no pressure done on a system, which is the case with the open system then we can say that;

$$w = -p\Delta V$$

Equation 2.20

For the adsorption process of a gas onto a catalyst this term, (w), is positive as work

can be seen to be done on the system. If we substitute the equation of work within an open system into the first law:

$$\Delta U = q - p\Delta V$$

Equation 2.21

For a closed system it is true that no work is being done on the system and therefore can be deemed:

$$\Delta U = q.$$

Equation 2.22

As the system is a fixed volume any change in internal energy is related to energy exchanged within the system. This is not so for an open system as there are other processes such as work being done outside the system that can occur. A value that is close to the actual internal energy can be defined but it is important to say it is not the true value. In most cases, and in this thesis, the enthalpy (H) is substituted for the change in internal energy:

$$H = U + PV$$

Equation 2.23

The enthalpy is denoted as the internal energy (U) added to the pressure and volume, PV respectively. The change in enthalpy can be stated to be:

$$\Delta H = \Delta U + P\Delta V + V\Delta P$$

Equation 2.24

The term for the change in internal energy can be substituted by using the equation for the first law of thermodynamics (Equation 2.19):

$$\Delta H = q - P\Delta V + P\Delta V + V\Delta P = q + V\Delta P$$

Equation 2.25

Working at constant pressure, (of an open system), means we can say that:

$$\Delta H = q$$

Equation 2.26

Both heat representations of internal energy, ΔH (for an open system) and q (for a closed 'static' system) can be plotted against the coverage of the amount adsorbed.

2.4.2 – Types of Calorimeter

There are three most commonly used calorimeters, heat accumulation, heat exchange and heat conduction (isothermal) calorimeters. A heat accumulation calorimeter measures the temperature change in a thermal reservoir caused directly by the compound producing the heat (exothermic or endothermic). An example of a heat accumulation calorimeter is a bomb calorimeter. A heat exchange calorimeter measures the difference in temperature between the compound producing the heat and the surroundings. An example of a heat exchange calorimeter is a heat-flux calorimeter. Finally, a heat conduction (isothermal) calorimeter is one that is used at a constant temperature, and where the conduction of heat between the sample and the surroundings, a relatively massive heat sink, is measured. As the temperature within the system is maintained, heat must be provided for any endothermic process and removed for any exothermic process where heat is evolved. A benefit to using this type of calorimeter is the high degree of sensitivity.

In this work a heat flux (heat flow) calorimeter has been used, a form of heat conduction calorimeter. In this instrument heat emitted by the sample in the sample cell is conducted through a thermopile which surrounds the sample cell, to a large thermal sink. When heat is produced in the cell, it is conducted to the heat sink through the sensitive thermocouple which records a transient signal which returns to zero as soon as thermal equilibrium is re-established. The thermopile is connected to a similar thermopile around the reference cell in such a way that voltage

differences between the two thermopiles are sensitive to differences between the two. As the heat flow from the sample cell rises and falls, so does the signal. This signal is the differential of the heat output and can be interpreted to give the heat output itself.

2.4.2.1 – Gases Used for Adsorption

There are many gaseous probe compounds that can be used to study the basicities and acidities of solids. In general, ammonia (base strength in water pKa 9.4) is most commonly used for studying acidity. Basicity measurements are commonly studied using SO_2 and CO_2. SO_2 is a stronger acid than CO_2, with pKa values of 1.89 and 6.37 respectively in water. SO_2 will probe the total number of basic sites, whereas CO_2 is more selective towards strong sites. A slight cause for concern with CO_2 is that under certain conditions it can interact sometimes with Lewis acid sites and behave as a base [15]. However the possibility of mixed oxides synthesised in this thesis exposing such sites (requiring very high temperatures) is remote. When referring to CO_2, the assumption is therefore made that all CO_2 chemisorption is related to the basicity of the solid.

2.5 – Scanning Electron Microscopy/Energy Dispersive Spectroscopy (SEM-EDS)

The scanning electron microscope (SEM) is a useful tool in characterising solid materials. The wavelength of electrons accelerated to energies of more than 10 KeV is very much less than that of visible light, reducing the effects of diffraction and therefore allowing greater magnification. In addition, much smaller apertures can be used, resulting in greater depth of field.

The principle of SEM is that the surface of a solid material is bombarded with electrons by the means of an electron gun. When the electrons hit the sample three different types of signals are generated. These signals can be described as x-rays,

and backscattered and secondary electrons (Figure 2.10). It is the secondary electron signal that can be interpreted as a high resolution image. X-rays resulting from bombardment of electrons allows elemental composition determination since their frequencies are characteristic of the elements from which they are emitted.
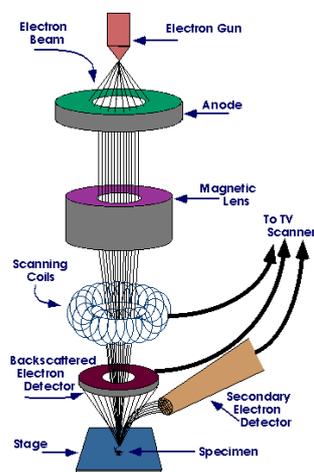
Figure 2.10 – Schematic of a Scanning Electron Microscope [16].

2.6 – Gas Chromatography (GC)

Gas chromatography (GC) is an analytical technique by which mixtures of organic compounds are separated and their components quantified. A small amount of sample is introduced to an injector which is set to a temperature hot enough to vaporise the sample. The vaporised mixture is then swept into the column by a carrier gas. The column inner walls are coated by an adsorbent material, the stationary phase. Interactions between the sample and the stationary phase cause the individual compounds in the mixture to pass through the column at different rates and to reach the detector at different times; the stronger the interaction between the compound and the stationary phase, the longer it takes for the compound to reach the detector. The column can be subjected to a temperature program if there is a requirement to separate materials with widely different boiling points.

Stationary phases are chosen depending on the compounds that require separation. In general, polar compounds will interact strongly with polar stationary phases and therefore will have longer retention times. As well as temperature, other variables

which affect separation include the column length, injection volume and the nature and flow rate of the carrier gas.

There are several types of detector, e.g. flame ionisation (FID), thermal conductivity (TCD), and electron capture (ECD). For all experiments in this thesis FID was used. An FID can be used to detect organic compounds with significant hydrocarbon content, and is used with a hydrogen-air flame. Organic compounds emerging from the column are burnt in the flame and the ions generated in the flame are detected via increased electrical conductivity across the gas flow. A potential difference of 200-300 V is applied across the flowing gas and the current that flows is measured, amplified and seen as a peak on a chromatograph.

2.7 – Atomic Absorption Spectroscopy (AAS)

Atomic absorption spectroscopy (AAS), was used to measure sodium levels in synthesised catalysts. This is a trace element analytical technique for measuring concentrations of elements to ppm or lower levels in aqueous solutions.

An aqueous solution is aspirated into a flame, in which any compounds or ions containing the element under analysis are decomposed so that only atomic species exist. The flame is irradiated using a high voltage lamp containing the vapour of the element under analysis. A detector records the absorption of the monochromatic light from the lamp by the atoms of the element in the flame. The extent of adsorption is then converted to concentration in the solution using a suitable calibration curve prepared using standard solutions of the element. Because AAS relies on discrete emissions and absorption lines in gas phase atomic spectra, there is virtually no interference between other elements in solution and the element being analysed. Sample preparation is therefore relatively simple.

2.8 – Heating Solids with Microwaves

Microwaves heat solids through coupling with dipolar species or with charge carriers [17].   Where solid state transformations occur, the transformation can be accompanied by dramatic changes in the way the solid interacts with the microwave field.   Under normal conditions this can lead to hot spots, cold spots, and, sometimes, temperature runaway. In addition to this, in some cases microwaves can induce quite different processes in solids to conventional heating, such as ion migration through the solid [18], especially close to surfaces [19]. Therefore, it is not surprising that solid phase transformations induced by microwaves are, in some cases, different to those brought about by conventional heating.   An important feature of microwave heating is that the direct heating effects are often less concentrated at the surface and are generally distributed through a material differently (depending on the nature of the sample and how the components present couple) to the effects of conventional heating. This gives rise to less pronounced, or at least different, temperature gradients to those generated under conventional heating. This is obviously important in cases where, for example, water vapour is expelled during heating (as with the calcination of metal hydroxides). The extent to which the water vapour has to diffuse to the surface through material which may or may not have already been dehydrated/dehydroxylated, differs between conventional and microwave heating.   At the least, the structural disruption caused by this diffusion, and the extent to which chemical equilibria are affected by resident water vapour, could be quite different, depending on the nature of the solid through which diffusion has to occur.

2.8.1 – Feedback-Controlled Microwave Heating

The problems with microwave-induced solid state transformations, of possible temperature runaway as the dielectric properties of the material change as the transformation occurs, can be reduced or eliminated by the application of feedback-controlled heating. Feedback-controlled heating methods were first developed to

increase resolution in thermal analysis experiments [20]. As a sample is subjected to a heating programme, continuous feedback is set up between a measured property of the sample, most commonly its temperature, and the power supplied to the sample furnace.   The power is controlled to maintain a constant rate of change of the property being monitored or a constant value of the property.   As well as sample temperature, control can be based on the mass of the sample or the partial pressure of an evolved gas, both resulting in reduced temperature gradients in the sample during crucial periods of heating programmes and improved resolution of events in thermal analysis experiments.

Feedback-controlled techniques (using both conventional and microwave heating) have been developed in our laboratories (as well as others). They have been scaled up for use in materials synthesis for samples of typically five grams. This is significant as it takes them from being analytical to preparative, or at least semi-preparative.

Figures 2.11 and 2.12 illustrate the value of controlled heating in a typical microwave calcination. Application of a linear increase in microwave power (in other words with no feedback control) to a layered double hydroxide seen here (Figure 2.11) results in dramatic changes in sample temperature response, with runaway above 450 ^{o}C. With feedback-controlled power set to provide a linear temperature increase (Figure 2.12) the temperature does indeed increase linearly. Note the continuously varying power is required to maintain this temperature ramp. This particular experiment did not extend beyond 400 ^{o}C but at higher temperature the power drops off rapidly to maintain the steady temperature rise through the region where runaway is detected in the absence of feedback-control.
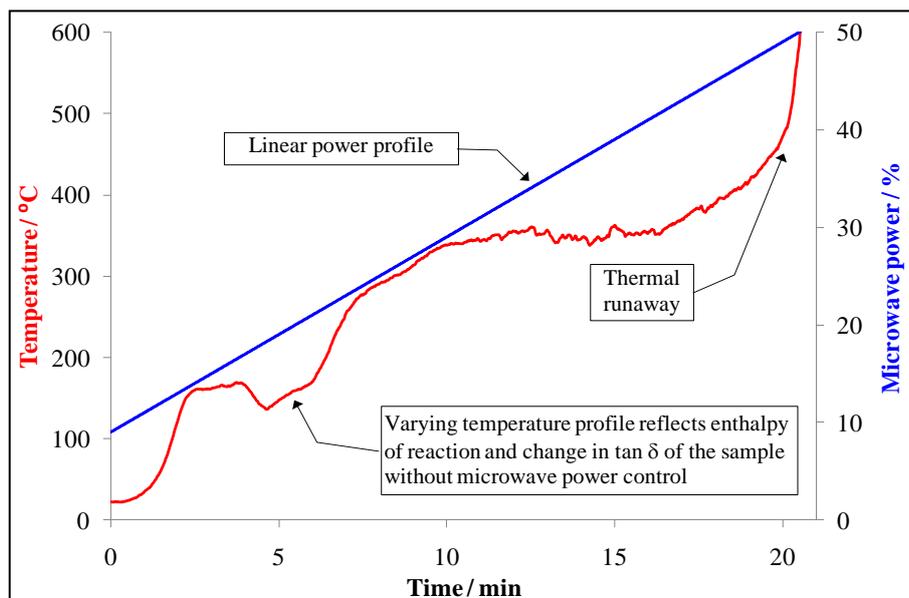
Figure 2.11 – Temperature/time and power/time where the rate of power increase kept constant for a typical hydrotalcite.
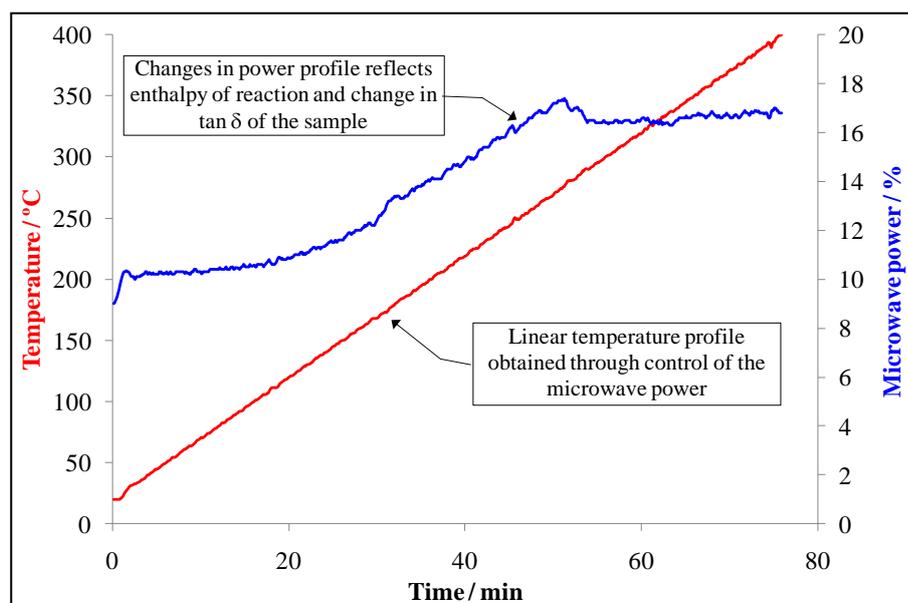
Figure 2.12 – Temperature/time and power/time where the rate of temperature increase is kept constant for a typical hydrotalcite.

Figure 2.13 illustrates a feedback-controlled experiment when a copper-containing LDH was heated with microwaves to 450 ⁰C controlling the power to maintain a linear temperature increase, and then held at that temperature for two hours. The interesting aspect of this experiment is that during the isothermal stage, at about 250 minutes, an event occurred resulting in a sudden rise in sample temperature. The microwave power can be seen to fall in response (by feedback-control) to bring the sample back to 450 ⁰C. Once stable again the power required to hold the temperature is slightly lower than it was before the event. P-XRD patterns taken before this point and immediately after show that an abrupt solid state transformation occurred, in which the hydroxide was converted to oxide. Nothing comparable to this has been observed under conventional heating.
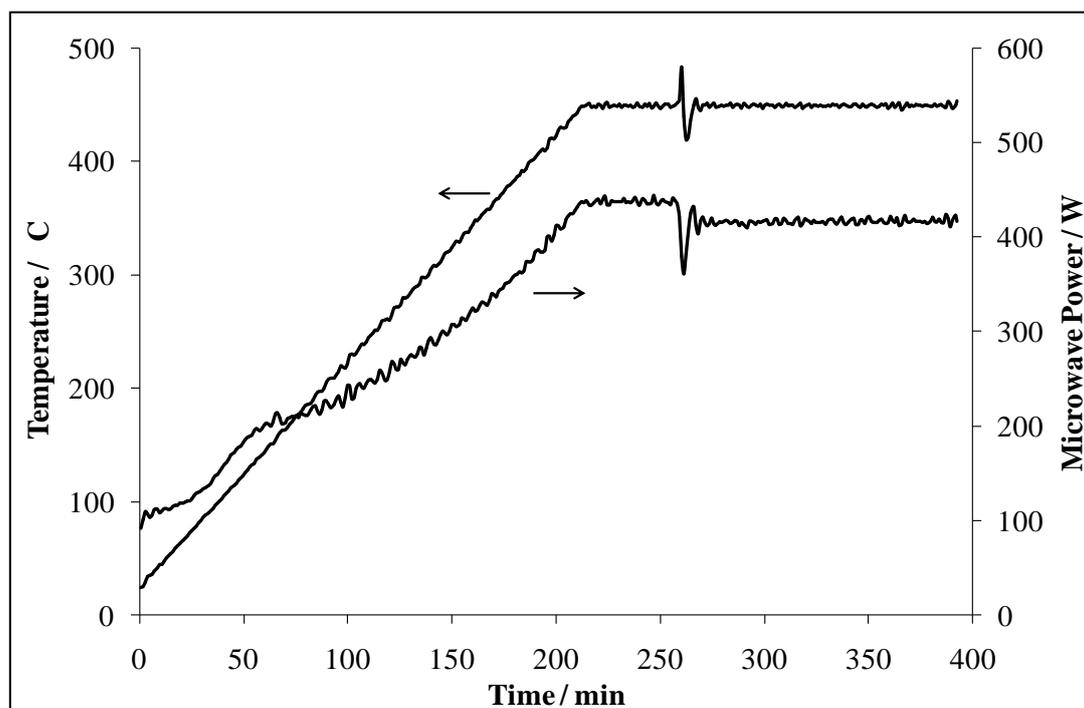
Figure 2.13 - Temperature/time and power/time plots for a copper-containing LDH under microwave heating, maintaining a constant heating rate followed by an isothermal period.

Practical Applications

2.9 – Powder X-ray Diffraction

Powder XRD patterns were obtained using a Bruker AXS – D8 Advance diffractometer with Cu Kα radiation, (wavelength 0.154 nm). Samples were scanned from 2θ = 0.6 ° to 70 ° with a scanning speed of 2 ° min^{-1} (step size 0.02 °). Powder XRD patterns were produced under atmospheric conditions. Powder XRD patterns of calcined hydrotalcites were measured promptly to minimise the contact of the mixed metal oxides with moisture and CO_2 which could affect the structure

2.10 – Nitrogen Adsorption

Nitrogen adsorption/desorption isotherms were generated for each sample using the sorption analyser (Micrometrics ASAP 2020). Adsorption isotherms were recorded at 77 K after degassing at 150 °C. The number of data points for an isotherm was 30. The adsorption isotherm was then used to calculate the BET surface area. Desorption isotherms were used to calculate pore volumes and pore size distributions using the BJH method.

2.11 – SEM-EDS

A JEOL JSM-6060 scanning electron microscope (SEM) fitted with an Oxford Instrument EDS system was used for the collection of high resolution images and elemental composition data. For each sample a small amount was placed on a double sided adhesive sheet on an aluminium disc. In order to ensure the sample was conducting, the sample was coated with a thin layer of palladium and gold (20:80). The voltage set was 15-20 kV.

2.12 – Catalytic Testing

2.12.1 – Transesterification of Tributyrin

Catalytic activities were measured in the transesterification of tributyrin with methanol. Catalyst (50 mg) was activated at 150 ^{o}C in a vessel (under flowing nitrogen) and added to a pre-heated mixture of 5.0 ml tributyrin and 11.0 ml methanol in the reaction vessel equipped with a reflux condenser and magnetic stirrer. The reaction temperature was 65 ^{o}C. The reaction was monitored in terms of conversion of tributyrin over two hours reaction time, using GC, with dihexyl ether as internal standard. In each reaction, the effect on the rate of reaction of removing the catalyst after one hour was examined, as a test for catalyst leaching. The effect of stirrer speed was also investigated to ensure that measurements were not taken in a diffusion controlled regime.

During the reaction, samples (100 μL), were taken periodically using a filtered syringe, including at zero minutes, and then held in an ice bath until they were analysed. Samples were filtered to remove any catalyst and to stop the reaction. A Perkin-Elmer Clarus 500 GC with FID was used, with a 25 m BP1 column at 1.4 ml min^{-1} helium flow, split ratio 28:1. A temperature program was used starting at 60 ^{o}C and heated to 150 ^{o}C at a rate of 10 ^{o}C min^{-1} followed by a second ramp of 20 ^{o}C min^{-1} to 280 ^{o}C. The injector and detector temperature was 240 ^{o}C.

2.13 – Adsorption Calorimetry

2.13.1 – Adsorption Microcalorimetry Measurements Using a Flow-Through System

Flow-through adsorption calorimetry using carbon dioxide and ammonia under flow conditions was performed using an indigenously developed system (Figure 2.14) based on a flow-through Setaram 111 differential scanning calorimeter (DSC) and an

automated gas flow and switching system, with a mass spectrometer detector for the down-stream gas flow (Hiden HPR20) connected via a heated capillary (at 175 °C) [21]. The powdered sample was held on a porous frit in the middle of a silica sample tube located in the DSC sample cell. In a typical experiment, the sample (~30-50 mg) was activated under dried helium (5 ml min^{-1}) for one hour at 150 °C. When using carbon dioxide, the sample was cooled to 120 °C for adsorption measurements. The adsorption temperature when using ammonia was 150 °C. Small pulses (typically 1 ml but depending of the volume of the sample loop) of the probe gas (1 % carbon dioxide or ammonia in helium) were then injected at regular intervals into the carrier gas stream from a gas sampling valve. Both gases were passed through drying tubes before exposing to the sample.

The concentration of carbon dioxide downstream of the sample was monitored with the mass spectrometer. The interval between pulses was chosen to ensure that the carbon dioxide or ammonia concentration in the carrier gas (including that adsorbed and then desorbed after the pulse has passed) returned to zero and the DSC heat flow baseline re-established itself. An important feature of the flow calorimetric technique is that net heat measurements relate only to carbon dioxide or ammonia bound irreversibly to the samples. Weakly bound (physisorbed) carbon dioxide or ammonia desorbs immediately the gas flow reverts to the carrier gas (Figure 2.9). The net amount of carbon dioxide irreversibly adsorbed from each pulse was determined by comparing the mass spectrometer signal during each pulse with a signal recorded during a control experiment through an empty sample tube. Net heat released for each pulse was calculated from the DSC thermal curve.

The Setaram 111 was connected to a computer using Setaram Setsoft 2000 software by which the heat flow signal could be integrated to obtain a heat value. An example of the data obtained is shown in Figure 2.15 and is the differential heat flow (mW) vs. time (s). The heat flow signal can be seen to decrease in area as more pulses are applied to the sample. This is indicative of the strongest sites adsorbing ammonia initially, followed by the weaker sites. The energy (in Joules) produced by the adsorption of the probe gas is obtained by the integration of a peak via the software. To determine if the sample has fully adsorbed the gas, ammonia was monitored during the experiment by the mass spectrometer. The mass spectrometer signal throughout the experiment corresponding to ammonia (m/z = 15)

is shown in Figure 2.15. This m/z ratio was chosen to avoid simultaneous detection of water (m/z = 18, 17, 16). In this example, ammonia is seen to be adsorbed fully by the sample up to the final five pulses.

It worth saying that attempts were made to gain data using a gas burette system in which probe gas reached equilibrium with the sample but experimental difficulties meant it was not possible to collect enough data on which to draw meaningful conclusions.
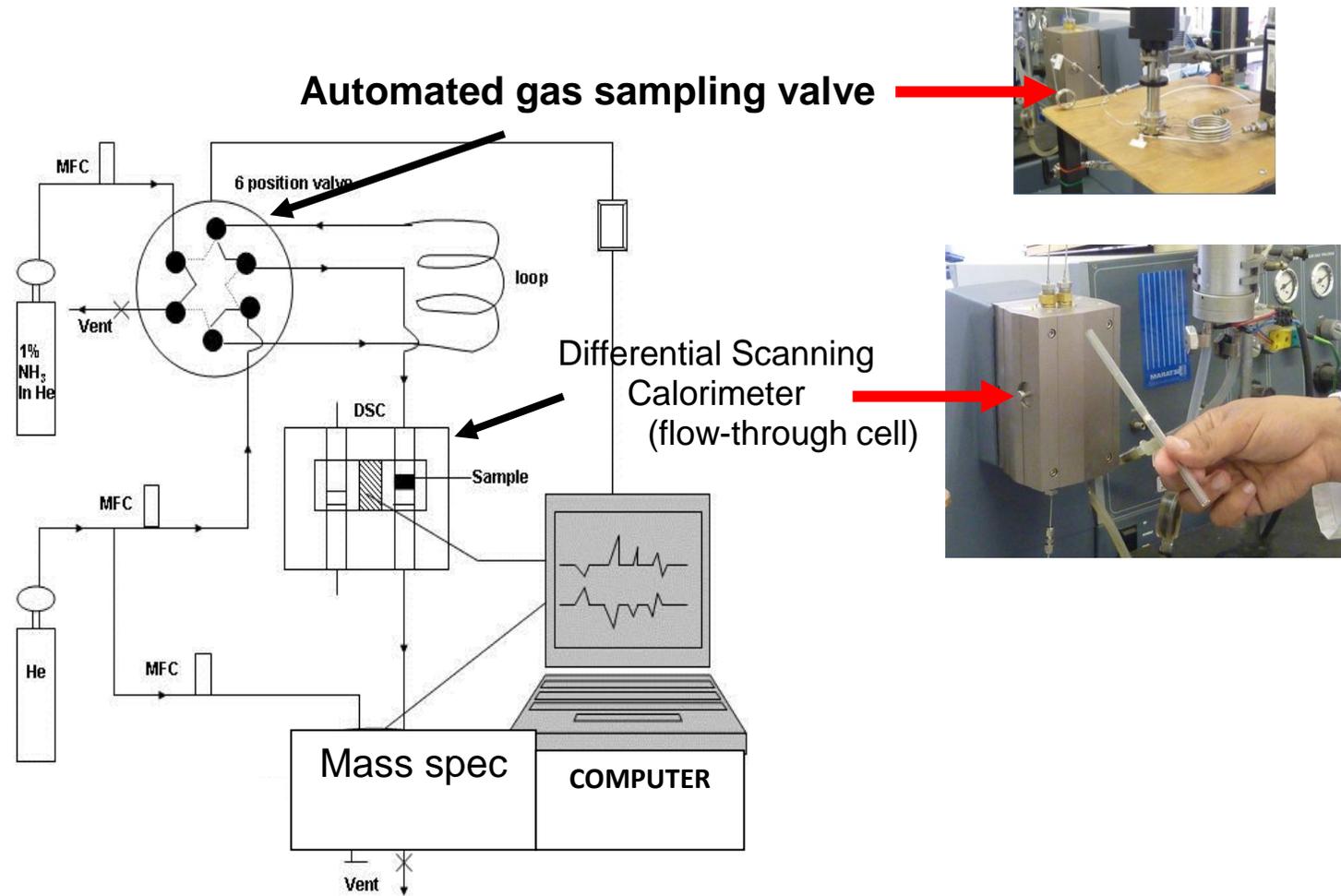
Figure 2.14 – Schematic diagram of the flow-through adsorption calorimeter system.

A "blank" experiment was performed in the same way as described above without a sample in the sample tube. Pulses of the probe gas were applied and monitored by the mass spectrometer. Typically 15 pulses of probe gas through the empty tube were integrated and the average integrated value used as an value of one pulse of probe gas. When there was breakthrough of probe gas during an experiment (i.e. the sample is not adsorbing all the gas), the percentage of gas adsorbed could be calculated and subsequently the amount of gas adsorbed calculated.
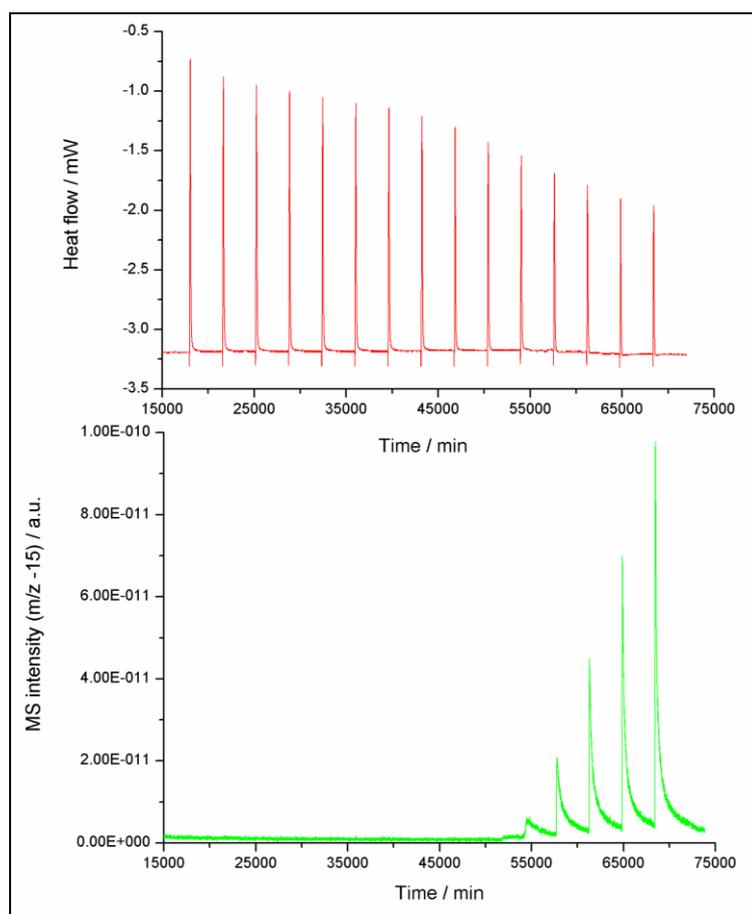
Figure 2.15 - An example of the heat signal obtained from the calorimeter (top) and the mass spectrometer signal obtained when probe gas (in this case ammonia). Note that for the first 10 pulses there is no breakthrough of ammonia.

The molar enthalpy of carbon dioxide or ammonia adsorption (ΔH^0_{ads}) was calculated for the carbon dioxide or ammonia adsorbed from each pulse. Each sample was analysed in duplicate or triplicate under the same experimental conditions. Data was

plotted as a profile of ΔH^0_{ads} vs. amount of carbon dioxide or ammonia irreversibly adsorbed. A spread sheet was set up to treat the raw data and the latest version of it is included in the Appendix 1.

2.14 – Atomic Absorption Spectroscopy

Each of the samples (0.100 g) was added to the minimum amount of concentrated nitric acid (Analar grade) needed to dissolve the solid, and then made up to 100 ml with deionised water. Absorption was measured at 519 nm using a sodium lamp. The instrument was a Perkin-Elmer AAnalyst 100. Sodium chloride, dried previously and maintained in a desiccator, (>99.9 %, Fisher), was used to prepare calibration standard solutions of sodium.

2.15 – Conventional Calcination

All samples (typically 2 g) were calcined using a conventional muffle furnace in a long ceramic boat to allow even exposure to the heat provided by the furnace. The calcination was carried out in static air, heating at 2 °C /min, followed by an isothermal stage. The rate of cooling was the same as heating and calcined samples were placed in a desiccator to ensure minimal moisture absorption.

2.16 – Microwave Calcination

The instrumental system and the algorithms used in this project were developed at the University of Huddersfield by Dr G M B Parkes [22-24]. A variable power (to 1 kW) microwave generator operating at 2.45 GHz feeds a wave guide with a three stub tuner and a resonant cavity which accommodates the sample.

The sample temperature is continuously measured by an infrared pyrometer located in one of the viewing ports of the microwave cavity. The pyrometer is calibrated against measurements made in a conventional furnace. The pyrometer output is used to control the power of the microwave generator to maintain a constant rate of sample temperature increases (most commonly at 2 °C /min), and to maintain a constant sample temperature during an isothermal stage.

Although not of direct relevance to this work it is worth mentioning that the sample, whilst in the cavity, is supported on the pan of a five figure balance. The software allows, when required, control of microwave power to be determined by the sample mass so that, for instance, it can be controlled to give a constant rate of sample mass change as the sample heats. The significance of this is that, in many cases, the rate of mass change of the sample is equivalent to the rate of reaction of the sample so this way of controlling microwave power allows for a constant reaction rate.

References

[1]   D. G. Cantrell, L. J. Gillie, A. F. Lee, K. Wilson, *Appl. Catal. A.,* 287 (2005) 183-190.

[2]   M. Zabeti, W. M. A. W. Daud, M. K. Aroua, *Fuel Process. Technol.,* 90 (2009) 770-777.

[3]   D. Siano, M. Nastasi, Patent, WO/2007/062825.

[4]   W. Xie, H. Peng, L. Chen, *J. Mol. Catal. A: Chem.,* 246 (2006) 24-32.

[5]   K. G. Georgogianni, A. P. Katsoulidis, P. J. Pomonis, M. G. Kontominas, *Fuel Process. Technol.,* 90 (2009) 671-676.

[6]   Di. Serio, M. Tesser, R. Dimiccoli, M. Cammarota, *Ind. Eng. Chem. Res.,* 45 (2006) 3009-3014.

[7]   W.L. Bragg, *Proceedings of the Cambridge Philosophical Society*, 17 (1913), 43–57.

[8]   [http://tap.iop.org/atoms/xray/530/page_47297.html], [cited 11/04/2011].

[9]   K.S.W. Sing, D.H. Everett, R.A.W. Haul, L. Moscou, *Pure Appl. Chem.*, 57 (1985) 603-619.

[10]   I. Langmuir, *J. Am. Chem. Soc.*, 40 (1918) 1361-1403.

[11]   S. Brunauer, P. H. Emmett, E. Teller, *J. Am. Chem. Soc.,* 60 (1938) 309-319.

[12]   E. P. Barrett, L. G. Joyner, P. P. Halenda, *J. Am. Chem. Soc.*, 73 (1951) 373-380.

[13]   A. Auroux, J. C. Vedrine, P. C. Gravelle, J. Rouquerol, K. S. W. Sing, *Stud. Surf. Sci. Catal.*, Elsevier, (1982) 305-322.

[14]   R. A. Sheldon, I. W. C. E, Arends, U. Henefeld, *Introduction: Green Chemistry and Catalysis*, Wiley-VCH Verlag GmbH & Co. KGaA, (2007).

[15]   S. P. Felix, C. Savill-Jowitt, D. R. Brown, *Thermochim. Acta.*, 433 (2005) 59-65.

[16]   L. Dussault, J. C. Dupin, E. Dumitriu, A. Auroux, C. Guimon, *Thermochim. Acta.*, 434 (2005) 93-99.

[17]   [http://www.purdue.edu/rem/rs/sem.htm], [cited 11/04/2011].

[18]   A. Harrison, R. Ibberson, G. Robb, G. Whittaker, C. Wilson, D. Youngson, *Faraday Discuss.,* 122 (2002) 363-399.

[19]   D. R.Baghurst, R. C. B. Copley, H. Fleischer, D. M. P. Mingos, G. O. Kyd, L. J. Yellowlees, A. J Welch, T. R Spalding, D. O'Connell, *J. Organomet. Chem.*, 447 (1993) C14-C17.

[20]   E.A Fesenko,.P. A Barnes, G. M. B. Parkes, O.T. Sorensen, J. Rouquerol, Sample Controlled Thermal Analysis. Hot Topics in Thermal Analysis and Calorimetry, 3; Springer: New York, U.S.A., (2004) 174-225.

[21]   M. P. Hart, D.R. Brown, *J. Mol. Catal. A Chem.*, 212 (2004). 315-322.

[22]   H. E. Cross, G. Parkes, D. R. Brown, *Appl. Catal. A-Gen.*, 429-430 (2012) 24-30.

[23]   H. M. Williams, G. M. B. Parkes, *Carbon.,* 46 (2008) 1169-1172.

[24]   G. M. B. Parkes, P. A. Barnes, G. Bond, E. L. Charsley, *Thermochimica Acta.,* 356 (2000) 85-96.

Chapter 3

Hydrotalcite and Mixed Metal Oxides: Synthesis, Calcination and Characterisation

Chapter 3

3.1 – Objectives

The objectives of the work reported here are:

1. to investigate methods of synthesis of layered mixed (double) hydroxides (LDHs) and identify the most suitable methods for preparing these materials for catalytic application,
2. to investigate the extent to which sodium salts can become entrained in mixed metal oxides prepared from LDHs using sodium hydroxide/sodium carbonate in the synthesis, to assess the impact on catalytic activity, and to modify the synthesis method to prevent the problem,
3. to investigate the effect of using microwave rather than conventional heating for the calcination of layered mixed (double) hydroxides on the properties of the mixed metal oxide catalysts formed, and to compare these with the properties of equivalent materials produced using conventional calcination techniques.

To achieve these objectives, the work reported here is based entirely on the layered double hydroxide $Mg_6Al_2(CO_3)(OH)_{16}.4H_2O$, in other words hydrotalcite, with the intention of applying the results to other materials, the preparation of which is reported in subsequent chapters.

3.2 – Introduction

3.2.1 – Hydrotalcite Synthesis

There are three most commonly used methods for the synthesis of hydrotalcite. All three involve starting with a solution of the two metals as nitrates and precipitating the mixed metal hydroxides by raising the pH. In the first method, the pH is controlled by the addition of NaOH solution to the nitrate solution, together with Na_2CO_3 which provides the exchangeable anion to occupy the hydrotalcite interlayer. This method has the advantage over others of being very simple and uses

inexpensive reagents. Its disadvantages are that the pH control is relatively difficult and there is a recognised danger that sodium salts can become entrained in the product and also the mixed metal oxide(s) formed on calcination [1]. This aspect and the consequence of entrained sodium salts are studied in some detail in this work and the results and conclusions are described later in this chapter.

The second method involves aqueous ammonia (NH_4OH) as a pH control agent in place of aqueous NaOH, and $(NH_4)_2CO_3$ in place of Na_2CO_3. The third method relies on the progressive hydrolysis of urea in-situ to gradually raise the pH and precipitate the hydrotalcite. Na_2CO_3 is not used in the last method because carbonate ions are formed in the hydrolysis reaction. The different levels of pH control from these methods are expected to give rise to different properties in the hydrotalcite. Othman *et al* reviewed methods of synthesis and related them to catalyst and adsorbent properties [2]. Workers have noted that the pH for the precipitation of metal ions should be that where the two metal hydroxide precipitation curves overlap [3]. Variations in precipitation pH in the initial LDH synthesis lead to different properties of the oxides formed after calcination [4]. Most hydroxides precipitate in the pH range 8-10 and it is generally accepted as the optimum range of pH to use for incorporation of both metal ions into the LDH structure. Outside this range, the compositions of products vary.

The third method uses urea. It is easy to use with solutions of metal salts, and the rate at which the hydroxides precipitate can be controlled using temperature control. The carbonate anion produced during the reaction also is of benefit. The hydrolysis reaction occurs at a suitable rate (typically overnight) when the temperature is raised to 90 °C. There are two reaction steps with ammonium cyanate formed initially which is then hydrolysed to ammonium carbonate, (Equation 3.1) [5]. Urea hydrolysis can be used for the precipitation of most metal salts in the range of pH 8-9 which makes it suitable for the formation of many LDHs, not only hydrotalcite.

$$CO(NH_2)_2 \rightarrow NH_4CNO$$
$$NH_4CNO + 2H_2O \rightarrow 2NH_4^+ + CO_3^{2-}$$
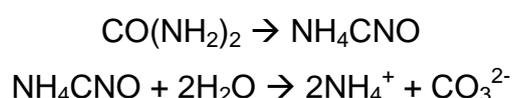
Equation 3.5

In addition to varying the reagents used, incorporating a precipitate ageing step involving several hours heating the aqueous suspension of the precipitate is reported to improve crystallinity, decrease particle size and increase the surface area [6]. This ageing aspect in the preparation of LDHs is studied in this chapter.

3.2.2 – Entrained Sodium in LDHs

The most straightforward and least expensive method for precipitating the hydroxide uses NaOH (and Na_2CO_3) but there is a possibility of sodium ions or sodium salts becoming entrained in the LDH [1,7]. Fraile et al has pointed out that control of alkali metal ions in hydrotalcite production is crucial if reproducible materials are to be synthesised [7]. They identified the presence of "leachable basicity" in LDHs containing high levels of residual alkali metal ions. Davis and co-workers have also shown that sodium can become entrained in magnesium/zirconium hydroxides at up to 3.4 % w/w unless washing of the product is extensive, and that this entrained sodium, while generally undesirable because of the risk of leaching, seems to boost the catalytic activity massively in base-catalysed transesterification reactions [8].

The precipitation of metal hydroxides to form an LDH by the three methods outlined above all involve the incorporation of carbonate as the exchangeable anion. LDHs prepared with other anions such as nitrate (when the synthesis step does not provide carbonate) tend to quickly convert to the carbonate from exposure to air but the incorporation of carbonate at the synthesis step ensures that there is no uncertainty over the nature of the exchangeable anion.

3.2.3 – LDH Calcination

LDHs are calcined to produce mixed metal oxides and it is the formation of these mixed metal oxides that is studied in this chapter using conventional heating and microwave heating. The method using $NaOH/Na_2CO_3$ was chosen for this calcination study because it is the most common form of synthesis used to generate catalytically active species.

Conventional calcination of LDHs and the mechanism(s) by which the LDH is converted to the oxide have been widely studied [9-11] but there are few reported studies of the use of microwaves in this process, and those reports that do exist do not involve any precise control of microwave power [12]. It is reasonable to expect that calcination of the hydroxides to form oxides under microwave heating would produce different properties in the oxide products compared to conventional calcination in a furnace.   The mechanism of microwave heating is different to conventional heating and microwaves usually heat solids in a more uniform way, heating throughout the bulk and not just from the surface, with associated temperature gradients [13].

As discussed earlier in Chapter 2, microwave heating is not always easy to control when used to induce solid state transformations because, in general, the products of reaction couple with microwaves in a different way to the reactants, meaning that the products of the transformation heat at a different rate to the reactants.   This inevitably leads to unpredictable temperature excursions. This can be overcome by applying the so-called "controlled rate" algorithms to microwave heating.   This approach to controlling microwave calcination is described later.

3.3 – LDH Synthesis and Entrained Sodium

3.3.1 – Experimental

All LDH materials were synthesised, unless stated, using a 3:1 $Mg^{2+}:Al^{3+}$ molar ratio. Hydrotalcite layered double hydroxide, $Mg_6Al_2(CO_3)(OH)_{16}.4H_2O$ was prepared by slowly adding simultaneously a solution of 250 ml magnesium and aluminium nitrates (99.9 % Aldrich) in a 3:1 molar ratio (total 1.0 mol dm^{-3}) and a 250 ml sodium carbonate solution (0.625 mol dm^{-3}) (99.9 % Aldrich) to a 1000 ml beaker, stirring rapidly as the mixture was formed. The pH of the solution was maintained at 7.6-8.0 by adding sodium hydroxide solution (0.20 mol dm^{-3}) (99.9 % Aldrich), under vigorous stirring. Once addition was complete and the pH was stabilised, it was filtered and the precipitate washed. The precipitate was dried at 100 °C overnight.

The level of washing was varied. The first samples were washed with deionised water at room temperature until the filtrate pH dropped below 7.6, which typically required 500 ml. The second set of samples was washed again with an additional 500 ml of deionised water to reach pH 7.0. Finally, the third set of samples was washed additionally with 500 ml deionised water which had been heated to 60 ^{o}C.

The same hydrotalcite compound was prepared using progressively hydrolysed urea (99.9 % Aldrich) as a precipitating agent [14]. Urea solution (250 ml, 0.047 mol dm^{-3}) was added to the 250 ml mixed metal nitrate solution and held at 90 °C overnight. The suspension was left to cool, and filtered. The precipitate was washed with deionised water at room temperature until the filtrate pH fell to 7.0. The precipitate was dried at 100 °C overnight.

A third synthetic method was used, in which a concentrated ammonia solution (34 % w/w) was used as the precipitating agent [15], by slowly adding simultaneously 250 ml of a solution of magnesium and aluminium nitrates (molar ratio Mg/Al 3:1) and 250 ml $(NH_4)_2CO_3$ (0.2 mol dm^{-3}) to a 1000 ml beaker, under vigorous stirring. The pH of the slurry was adjusted to 7.6–8.0 by the drop-wise addition of the ammonia solution. The slurry was stirred vigorously and then filtered and washed with deionised water to pH 7.0**.** For this first part of the study all LDHs were calcined in a muffle furnace to 500 °C raising the temperature at a rate of 2 °C min^{-1}. This temperature was held for four hours in static air to produce the mixed metal oxides.

Aluminium and magnesium analyses of oxides were obtained using SEM-EDS and sodium contents of the oxides were determined by atomic absorption spectroscopy (AAS) following digestion in concentrated nitric acid. Nitrogen adsorption/desorption isotherms were generated for all samples at -196 ^{o}C after degassing at 150 ^{o}C. Surface areas (adsorption isotherms, BET), pore volumes and size distributions (desorption isotherms, BJH) were determined.

Catalytic activities were measured in the transesterification reaction of tributyrin with methanol, monitoring the conversion of tributyrin, as described in Chapter 2 (page 60). In each reaction, the effect on the rate of reaction of removing the catalyst after

one hour was examined, as a test for possible leaching of catalytically active material into solution. The stirring rate was set to ensure that the reaction rate was not under diffusion control.

The effect of ageing the metal nitrates solution during synthesis was investigated. Hydrotalcite was synthesised using the NaOH/Na$_2$CO$_3$ precipitation method, after which the mixture was left stirring at 150 rpm for 30 minutes. After this point, the mixture was split into three. One sample was left under vigorous stirring and heated to 65 °C for three hours. The second was left under vigorous stirring at room temperature. Both samples were then filtered under gravity. The third sample was filtered under gravity immediately without ageing. All three samples were washed three times after filtering with two aliquots of 500 ml cold deionised water and one of 500 ml of deionised water heated to 60 °C. The hydrotalcites synthesised were not calcined.

Powder X-ray diffraction (p-XRD) patterns were recorded for the hydrotalcite and the calcined hydrotalcite using Cu K$_\alpha$ radiation, minimising the exposure of the calcined products to air to reduce the chances of rehydration to the hydroxides.

Surface basicities of the calcined products were determined by CO$_2$ adsorption calorimetry under flow conditions, as described in detailed in Chapter 2 (section 2.13.1).

3.3.2 – Results and discussion

3.3.2.1 – Powder X-ray Diffraction

The assignments of reflections are given for a typical hydrotalcite p-XRD pattern in Figure 3.1. The LDH used for this experiment was prepared using the urea hydrolysis method. Similar patterns were seen for LDHs prepared using other methods but peaks were not as well defined.
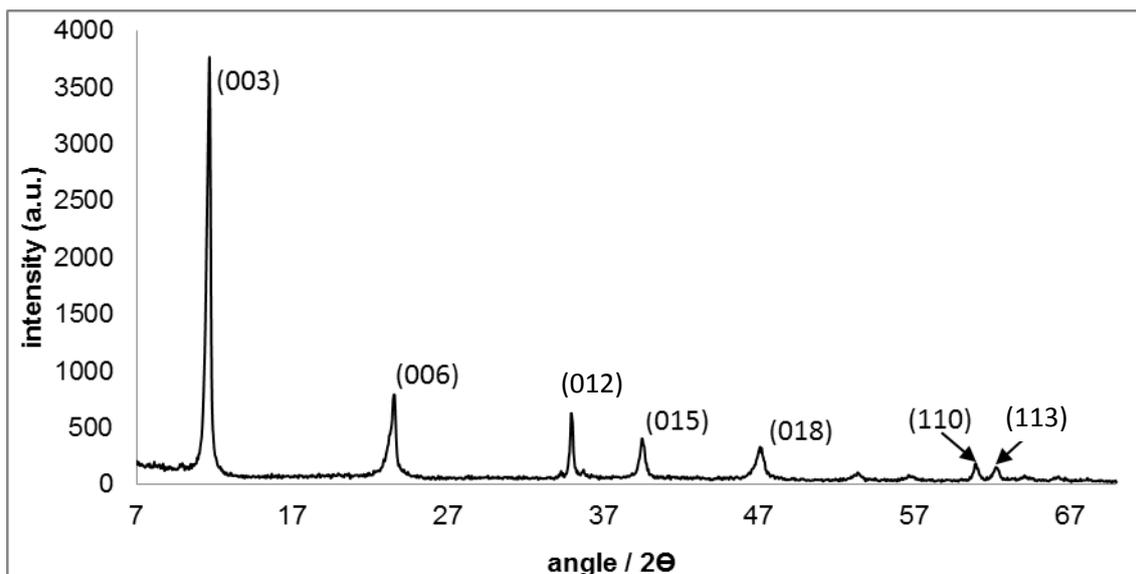
Figure 3.1 – Powder X-ray diffraction pattern typical of hydrotalcite synthesised using the urea hydrolysis method.

The p-XRD pattern for the LDH prepared using sodium hydroxide (two 500 ml cold deionised water wash) is shown in Figure 3.2. Diffraction patterns for other LDHs prepared using sodium hydroxide showed the same reflections and exhibited similar line widths.

The only difference between the diffraction pattern shown in Figure 3.2 and those of the same LDHs after prolonged washing is the presence of a sharp but weak reflection at 29.5 $^{\circ}$. This is not seen for samples washed more thoroughly. This reflection has been seen in diffraction patterns for LDHs prepared using NaOH at various intensities by others, notably Tichit *et al*, and has been assigned to sodium nitrate [18]**.** These workers recognised that it is difficult to wash out the sodium nitrate from the LDHs and suggested that it might be occluded in the crystal structure. Our results support this view.
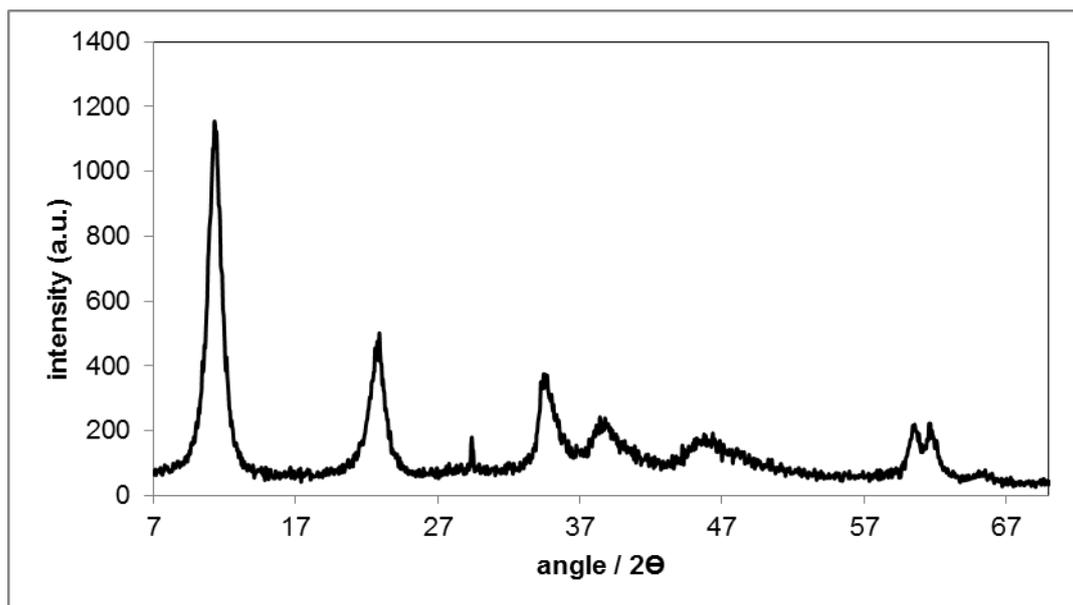
Figure 3.2 – $Mg_6Al_2(CO_3)(OH)_{16}.4H_2O$ – following the first washing with deionised water to pH 7.0-7.5. Synthesised using the $Na_2CO_3/NaOH$ method.

The crystallite size for each LDH sample was calculated from the 110 reflection using the Scherrer equation (Table 3.1) based on the width of the peak at half height. For the three preparative methods, the crystallite size differs quite significantly, with urea and ammonia methods seeming to produce the largest crystallites. For the urea method of precipitation, this could be due to the finely controlled pH and the very gradual precipitation rate. There is a decrease in crystallite size when samples made using the $NaOH/Na_2CO_3$ preparative method are progressively washed with hot deionised water.

Documented for each LDH synthesised, in Table 3.1, are values for d_{003} which is equal to the unit cell dimension 'c'. This dimension is calculated from the 2θ value for the third order, 003, reflection. This distance includes the interlayer spacing. It is sensitive to interactions between the anions in the interlayer and between these anions and the lattice. It is also dependant on the level of hydration of the material and small differences in 'c' between samples are not necessarily significant in terms of the LDH structure.

Preparation	a (Á) 2d$_{(110)}$	c (Á) 3d$_{(003)}$	^{a}L$_{110}$ (Á)
NaOH **1st washing — room temperature washed to below pH 7.6 with 500 ml cold deionised water**	3.06	23.61	111
NaOH **2 x 500 ml cold deionised water and 500 ml 60 °C deionised water**	3.04	23.27	44
NH$_3$ **washed to pH 7.0–7.5**	3.04	23.58	248
(NH$_2$)$_2$CO **washed to pH 7.0–7.5**	3.03	22.71	241

Table 3.1 – Powder X-ray diffraction data for $Mg_6Al_2(CO_3)(OH)_{16}.4H_2O$ synthesised by three different preparative methods.

^{a}Calculated using the Scherrer Equation.

In addition, d_{110} values are also shown and this spacing is related to the unit cell dimension 'a', with 'a' being $2d_{110}$. The value of 'a' is dependent on the metal ions in the LDH lattice [19]. Valente *et al* incorporated transition metals, such as copper, nickel and zinc, into the hydrotalcite structure. In general it was seen that the 'a' value, measured by p-XRD, changed in line with the ionic radius of the transition metal incorporated into the lattice.

Small variations in "c" between LDHs prepared by the three methods are not unexpected and are not significant. The fact that "c" for LDHs prepared by the three methods are very similar suggests that the elemental compositions are essentially the same. Data shows that ammonia and urea methods produce the largest crystallites, not surprising for urea which is known to hydrolyse relatively slowly, but less easy to explain in the case of ammonia, except in as much as it is a weak base and therefore might give more progressive pH control than NaOH. The NaOH method produces the smallest crystallites, as expected. It is surprising that washing decreases crystallite size. Conceivably, this is due to attrition and breaking up of the crystallites as suspensions are stirred.

3.3.2.2 – Elemental Analysis

SEM-EDS was used to calculate the molar ratios of the metallic elements in the lattices of the LDHs (Table 3.2.). This is a surface, or close-to-surface technique, but it is useful to look at the elemental concentration at the surface since it is the metal cations located on the surface that would be expected to play a substantial role in the catalytic activity. And in any case there is no obvious reason why the composition near the surface would be substantially different to the composition in the bulk. However, the SEM-EDS results described below show more variation in the Mg:Al ratio than was expected and it is certainly possible that there is, in all cases, some variation in the Mg:Al ratio throughout the crystals.

Elemental analysis data for the mixed metal oxides in Table 3.2 show significant sodium levels in materials derived from LDHs that were not washed extensively, up to 2 % w/w in the material which was washed with only 500 ml deionised water. This

corresponds to approximately 1 mmol g^{-1} of sodium based on the oxides. If this sodium is in the form of sodium nitrate (before calcination), as suggested earlier, then our results support those of Tichit *et al* [18] in observing a remarkable resistance to dissolution of the salt as the LDH is washed. A question concerns the form taken by the sodium ions in the calcined materials in which clearly the nitrate salt can no longer exist.

Table 3.2 shows that the Mg:Al ratio in the LDHs prepared and washed in different ways varies significantly. Extensive washing evidently reduces the Mg content. A possible explanation, as suggested above, is that Mg and Al are not evenly distributed through the crystallites and extensive washing exposes part of the crystallite that was originally in the bulk of the crystallite. This could be due to some of the metal nitrates not precipitating into hydroxides and therefore washed out during this extensive washing process. This result could be because of the ageing step being omitted, due to limiting the amount of sodium entrained in the LDH. This is very speculative however and the observed variations are surprising.

Preparation	[a]Mg:Al molar ratio	[b]Na / % w/w
NaOH 1st washing — room temperature deionised water to below pH 7.6	3.5 (± 0.5)	2.10 (± 0.05)
NaOH 2nd washing — additional 500 ml deionised water (pH ca. 7.0)	1.4 (± 0.5)	0.58 (± 0.05)
NaOH 3rd washing — additional 500 ml 60 °C deionised water (pH below 7.0)	1.5 (± 0.5)	0.042 (± 0.05)
NH$_3$ washed to pH 7.0–7.5	1.8 (± 0.5)	-
(NH$_2$)$_2$CO washed to pH 7.0–7.5	2.5 (± 0.5)	-

Table 3.2 – Elemental data for samples of $Mg_6Al_2(CO_3)(OH)_{16}.4H_2O$. [a]SEM-EDS measurements. [b]AAS measurements.

3.3.2.3 – Morphology and Surfaces

SEM micrographs are shown in Figure 3.3 of hydrotalcite prepared using the three preparative methods, including samples of $NaOH/Na_2CO_3$ prepared hydrotalcite subjected to the first and the final washing. It can be seen that the $NaOH/Na_2CO_3$ prepared samples differ considerably after the third washing compared to the first. Hydrotalcite prepared using ammonia can be seen to be similar to that after the third, hot water washing of $NaOH/Na_2CO_3$ prepared samples. The hydrotalcite prepared using urea as a precipitating agent shows a very different texture. It is difficult to draw firm conclusions from these images except in so far as they confirm that significant differences in morphology are associated with different methods of preparation.
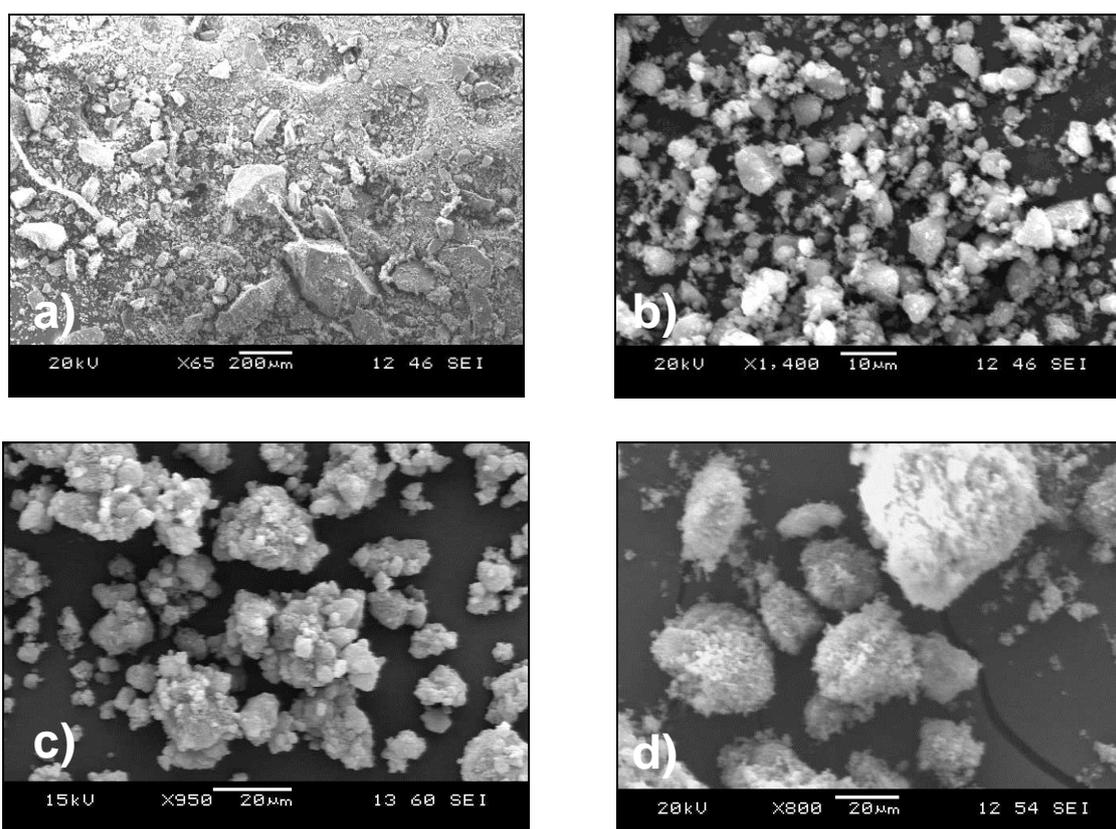
Figure 3.3 – SEM micrographs of $Mg_6Al_2(CO_3)(OH)_{16}.4H_2O$ a) prepared using NaOH and washed once, b) prepared using NaOH and washed three times c) prepared using NH_3 and d) prepared using $(NH_2)_2CO$.

Surface areas and pore volumes for mixed oxides derived from LDHs prepared by the various routes are shown in Table 3.3, and are in general fairly typical for mixed metal oxide materials derived from LDHs [15]. It is interesting to note that the surface area of the mixed metal oxides prepared using urea, while not exceptional, is significantly greater than those of the oxides generated from LDHs prepared using the other routes. This is surprising in view of the larger crystallite sizes for the precursor material, as identified from the p-XRD patterns. The pore volume is broadly similar for all synthetic routes.

The sodium levels in each of the oxides are also shown. Catalytic activities are also presented in Table 3.3, expressed as the % conversions of tributyrin after 20 minutes reaction time. The most significant aspect of the relative catalytic activities is that there is a broad correlation between the activity of the catalyst and the sodium content. It is not certain whether the activity enhancement associated with entrained sodium is due to additional heterogeneous catalysis at the surface of the solid or whether the entrained sodium can leach into the reaction medium so that homogeneous catalysis occurs. The magnitude of the enhancement suggests that it is most likely due to the latter. If so, it is an undesired feature of the transesterification catalyst because contamination of biodiesel with sodium is unacceptable if the fuel is to be used in combustion engines.

Preparation	Surface area / m^2 g^{-1}	Pore volume / cm^3 g^{-1}	Na content / % w/w	Catalytic activity in transesterification of tributyrin / % conversion at 20 minutes
NaOH 1st washing — room temperature deionised water to below pH 7.6	60	0.23	2.10 (±0.05)	94
NaOH 2nd washing — additional 500 ml deionised water (pH ca. 7.0)	79	0.22	0.58 (±0.05)	15
NaOH 3rd washing — additional 500 ml 60 °C deionised water (pH below 7.0)	110	0.21	0.042 (±0.05)	4
NH_3 washed to pH 7.0–7.5	85	0.21	0.00	6
$(NH_2)_2CO$ washed to pH 7.0–7.5	170	0.18	0.00	15

Table 3.3 – Characterisation data for mixed metal oxides formed from the conventional calcination of $Mg_6Al_2(CO_3)(OH)_{16}.4H_2O$ (calcined, 500 °C four hours).

The nitrogen adsorption isotherms are shown for calcined products obtained from LDHs prepared by all three methods in Figures 3.4, 3.5 and 3.6.   The three isotherms differ significantly.   Figure 3.4 displays the adsorption isotherm for the mixed metal oxides obtained from the calcination of hydrotalcite prepared using $NaOH/Na_2CO_3$. The isotherm shows an H2 hysteresis loop, inferring that the pores are heterogeneous in distribution and/or size meaning that there is likely to be a broad pore size distribution [20]. Figure 3.5 displays the adsorption isotherm for the mixed metal oxides obtained from the calcination of the hydrotalcite prepared using urea hydrolysis and this isotherm shows an H4 hysteresis loop, and a much narrower pore size distribution, as explained in the more detail in the experimental section. Figure 3.6 is the adsorption isotherm for the mixed metal oxides obtained from the calcination of hydrotalcite prepared using ammonia and it can be seen that the isotherm shape is indicative of larger pores, displaying an H3 hysteresis loop. It is not clear why the three synthesis routes lead to such different pore structures.
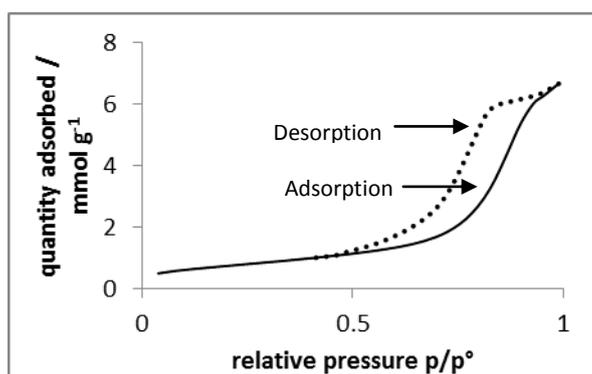
Figure 3.4 – Nitrogen adsorption isotherm for $Mg_6Al_2(CO_3)(OH)_{16}.4H_2O$ prepared using $NaOH/Na_2CO_3$ and washed to pH 7.0, calcined for four hours at 500 °C.
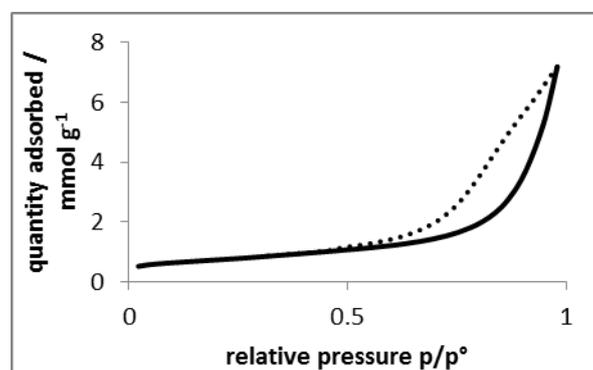
Figure 3.5 – Nitrogen adsorption isotherm for $Mg_6Al_2(CO_3)(OH)_{16}.4H_2O$ prepared using NH_3 and washed to pH 7.0, calcined for four hours at 500 °C.
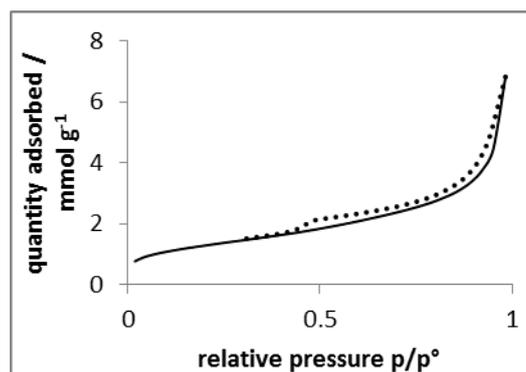
Figure 3.6 – Nitrogen adsorption isotherm for $Mg_6Al_2(CO_3)(OH)_{16}.4H_2O$ prepared using urea hydrolysis and washed to pH 7.0, calcined for four hours at 500 °C.

3.3.2.4 – CO$_2$ Adsorption Calorimetry

CO_2 adsorption calorimetric data is shown in Figures 3.7 and 3.8. Figure 3.7 shows a comparison between the CO_2 molar enthalpy of adsorption vs. coverage profile for calcined LDHs prepared using sodium hydroxide, subject to two successive cold deionised water washings and that for an LDH washed with deionised water at 60 °C. Equivalent plots for calcined LDHs prepared using urea and the ammonia methods are shown in Figure 3.8.

From the data in Figure 3.7 we can see that the three samples show significant differences in their basicities. Data shown in Figure 3.7 suggests that the strength of the sites for mixed metal oxide formed from the calcined hydrotalcite washed once with 500 ml of cold deionised water is significantly higher than for the other two washed samples. The coverage is also much greater, suggesting that there are more basic sites existing in this sample (based on the assumption that significantly basic sites adsorb CO_2 with an enthalpy of adsorption of at least 90 kJ mol^{-1} [21]). As the sample is progressively washed, the coverage or concentration of basic sites progressively falls. And the strongest basic sites (those populated by the first pulses of CO_2) seen for the sample washed only once with molar enthalpy of adsorption over 135 kJ mol^{-1} are not present in the two catalysts washed more than this.
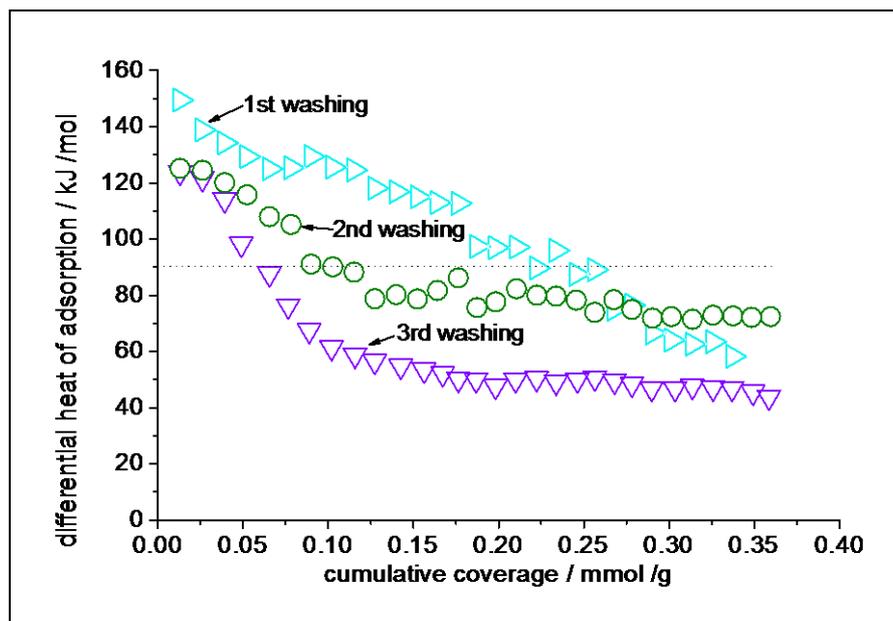
Figure 3.7 – Differential molar enthalpy of CO_2 adsorption
against amount of CO_2 adsorbed for calcined $Mg_6Al_2(CO_3)(OH)_{16}.4H_2O$ prepared
using NaOH washed to pH 7.0-7.5 (1st washing), washed with an additional 500 ml
cold water (2nd washing), and washed with 500 ml 60 °C water (3rd washing).

Figure 3.8 shows the differential heat of adsorption of CO_2 vs. coverage data for the
two mixed metal oxide samples formed from hydrotalcite prepared using ammonia
and urea hydrolysis.   The results show that these oxides exhibit similar or lower
initial heats of adsorption to the hydrotalcite washed two and three times in Figure
3.7.   There appear to be many more sites with adsorption enthalpies in the 70-90 kJ
mol^{-1} range on these materials than on those made using NaOH (and thoroughly
washed with hot water) but these sites are only marginally basic and, given the
experimental error in this data, it is difficult to conclude that they differ in basicity
from the catalysts prepared using NaOH.

Nevertheless, it does appear that the concentration of surface basic sites, even if
only marginally basic, is lower on catalysts prepared using NaOH and thoroughly
washed with hot, water, than on those prepared using urea or ammonia.   The fact
that hot water washing seems to reduce both the abundance and the strength of
surface base sites is surprising.   It is possible that the hot water wash acts a little like
an ageing step and that, after this process, the number of surface defects sites,

which might be responsible for the relatively weak base sites that are most affected, is reduced.
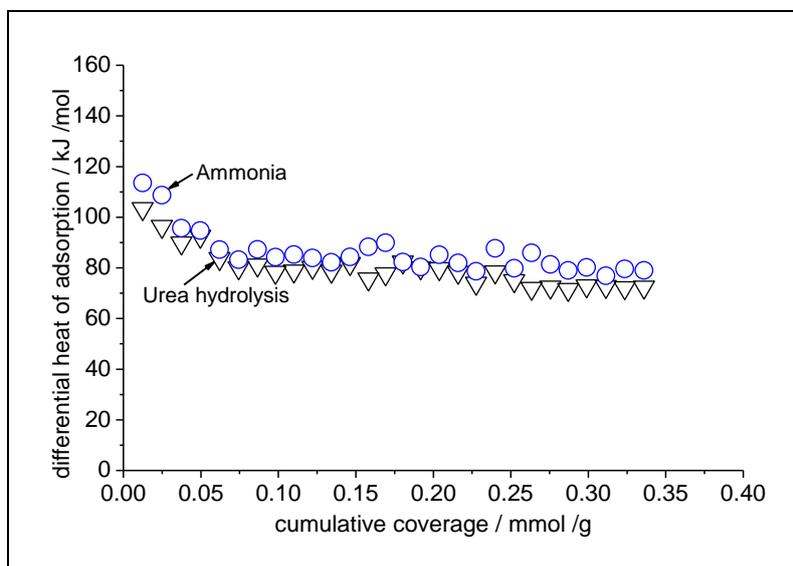
Figure 3.8 – Differential molar enthalpy of CO_2 adsorption against amount of CO_2 adsorbed for calcined $Mg_6Al_2(CO_3)(OH)_{16}.4H_2O$ prepared using the ammonia and the urea methods.

3.3.2.5 – Effect of ageing

Figure 3.9 shows an XRD pattern of hydrotalcite synthesised using $NaOH/Na_2CO_3$ with an additional step of vigorous stirring and heating of the hydrotalcite suspension at 65 °C for three hours at room temperature. Figure 3.10 is an XRD pattern of hydrotalcite following vigorous stirring at room temperature for three hours. Figure 3.11 is an XRD diffraction pattern of hydrotalcite with no ageing step.

The first thing to note is that line widths are not significantly affected by ageing. The double feature at 60.5 ° is possibly slightly better resolved for the most extensively aged precipitate than for the others but only marginally. The overall conclusion drawn in this work is that ageing has a negligible effect on crystallinity. It has not been employed in the rest of the work reported in this thesis.

It is interesting to note that the XRD pattern for the hydrotalcite that has been aged by heating has reflections (highlighted) denoting sodium nitrate in the sample. This is not seen in the XRD pattern for the precipitates that were not heated. It is difficult to explain this.   Evidently the re-dissolving, re-precipitating processes that occur during ageing somehow promote the incorporation of sodium nitrate in the crystalline precipitate.
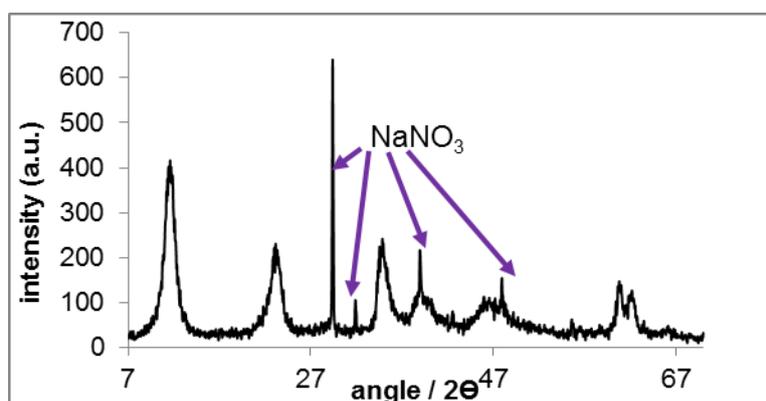
Figure 3.9 – Powder XRD pattern for $Mg_6Al_2(CO_3)(OH)_{16}.4H_2O$. Precipitation mixture was vigorously mixed and heated to 65 °C for three hours.
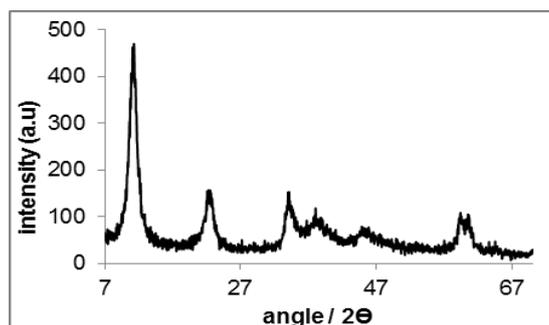
Figure 3.10 – Powder XRD pattern for $Mg_6Al_2(CO_3)(OH)_{16}.4H_2O$. Precipitation mixture was vigorously mixed for three hours.
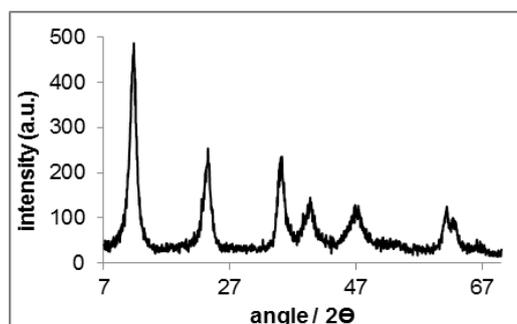
Figure 3.11 – Powder XRD pattern for $Mg_6Al_2(CO_3)(OH)_{16}.4H_2O$. Precipitation mixture was filtered under gravity immediately without ageing.

3.3.3 – Conclusions

3.3.3.1 – Sodium Entrainment

1. Using NaOH for pH control in hydrotalcite synthesis leads to entrainment of $NaNO_3$ in the LDH. Reasonable washing can still leave up to 2.0 % w/w sodium in the products of calcination. To avoid this, extensive washing at elevated temperature needs to be applied.

2. Ageing at high temperatures in LDH synthesis appears to promote sodium entrainment.

3. Entrained sodium increases the concentration and strength of basic sites of the products, and enhances basic catalytic activity.

4. It seems possible that sodium can leach into a reaction mixture and act as a homogeneous catalyst, although this has not been verified.

3.3.3.2 – Synthetic Methods

1. Of the three methods investigated, that based on $NaOH/Na_2CO_3$ as the precipitating agent is the simplest, but reproducible pH control can be difficult and entrainment of sodium as the nitrate and possibly other forms is a significant problem.

2. Ageing of the LDH suspension at elevated temperatures is not beneficial in terms of crystallinity.

3. Using ammonia avoids the risk of sodium entrainment. The crystallinity of products formed are similar to those of the products formed when using $NaOH/Na_2CO_3$. The pH is difficult to control uniformly using ammonia.

4. The urea method yields material with larger crystallites but similar surface areas for the resultant mixed oxides. In the transesterification reaction of tributyrin there seems to be no catalytic advantage to having highly crystalline LDH precursors. An advantage of using urea is that pH control during precipitation is essentially automatic. A disadvantage is that it is difficult to

achieve pH greater than 9.0 which might be needed when incorporating some metals in the LDH.

3.4 – Calcination of $Mg_6Al_2(CO_3)(OH)_{16}$ using Conventional and Microwave Heating

3.4.1 – Introduction

Mixed metal oxides are formed when hydrotalcite is calcined at temperatures above 400 °C. Two methods have been used to achieve this, microwave controlled heating and conventional heating. The mixed metal oxides formed using microwaves and also conventional heating are characterised in terms of physical and chemical properties.

Over the past decade there have been many papers reporting work on LDHs synthesised using the $NaOH/Na_2CO_3$ precipitation method [22-28]. It is because LDHs prepared this way have been so well characterised that it is this approach that has been used to prepare materials for the calcination study in this thesis.

The objective here has been to evaluate differences in calcination products generated through microwave calcination and conventional calcination. The unique aspect of this work is that microwave heating has been carried out under feedback control to ensure continuous temperature control as solid state transformations occur.

There has been extensive research in the understanding of the hydrotalcite calcination process under conventional heating. Frost *et al* have shown that hydrotalcite undergoes dehydration up to roughly 225 °C, after which at 300 °C dehydroxylation and decarbonisation begin. When 400 °C is reached, all hydroxyl and most carbonate interlayer groups have been decomposed and metal oxides dominate. At temperatures above 600 °C, spinel is formed, $MgAl_2O_4$.

Very little research into the use of microwaves for the calcination of LDHs has been published, largely, as far as we can see, because of difficulties in temperature control [10,11]. In contrast, it is worth mentioning that there has been a substantial amount of research on the use of microwaves for the ageing process applied to the LDH precipitate in aqueous suspension with the objective to improve crystallinity [28-31].

3.4.2 – Experimental

Hydrotalcite for the calcination study here was synthesised using aluminium and magnesium nitrates, and Na_2CO_3 with NaOH to control the pH. The hydroxides were prepared by slowly adding simultaneously a 250 ml solution of the metal nitrates (1.0 mol dm^{-3}) and a 250 ml sodium carbonate solution (0.625 mol dm^{-3}) to a 1000 ml beaker, stirring rapidly as the mixture was formed. The pH of the solution was maintained at 8-10 by adding sodium hydroxide solution (0.20 mol dm^{-3}), under vigorous stirring. The resulting mixture was filtered and the precipitate washed thoroughly as described previously. The precipitate was dried overnight at 100 ºC. Several samples of the powder were taken for calcination studies. Conventional calcination was performed in a muffle furnace, and temperatures from 500 ºC up to 1000 ºC were studied. Microwave heating was applied at 500 ºC. Using the feedback-control apparatus described in 2.16. Both methods involved heating rates of 2 ºC min^{-1} with the final temperature held for four hours.

3.4.3 – Results

The powder XRD pattern for the parent hydrotalcite is shown in Figure 3.12. The p-XRD patterns for conventionally heated hydrotalcite heated from 500 ℃ to 1000 ℃ are shown in Figure 3.13. Under conventional heating, the LDH pattern is lost at 500 ℃. Reflections due to MgO are detected at 500 ℃. Reflections become sharper as the calcination temperature is increase, indicative of sintering during the

formation of MgO crystallites increasing in size. At 900 ℃ reflections assigned to spinel $MgAl_2O_4$ appear.
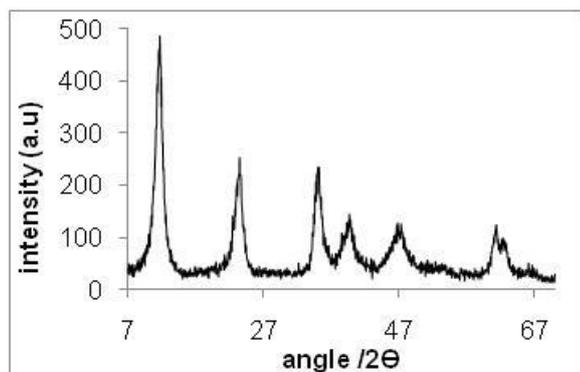
Figure 3.12 – Powder X-ray diffraction pattern of $Mg_6Al_2(CO_3)(OH)_{16}.4H_2O$ synthesised using $NaOH/Na_2CO_3$.
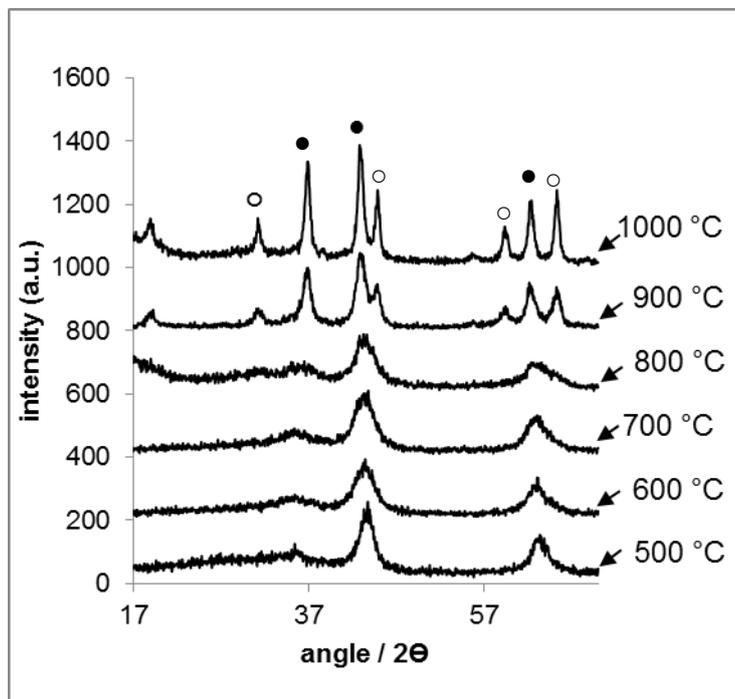
Figure 3.13 – Powder X-ray diffraction patterns of $Mg_6Al_2(CO_3)(OH)_{16}.4H_2O$, 500 °C to 1000 °C (●=MgO, ○=$MgAl_2O_4$)

Feedback-controlled (to maintain a linear temperature increase) microwave heating was performed on hydrotalcite up to 500 °C (restricted to this maximum by instrumental factors but for some samples this temperature could be exceeded using microwave heating).   This temperature was held for four hours.   In order to conmppare the effect of the two types of heating, the diffraction pattern for the LDH calcined under conventional heating at 500 °C for four hours is shown again in Figure 3.14, with the XRD pattern for the equivalent material calcined under microwave heating in Figure 3.15.   Both show poorly crystalline MgO and the diffraction patterns are, in general, very similar. However, the material calcined using microwaves possibly exhibits slightly sharper reflection for MgO at 36 °.
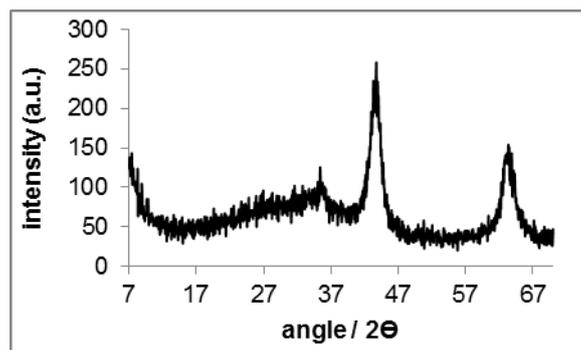
Figure 3.14 – Powder X-ray diffraction pattern of $Mg_6Al_2(CO_3)(OH)_{16}.4H_2O$, heated conventionally to 500 °C.
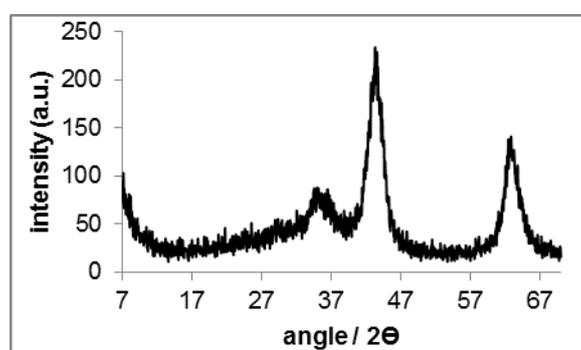
Figure 3.15 – Powder X-ray diffraction pattern of $Mg_6Al_2(CO_3)(OH)_{16}.4H_2O$, heated with microwaves to 500 °C.

The plots of differential enthalpy of CO_2 adsorption against the amount of CO_2 adsorbed for calcined hydrotalcite using conventional heating at 500 °C and microwave heating at 500 °C are shown in Figures 3.16 and 3.17 respectively. It is possible to quantify this data as follows. The concentration of basic sites on the catalyst is assumed to be equal to the concentration of CO_2 that adsorbs with molar enthalpy greater than 90 kJ mol^{-1}. An indication of average base site strength is given by the average of the enthalpies recorded on these plots that lie above 90 kJ mol^{-1}. In the case of conventionally calcined hydrotalcite the average differential heat of irreversible adsorption is 116 mmol g^{-1}. An additional indication of base strength is the highest differential enthalpies recorded for CO_2 adsorption on a single sample. This normally means the ΔH^0_{ads} values for the first two points plotted. They represent adsorption on the strongest basic sites. For conventionally calcined hydrotalcite the two highest recorded heats are 123 and 121 kJ mol^{-1} (total

adsorption 0.05 mmol g^{-1}). For microwave calcined hydrotalcite the two values are 139 and 138 kJ mol^{-1} (total adsorption 0.17 mmol g^{-1}). It is worth noting that other workers have typically recorded differential enthalpies of CO_2 adsorption on calcined hydrotalcite of 120-130 kJ mol^{-1} in line with the data here [19].

The conclusion from this work on hydrotalcite, calcined in the two ways, is that microwave calcination results in a significantly higher concentration of accessible basic sites. The average and maximum strengths of these basic sites are higher when generated by microwave calcination than are found in conventionally calcined hydrotalcite.
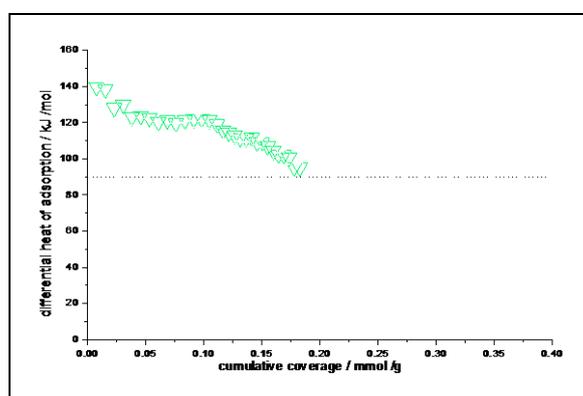
Figure 3.16 -– Differential molar enthalpy of CO_2 adsorption against amount of CO_2 adsorbed for calcined $Mg_6Al_2(CO_3)(OH)_{16}.4H_2O$ under microwave heating to 500 °C.
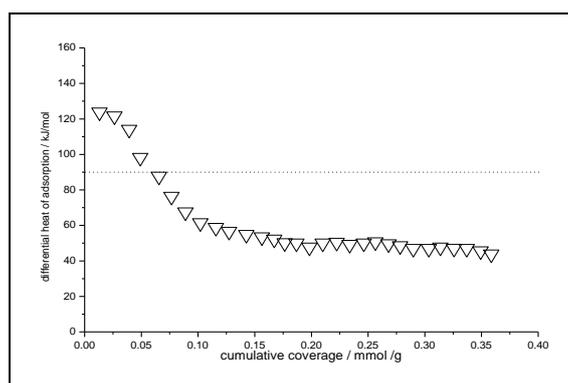
Figure 3.17– Differential molar enthalpy of CO_2 adsorption against amount of CO_2 adsorbed for calcined $Mg_6Al_2(CO_3)(OH)_{16}.4H_2O$ under conventional heating to 500 °C.

Nitrogen adsorption/desorption isotherms obtained for the samples using the two different types of heating can be seen in Figure 3.18 and Figure 3.19. The pore size distributions calculated from the desorption isotherms are displayed also. Both adsorption isotherms portray a mesoporous-like structure and have the corresponding type IV hysteresis loops accordingly. Hydrotalcite calcined conventionally exhibits a hysteresis loop between H1 and H2 types and this is indicative that the pore sizes and shapes are not uniform.
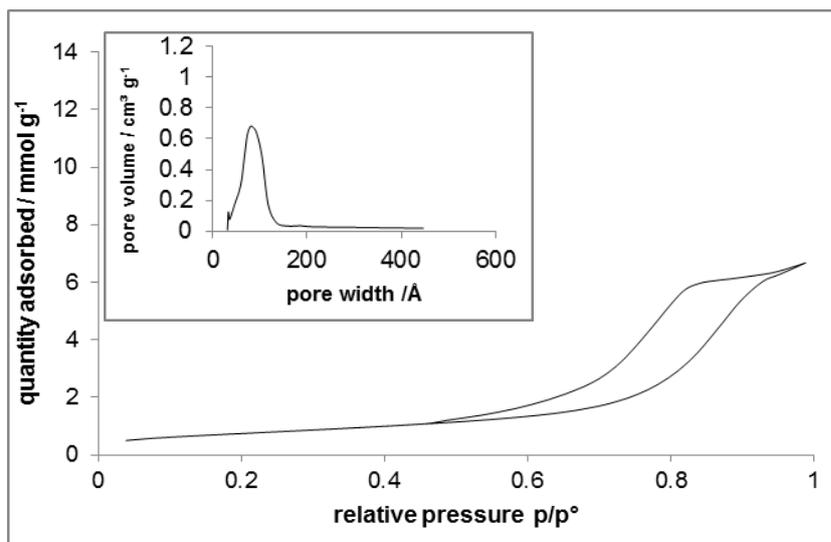
Figure 3.18 – Nitrogen adsorption/desorption isotherm and pore size distribution for $Mg_6Al_2(CO_3)(OH)_{16}.4H_2O$ calcined conventionally at 500 °C.
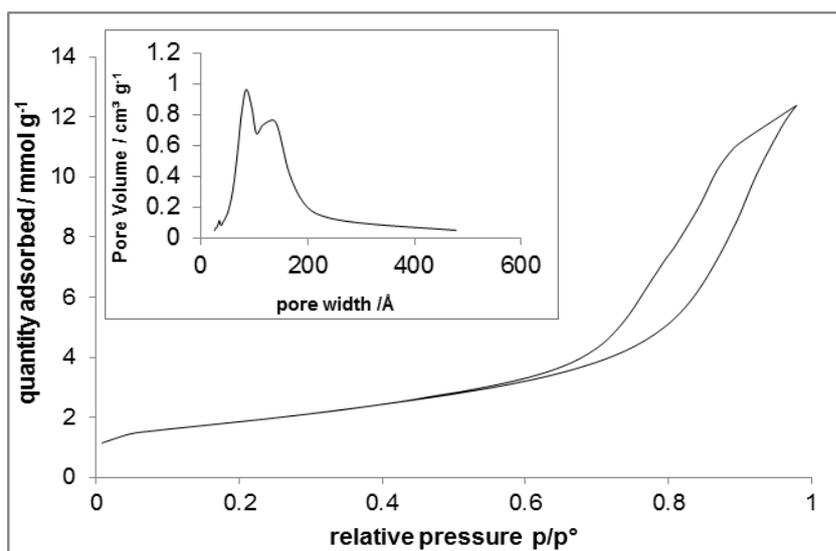
Figure 3.19 – Nitrogen adsorption/desorption isotherm and pore size distribution for $Mg_6Al_2(CO_3)(OH)_{16}.4H_2O$ calcined with microwaves at 500 °C.

Surface area, pore volume and catalytic activity data for the mixed metal oxides obtained from the hydrotalcite precursors can be seen in Table 3.5. The surface area for the microwave calcined hydrotalcite is significantly higher than for the conventionally heated sample. This higher surface area can be related to the increase in activity seen by the sample heated with microwaves. Pore volumes show the same trend. This could have an impact on the amount and number of active sites that are accessible which would perhaps account for the increase in the concentration of basic sites (if not their strength) measured using adsorption calorimetry.

Preparation	Surface area / $m^2\ g^{-1}$	Pore volume / $cm^3\ g^{-1}$	Catalytic activity in transesterification of tributyrin reaction / % conversion at 20 minutes
$Mg_6Al_2(CO_3)(OH)_{16}.4H_2O$ Microwave heating 500 °C	144	0.44	26
$Mg_6Al_2(CO_3)(OH)_{16}.4H_2O$ Conventional heating 500 °C	60	0.23	4

Table 3.5 – Physical characteristics and catalytic data for mixed metal oxides obtained from hydrotalcite subjected to microwave and conventional calcination.

The catalytic activity, based on tributyrin transesterification and conversion of tributyrin after 20 minutes reaction, of microwave calcined LDHs is very much higher than that of the conventionally heated hydrotalcite. Additional kinetic data are shown in Table 3.6, where pseudo-first order rate constants (first order in tributyrin) are shown for reactions catalysed by conventionally calcined hydrotalcite at a range of calcination temperatures and microwave-calcined hydrotalcite calcined at 500 °C. Note that the other reactant, methanol, was used in excess so that its concentration will effectively remain constant during the reaction, justifying the application of pseudo-first order kinetics.

These rate constants are based on the initial rates of reaction. In all cases first order plots were essentially linear for typically the first 20 minutes of reaction and this is the range from which first order rate constants were calculated.

$Mg_6Al_2(CO_3)(OH)_{16}.4H_2O$	Calcination temp / °C	[a]k /s^{-1}
Conventional	500	0.52
	600	0.52
	700	0.29
	800	0.025
	900	0.12
	1000	0.24
Microwave	500	2.27

Table 3.6 – Dependence of transesterification rate constant on the mode and temperature of catalyst calcination.   [a]Obtained for the first 20 minutes of the reaction.

The data shows clearly that for $Mg_{7.2}Al_2(CO_3)(OH)_{16}.4H_2O$, the reaction rate is very much higher with calcination using microwaves at 500 °C than calcined conventionally at all temperatures tested. It is tempting to think that the enhanced catalytic activity of microwave-calcined LDHs may be due to local temperature excursions brought about uniquely by microwave calcination that are not reflected in the recorded calcination temperature of 500 °C. But, assuming that these excursions

would not go above 1000 ºC locally, the data in Table 3.6 suggests this may not be the case as it clearly shows that materials calcined conventionally at up to 1000 ºC all have much lower activities that the microwave-calcined LDH (at 500 ºC), with maximum activity achieved on conventional calcination at 500-600 ºC.

3.4.4 – Conclusions

The results of this work suggest that the properties of the mixed oxides generated by microwave calcination of hydrotalcite can be very different to those of oxides generated by conventional calcination. It is not unreasonable that different morphologies result from the two types of calcination. One reason, for example, is that, under conventional heating, conversion of hydrotalcite to oxide would first occur on the outsides of the particles. Subsequently, water that evolves from hydroxides in the inside of particles would have to diffuse through the outer oxide crust to desorb. This would happen to a lesser extent under the even heating provided by microwaves. The effect of this water diffusion process might 1) result in a heavily disrupted outer oxide layer on the particle and 2) increase the partial pressure of water in the particles, perhaps affecting the rates of solid state conversion. It is not easy to see how differences linked to these effects might affect basicity and activity but it is certainly reasonable to expect some differences between materials prepared in the two ways, as indeed we observe in this work here. Our overall conclusion is that this work shows that microwave calcination has the potential for generating new and different properties in calcined materials, with important potential applications in catalyst preparation.

References

[1]   J. M. Fraile, N. García, J. A. Mayoral, E. Pires, L. Roldán, *Appl. Catal. A-Gen.*, 387 (2010) 67-74.

[2]   Z. Helwani, M.R. Othman, N. Aziz, J. Kim, W.J.N. Fernando. *Appl. Catal. A-Gen.*, 363 (2009) 1-9.

[3]   J. Theo Kloprogge, Leisel Hickey, R. L. Frost, *J. Solid State Chem.,* 177 (2004) 4047-4055.

[4]   A. Seron, F. Delorme, *J. Phys. Chem. Solids.*, 69 (2008) 1088-1090.

[5]   D.G. Evans, X. Duan, *Layered Double Hydroxides*, Springer, New York, 2006.

[6]   Y. Zhao, F. Li, R. Zhang, D. G. Evans, Xue Duan, *Chem. Mater.*, 14 (2002) 4286-4291.

[7]   J.M. Fraile, N. Garcia, J.A. Mayoral, E. Pires, L. Roldan. *Appl. Catal. A-Gen.*, 364 (2009) 87-94.

[8]   J.T. Kozlowski, M.T. Aronson, R.J. Davis. Appl. Catal., B., 96 (2010) 508–515.

[9]   M.J Holgado, F.M Labajos, M.J.S Montero, V Rives, *Mater. Res. Bull.*, 38 (2003) 1879-1891.

[10]   M. del Arco, V. Rives, R. Trujillano, *Stud. Surf. Sci. Catal.*, 87 (1994) 507-515.

[11]   V. Rives, *Mater. Chem. Phys.* 75 (2002) 19-25.

[12]   M. Herrero, P. Benito, V. Rives, *Catal. Today.*, 128 (2007) 129-137

[13]   G.M.B. Parkes, P.A. Barnes, G. Bond, E.L. Charsley, *Thermochim. Acta.*, 356 (2000) 85-96.

[14]   J.M. Oh, S.H. Hwangm, J.H. Choy, *Solid State Ionics.,* 151 (2002) 285-293.

[15]   D. Cantrell, L.J. Gillie, A.F. Lee, K. Wilson, *Appl. Catal. A-Gen.*, 287 (2005) 183-201.

[16]   S. Casenave, H. Martinez, C. Guimon, A. Auroux, V. Hulea, A. Cordoneanu, E. Dumitriu, Thermochim. Acta., 379 (2001) 85-92.

[17]   H.A. Prescott, Z.J. Li, E. Kemnitz, A. Trunhke, J. Deutsch, H. Lieske, A. Auroux, J. Catal., 234 (2005) 119-132.

[18]   S. Abelló, F. Medina, D. Tichit, J. Pérez-Ramírez, X. Rodríguez, J.E. Sueiras, P. Salagre, Y. Cesteros, *Appl. Catal. A-Gen.*, 281 (2005) 191-203.

[19]   J. S. Valente, J. Hernandez-Cortez, M. S. Cantu, G. Ferrat, E. López-Salinas*, Catal. Today.*, 150 (2010) 340-345.

[20]   P. Benito, F.M. Labajos, J. Rocha, V. Rives, *Micropor. Mesopor. Mat.,* 94 (2006) 148-15.

[21]   M. Leon, E. Diaz, S. Bennici, A. Vega, S. Ordonez, A. Auroux, *Ind. Eng. Chem. Res.*, 49 (2010) 3663-3671.

[22]   R. Prihod'ko, M. Sychev, I. Kolomitsyn, P. J. Stobbelaar, E. J. M. Hensen, R. A. van Santen, *Micropor. Mesopor. Mat.,* 56 (2002) 241-255.

[23]   J. Zhang, F. Zhang, L. Ren, D. G Evans, X. Duan, *Mat. Chem. Phys.*, 85 (2004) 207-21.

[24]   H.-W. Olfs, L.O. Torres-Dorante, R. Eckelt, H. Kosslick, *Appl. Clay Sci.*, 43 (2009) 459-464.

[25]   S. Miyata, *Clays Clay Miner.*, 28 (1980) 50-64.

[26]   V.R.L. Constantino, T.J. Pinnavaia, Inorg. Chem., 34 (1995) 883-897.

[27]   V.K. Diez, C.R. Apesteguia, J.I. Di Cosimo, J. Catal., 215 (2003) 220-234.

[28]   M. Herrero, P. Benito, F.M. Labajos, V. Rives*, J. Solid State Chem.*, 180 (2007) 873-884.

[29]   P. Benito, M. Herrero, F.M. Labajos, V. Rives, *Appl. Clay Sci.*, 48 (2010) 218-227.

[30]   P. Benito, M. Herrero, F.M. Labajos, V. Rives, C. Royo, N. Latorre, A. Monzon, *Chem. Eng. J.*, 149 (2009) 455-462.

[31]   L. Wang, B. Li, M. Yang, C. Chen, Y. Liu, *J. Colloid Interface Sci.*, 356 (2011) 519-525.

Chapter 4

Synthesis and applications of copper doped mixed oxides and their precursors

Chapter 4

4.1 – Objectives

The objectives of the work reported here are:

1. to investigate the effects of isomorphous substitution of copper (II) in LDH structures on physical and chemical properties, and on catalytic properties for base catalysed reactions.

2. to investigate the effect of microwave calcination compared to conventional calcination on the same properties

4.2 – Introduction

It is known that transition metal oxides often have useful catalytic properties because of their ability to exist in more than one oxidation state [1]. Therefore it could reasonably be expected that it might be possible to enhance the activity of the conventional hydrotalcite LDH by the addition of a transition metal into the lattice.

In this work copper was chosen to dope the most common LDH, hydrotalcite, for applications as a basic catalyst. Copper is one of the most useful transition metals to incorporate as it is readily available, inexpensive and forms one of the most catalytically active metal oxides [2].

Copper, existing as Cu^{2+}, has been successfully incorporated into the hydrotalcite lattice by many researchers, replacing some of the Mg^{2+} [3-9]. These copper doped LDH precursors have been calcined and used as catalysts for many reactions, including oxidation and dehydrogenation reactions [10-14].

Copper was also chosen because its oxide is known to exhibit activity in base catalysed reactions [15-20]. In addition, copper (II) is known to couple well with microwave fields so it was anticipated that copper-containing LDHs would be relatively easy to heat using microwaves. As discussed in Chapter 1, the ionic radius of a cation determines whether it can be incorporated in the hydrotalcite structure and the copper (II) cation

radius is 0.72 Å (Pauling, octahedral co-ordination), identical to that of magnesium (II) [21]. Vaccari suggested that the formation of an LDH consisting solely of the divalent copper cation and trivalent aluminium is unfavoured but substitution by copper (II) for a proportion of the magnesium (II) in hydrotalcite is possible. Typically, when an LDH is calcined, the only crystalline oxide phase detected by powder XRD is that of the most abundant cation. Therefore it was decided to synthesise copper containing LDHs in two stoichiometries, with copper levels higher than, and equal to those of magnesium. This enables comparisons to be made on the effects of incorporating copper into the lattice, in terms of structure and activity. At the same time, and to ensure direct comparability, a batch of standard hydrotalcite was also prepared.

Valente and co-workers have looked at the properties of LDHs, prepared using the conventional co-precipitation method, containing three cations, magnesium, aluminium and a transition metal [23], one of which was copper (II). The main interests in this study were acid-base properties formed when the transition metal doped LDHs were calcined and tested in a reaction that is selective to either acid or base catalysed formation of products. The reaction was the dehydrogenation or dehydration of 4-methyl-2-pentanol, with the dehydrogenation reaction responding to base catalysis and the dehydration reaction responding to acid catalysis. In this reaction a calcined copper doped LDH has been found to catalyse the dehydrogenation reaction with selectivity of 100 %. It was interesting to note that LDHs containing other transition metals could also catalyse the dehydration reaction, indicating a mixture of acid and base sites. The reaction was also tested with the conventional hydrotalcite LDH (calcined) and it was found that it exhibited selectivity to the dehydrogenation reaction, indicating presence of basic sites only.

Dussault and co-workers also looked at the properties of the corresponding oxides formed from the calcination of LDHs that have divalent transition metals replacing various amounts of magnesium [24]. The method of synthesis was also by co-precipitation. In this work, copper was incorporated alongside nickel. Results show that when the level of copper is increased, the acidity of the LDH decreases which is in good agreement with Valente.

To date, much of the literature seems to concern the use of transition metals in LDHs to provide both acid and base properties without the tailoring of a transition metal LDH for

a specific reaction requiring either base or acid catalysis [25-31]. In this work the object is to enhance the basicity of hydrotalcite through incorporation of copper (II) with an eventual view to developing a solid base catalyst for the transesterification of triglycerides. At this present time the reaction to produce biodiesel, the transesterification of triglycerides, has been tested using a variety of solid basic catalysts [32-41]. However, these heterogeneous catalysts are very much lower in activity than typical basic homogeneous catalysts. This barrier should be addressed if there is to be a possibility of employing solid catalysts in place of liquid catalysts in the transesterification of vegetable oils.

The processes that occur when an LDH is calcined have been described previously and are reported in the literature [42,43]. In this work, calcination has been carried out using microwave heating. A feature of copper-doped LDHs is that copper was also chosen as copper is known to couple strongly with microwaves [44-48] making it relatively easy to heat in this way. As far as we known this is the first occasion on which a transition metal doped hydrotalcite has been calcined using controlled microwave heating. Evidence of copper's sensitivity to microwave heating is provided by the microwave-induced calcination of copper-containing high temperature superconducting mixed oxides in which calcination times have been reduced from 24 hours to 30 minutes [49]. However, this process of using microwaves involved little temperature control so it is not possible to easily rationalise differences in behaviours in the two heating regimes.

Calcination of typical hydrotalcite at around 500 ^{o}C is characterised by broad lines in the powder XRD pattern associated with the oxide of the most/more abundant metal in the precursor, indicative of small crystallites of the oxide. Raising the temperature beyond this result in sintering of the oxides, formation of spinel phases and, generally, a reduction in solid base catalytic activity [50]. When transition metals are isomorphously substituted for magnesium additional processes can occur, for example reduction of the transition metal to a lower oxidation state. Studies of copper-containing mixed hydroxides for instance show that activity towards dehydrogenation reactions is maximised following calcination at typically greater than 600 ºC although, oddly, base strength is relatively low [51].

The importance of the intimately mixed oxides formed on calcination of LDHs for catalysis is partly that they exhibit large numbers of active surface defect sites. They have been used in many organic syntheses and are studied widely in base-catalysed transesterification reactions [52-56]. With transition metals substituted in the lattice, they have shown activity as acid and base, and redox catalysts. They are now also being studied in the catalytic oxidation of VOCs, in NOx reduction and soot combustion in diesel engine exhausts and SO$_X$ reduction [57]. Another potential use is in CO$_2$ storage/removal [58].

Studies of mixed hydroxides under conventional heating have been carried out, characterising the effects of varying heating rates and over-gases in furnaces. Process-controlled conventional heating techniques, on an analytical scale, have been applied [59] but, crucially, these have not been linked to microwave heating. Microwave calcinations of LDHs have been studied but without temperature control and so conclusions and also comparisons are of limited value. It is the use of microwaves, combined with process-control and the associated control of reaction rates and hence crystal nucleation rates, that is the key to the work described here.

In this work, comparisons between microwave controlled heating and conventional heating in air for the calcination of copper doped hydrotalcites are reported and compared in terms of the catalytic activities and structural characteristics of the mixed oxides produced on calcination.

4.3 – Experimental

4.3.1 – Synthesis of Cu$_x$Mg$_{6-x}$Al$_2$(CO$_3$)(OH)$_{16}$.4H$_2$O and Mg$_6$Al$_2$(CO$_3$)(OH)$_{16}$.4H$_2$O

Hydrotalcite layered double hydroxide, Mg$_6$Al$_2$(CO$_3$)(OH)$_{16}$·4H$_2$O was prepared, as before, by slowly adding simultaneously a solution of 250 ml magnesium and aluminium nitrates in a 3:1 molar ratio (total 1.0 mol dm^{-3}) and a 250 ml sodium carbonate solution (0.625 mol dm^{-3}) to a 1000 ml beaker, stirring rapidly as the mixture was formed. The pH of the solution was maintained at about 8.0 by adding sodium hydroxide solution (0.20 mol dm^{-3}), under vigorous stirring. The resulting mixture was filtered and

thoroughly washed with hot water to ensure removal of sodium salts. The powder was dried at 100 °C overnight.

Mixtures of copper nitrate, magnesium nitrate and aluminium nitrate were used in the same precipitation method to form the corresponding LDHs. The pHs of the solutions were kept at 9.0 ± 0.5 throughout the precipitation process as this was the range in which the copper nitrate would precipitate as copper hydroxide. Target products were Cu$_3$Mg$_3$Al$_2$(CO$_3$)(OH)$_{16}$.4H$_2$O and Cu$_{1.2}$Mg$_{4.8}$Al$_2$(CO$_3$)(OH)$_{16}$.4H$_2$O.

Powders were calcined conventionally in a muffle furnace at temperatures between 400 °C and 800 °C, heating at 2 °C min^{-1} in air with a hold time of 4 hours, to produce the mixed oxide catalysts. Microwave heating was also used but instrumental limitations meant that only Cu$_3$Mg$_3$Al$_2$(CO$_3$)(OH)$_{16}$.4H$_2$O was heated above 600 °C (to 750 °C) using microwaves. Cu$_{1.2}$Mg$_{4.8}$Al$_2$(CO$_3$)(OH)$_{16}$.4H$_2$O was heated only to 600 °C. All catalyst precursors and oxides were kept in a desiccator to ensure minimal contact with water.

For comparison, the oxides of the individual metals used in this work, were also prepared by the calcination of the single hydroxides. The individual hydroxides were synthesised from the relevant metal nitrates using sodium hydroxide at the same pH used to synthesise the LDHs. The oxides were mixed together to form the equivalent molar species to those expected from the LDHs.

Copper doped LDHs and the corresponding mixed oxides were characterised using N$_2$ adsorption, powder XRD, SEM-EDS and adsorption microcalorimetry using CO$_2$. Powder XRD patterns were obtained as quickly as possible after the oxides were synthesised to prevent rehydration in air.

It is worth noting that neither the urea method nor the ammonia method of precipitating the LDHs could be used because of the solubility of copper (II) in ammonia solutions through complexation [60].

4.4 – Results and Discussions

4.4.1 - Elemental Analysis

Elemental analysis was carried out using SEM-EDS and calculated elemental compositions can be seen in Table 4.1. It is acknowledged that this technique is only sensitive to the elemental compositions close-to or at the surface of the solid, but there is no reason to support that the bulk composition would differ significantly from that determined by SEM-EDS. Stoichiometries were also obtained using XPS and although the stoichiometries were not identical to the results seen here, the trends were the same (i.e. the copper amount increased two-fold in the higher copper containing sample). The results indicate that the elemental compositions of all three LDHs are not close to the metal nitrate compositions employed in the synthesis step. However, the copper LDHs show a clear difference in the amount of copper incorporated into the lattice. The formulae presented in this thesis reflect the elemental compositions determined using the results in Table 4.1. The EDS data gives the relative molar abundance of each element. In order to derive the formulae, we have assumed that the aluminium content in each LDH is the same and determined formulae for the LDHs based on this.

Catalyst	O	Mg	Al	C	Cu	Na	M:Mg:Al molar ratio
$Mg_6Al_2(CO_3)(OH)_{16}.4H_2O$	25.47	3.80	1.00	4.24	-	-	$Mg_{7.2}Al_2$
$Cu_3Mg_3Al_2(CO_3)(OH)_{16}.4H_2O$	68.36	8.94	3.08	16.76	1.00	-	$Cu_{1.32}Mg_{2.98}Al_2$
$Cu_{1.2}Mg_{4.8}Al_2(CO_3)(OH)_{16}.4H_2O$	28.84	2.27	1.52	7.51	1.00	-	$Cu_{0.64}Mg_{5.8}Al_2$

Table 4.1 – Elemental data of LDHs incorporating copper, determined by SEM-EDS. The numbers shown are relative molar abundances and are unit-less.

4.4.2 – Powder XRD

Figure 4.1 shows the powder XRD diffraction patterns for the as-synthesised copper LDHs. All catalyst precursors before calcination exhibited broad peaks at values of 2θ which were characteristic of the hydrotalcite structure. Figure 4.2 is the powder XRD diffraction pattern for $Mg_{7.2}Al_2(CO_3)(OH)_{16}.4H_2O$ subjected to conventional calcination up to 1000 °C. Heating above 150-200 °C resulted in loss of the characteristic LDH reflections (data not shown) and at 500 °C broad lines attributed to MgO can be seen. Calcination temperatures above 800 °C resulted in the formation of spinel, $MgAl_2O_4$, (reflections at 20 °, 27 °, 43 °, 61 °, 62 ° and 65 °) [61].
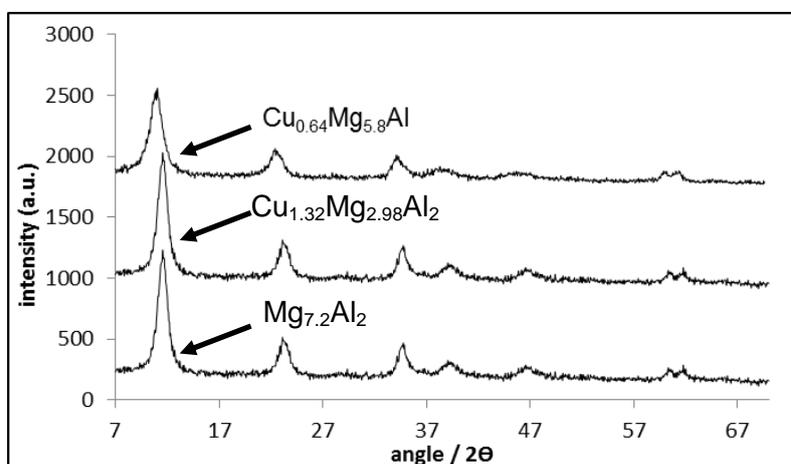
Figure 4.1 – Powder XRD patterns for synthesised LDHs.
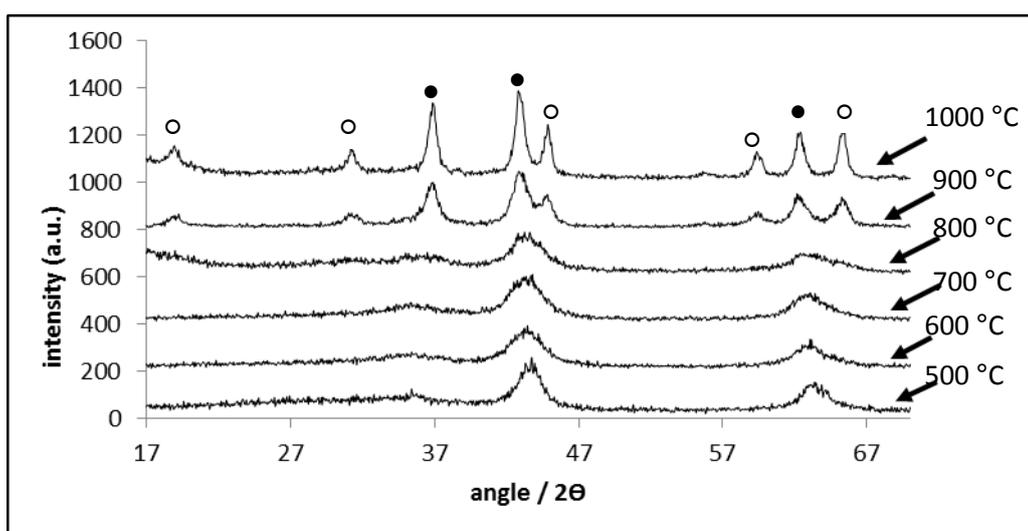
Figure 4.2 – Powder XRD patterns of $Mg_{7.2}Al_2(CO_3)(OH)_{16}.4H_2O$, calcined for four hours under conventional heating (heating ramp of 2 °C min^{-1}). (● =MgO, ○ =MgAl$_2$O$_4$).

Figure 4.3 shows the powder XRD patterns of $Cu_{0.64}Mg_{5.8}Al_2(CO_3)(OH)_{16}.4H_2O$ through progressive conventional heating. The first significant transformation occurred at 500 °C when broad peaks assigned to a poorly crystalline MgO phase were seen. As the temperature was increased to 800 °C, significantly narrower peaks assigned to MgO could be seen, together with reflections assigned to CuO. The CuO diffraction pattern largely disappeared when a temperature of 1000 °C was reached, and MgO reflections [62] became sharper, suggesting that MgO crystals were sintering under heating. This was accompanied by the appearance of a spinel phase in line with behaviour of $Mg_{7.2}Al_2(CO_3)(OH)_{16}.4H_2O$.
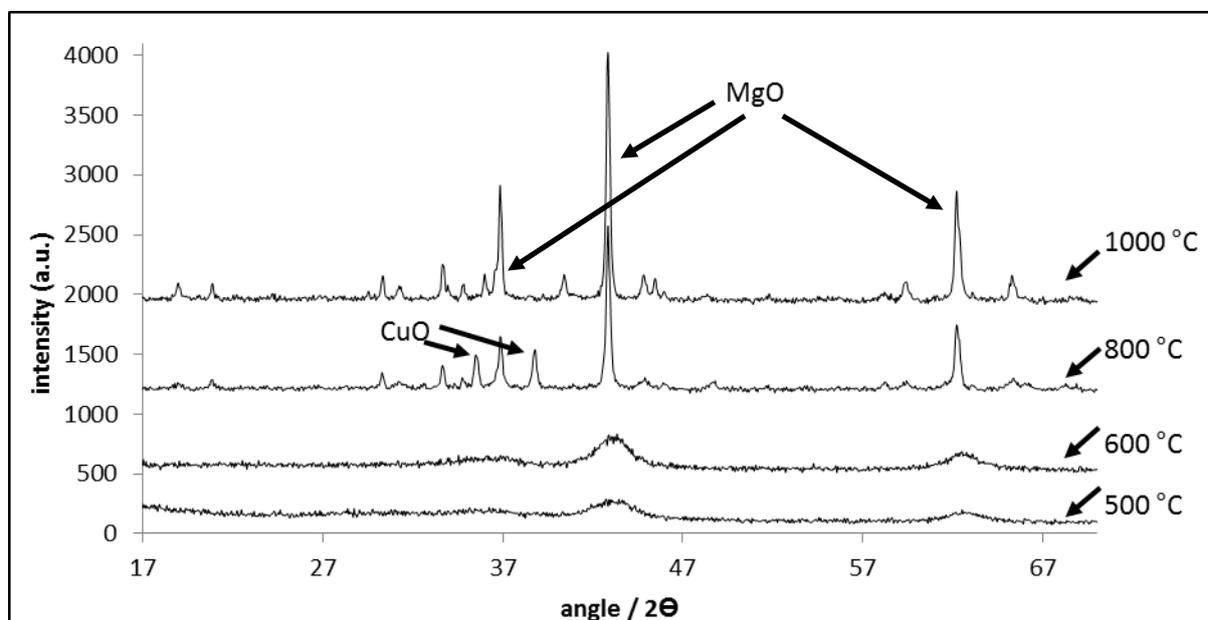
Figure 4.3 – Powder XRD pattern of $Cu_{0.64}Mg_{5.8}Al_2(CO_3)(OH)_{16}.4H_2O$, calcined for four hours under conventional heating following a heating ramp of 2 °C min^{-1}.

Figure 4.4 shows the powder XRD patterns for $Cu_{0.64}Mg_{5.8}Al_2(CO_3)(OH)_{16}$ under progressive heating using the process-controlled microwave technique. Only two temperatures were studied, 500 °C and 600 °C as studied previously. We can see broad reflections assigned to MgO and CuO at 500 °C. When the controlled microwave heating temperature was increased to 600 °C, these reflections abruptly sharpened, suggesting sintering of both CuO and MgO crystallites.
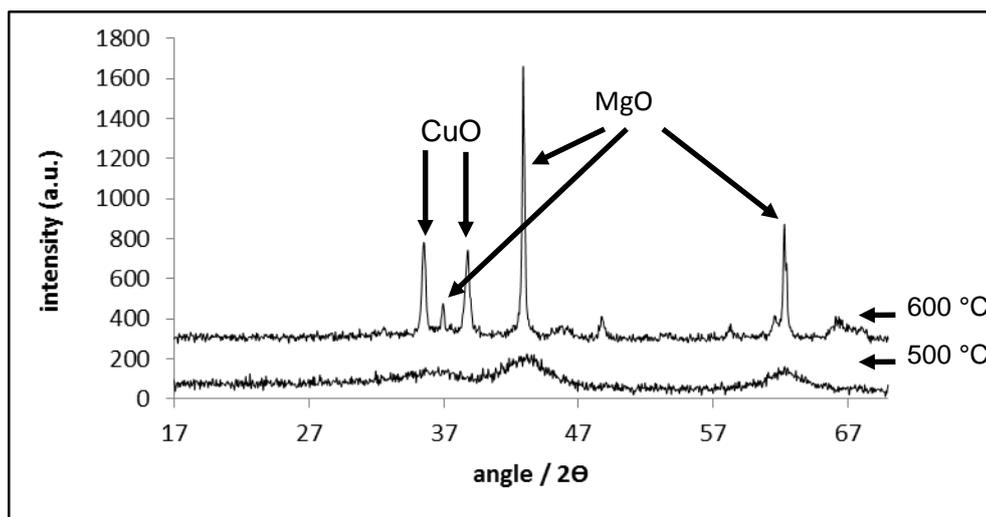
Figure 4.4 – Powder XRD pattern of Cu$_{0.64}$Mg$_{5.8}$Al$_2$(CO$_3$)(OH)$_{16}$.4H$_2$O, calcined for four hours under microwave heating following a heating ramp of 2 °C min^{-1}.

There are clear differences between the products of calcination using the two methods of heating. The well-defined pattern for CuO together with sharp MgO reflections appear by 600 °C under microwave heating whereas these are only seen at 800 °C when conventional heating is used. The relative amounts of CuO and MgO are different also, with CuO exhibiting a relatively strong diffraction pattern at 600 °C under microwave heating but the CuO pattern is less intense in the sample calcined conventionally. The conclusion is that both CuO and MgO are formed at lower temperatures with microwaves than with conventional heating.

The powder XRD patterns are shown for the high-copper LDH, Cu$_{1.32}$Mg$_{2.98}$Al$_2$(CO$_3$)(OH)$_{16}$.4H$_2$O heated to 1000 °C by conventional heating in Figure 4.5. It can be seen that from 500 to 700 °C there is evidence of poorly crystalline MgO. In addition to MgO, as the LDH is heated to 700 °C, reflections due to CuO are seen. These are more intense than those detected for the low copper LDH. At 1000 °C the MgO reflections are much narrower than at lower temperatures and reflections assigned to spinel MgAl$_2$O$_4$ are detected. CuO reflections are no longer visible at 1000 °C.
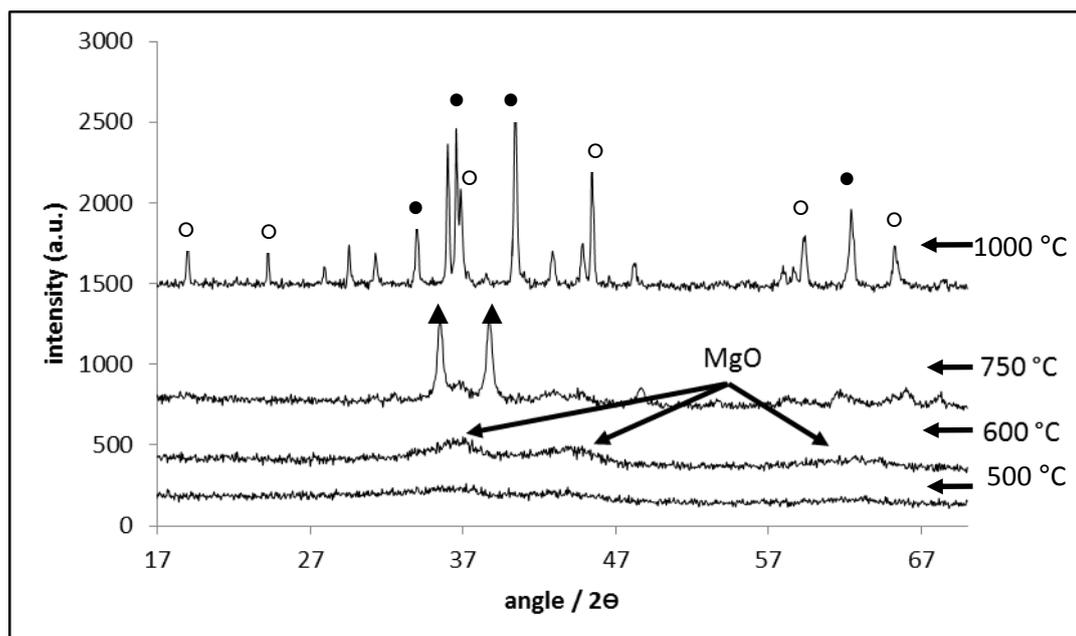
Figure 4.5 – Powder XRD pattern for Cu$_{1.32}$Mg$_{2.98}$Al$_2$(CO$_3$)(OH)$_{16}$.4H$_2$O, calcined for four hours under conventional heating following a heating ramp of 2 °C min^{-1} (▲=CuO ● =MgO, ○ =MgAl$_2$O$_4$).

Using temperature controlled microwave heating it was possible to heat the high copper LDH to the higher temperature of 750 °C because it coupled so strongly with the microwave field. In this case also, an additional patterns after 400 °C is shown. The diffraction patterns recovered after microwave calcination to 400, 500 and 750 °C are shown in Figure 4.6. The material loses the hydrotalcite structure and broad overlapping reflections due to MgO and CuO appear (Figure 4.6) at 400 °C. At 500 °C, it can be seen that CuO reflections abruptly sharpen followed by a sudden reduction in peak width for MgO at 750 °C. Reflections assigned to spinel, MgAl$_2$O$_4$, are seen at 750 °C. In fact, these could be due to a copper-containing spinel [63], the XRD pattern for which may be indistinguishable from that of MgAl$_2$O$_4$.

The XRD patterns of MgO and CuO sharpen very abruptly during the heating process, implying that sintering of the small oxide crystallites responsible for the broad line patterns occurs quite suddenly. There is not a great deal of difference in the way this occurs under the two heating regimes but, in general, material heated using microwaves exhibits more intense and better resolved lines for CuO, MgO and for spinel, suggesting that greater crystallinity is achieved using microwave compared to

conventional heating.   Furthermore, the appearance of these phases occurs at nominally slightly lower temperatures under microwave heating (compare the 500 ^{o}C patterns under the two heating regimes).
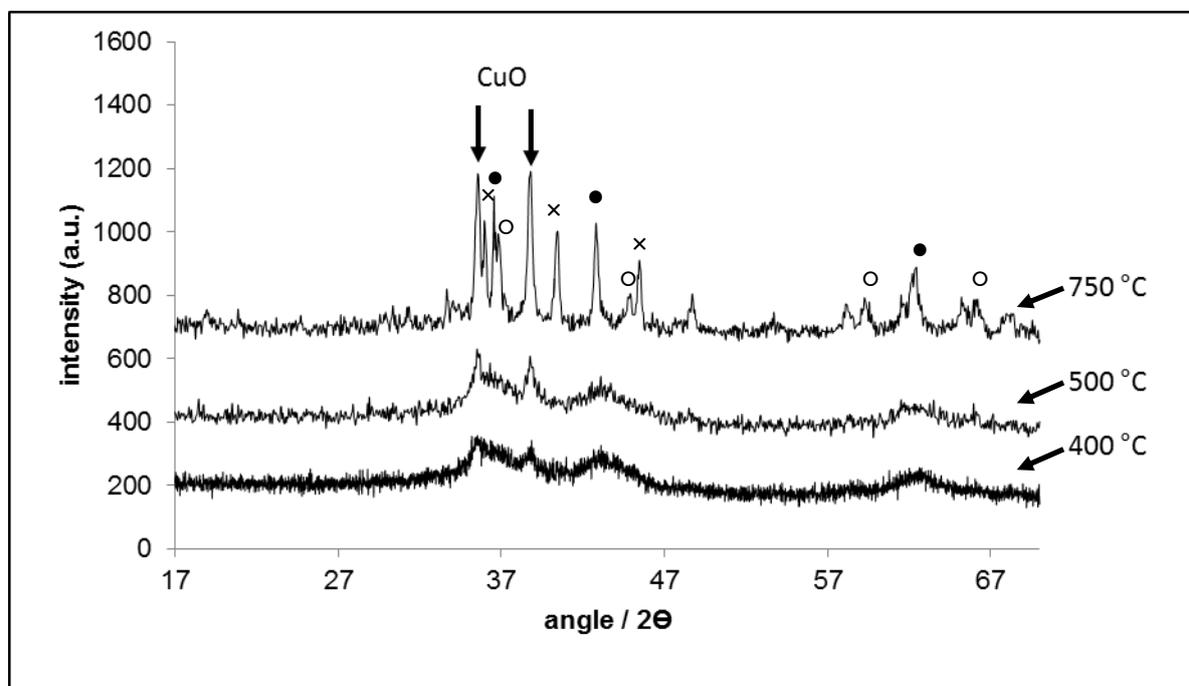
Figure 4.6 – Powder XRD pattern for Cu$_{1.32}$Mg$_{2.98}$Al$_2$CO$_3$(OH)$_{16}$.4H$_2$O, calcined for four hours under microwave heating following a heating ramp of 2 °C min^{-1} (● =MgO,

○ =MgAl$_2$O$_4$, ✗ =Cu$_2$MgO$_3$).

At higher temperatures, illustrated by the results at 750 ^{o}C in Figure 4.6, the CuO phase is clearly visible.   But an additional phase is also seen at this temperature when microwaves are used.   Reflections in the 750 ^{o}C microwave XRD pattern associated with this new phase can be matched to those of Cu$_2$MgO$_3$, gueggonite [64]. This compound has been detected by others on heating simple solid mixtures of CuO and MgO, but only at 1000 ^{o}C using conventional heating [65].   It is significant to note that, while Cu$_2$MgO$_3$ was detected at 750 ^{o}C under microwave heating in this work, no evidence for it was found when Cu$_{1.32}$Mg$_{2.98}$Al$_2$(CO$_3$)(OH)$_{16}$.4H$_2$O was calcined using conventional heating to 1000 ^{o}C and even beyond, despite the existence of a CuO/MgO mixture at temperatures above 500 ^{o}C.   Note, however, that the published report of

Cu$_2$MgO$_3$ formed from CuO/MgO mixtures also describes how, prior to formation of this new phase, a solid solution exists of CuO and MgO. This evidently shows up through shifted reflections in the MgO XRD pattern [66]. In the work reported in this Chapter, no evidence for this solid solution was found so if this solid solution is a precursor to Cu$_2$MgO$_3$, it is conceivable that conditions exist in the calcined mixed hydroxides, when conventionally heated anyway, which prevent its formation.

Although not referred to in the experiment section, attempts were made to incorporate more copper in the LDH layered structure. As can be seen from the powder XRD pattern shown in Figure 4.7 for Cu$_{3.6}$Mg$_{2.4}$Al$_2$(CO$_3$)(OH)$_{16}$.4H$_2$O, crystallinity is low. It appears that LDH's cannot easily be prepared with this much copper in the lattice. For this work, we assumed that Cu$_{1.32}$Mg$_{2.98}$Al$_2$(CO$_3$)(OH)$_{16}$.4H$_2$O represents the highest copper content LDH that can be readily prepared.
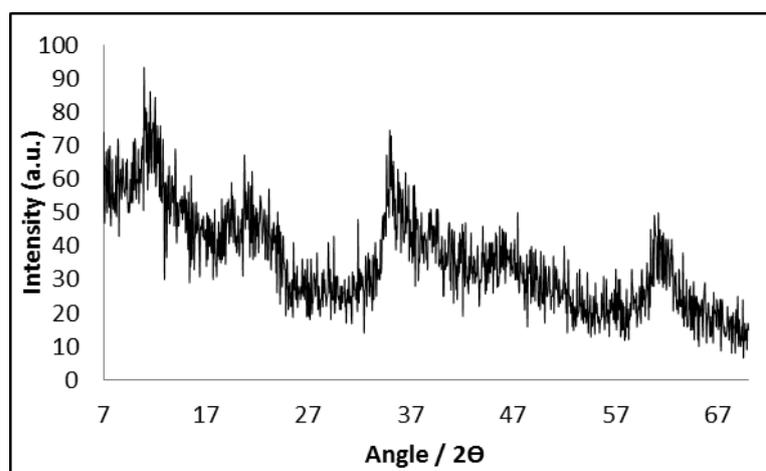
Figure 4.7 – Powder XRD diffraction pattern for Cu$_{3.6}$Mg$_{2.4}$Al$_2$(CO$_3$)(OH)$_{16}$.4H$_2$O.

4.4.3 – CO$_2$ Adsorption Microcalorimetry

Conventionally calcined and microwave calcined copper-doped hydrotalcites were characterised using CO$_2$ adsorption microcalorimetry and results can be seen in Figures 4.8-4.11. Data is portrayed using the molar enthalpy of adsorption, (measured for each measured dose of CO$_2$), plotted against the total amount of CO$_2$ adsorbed by

the catalyst. The enthalpy of adsorption is a good indicator of the strength of the basic sites and it is assumed that the basic sites react with CO_2 in order of decreasing strength (constrained by the Boltzmann distribution governing the relative populations of sites of different strengths) [67]. Catalyst basicities can be compared using these profiles, taking note of the extent of CO_2 adsorption with enthalpies greater than 90 kJ mol^{-1} (generally thought to differentiate between chemisorption and physisorption) [68]. Another important indicator is the adsorption enthalpy for the first few pulses of CO_2, as a comparative indicator of the strength of the strongest basic sites on the catalysts.

The profiles for CO_2 adsorption on $Cu_{1.32}Mg_{2.98}Al_2(CO_3)(OH)_{16}.4H_2O$ following calcination at 500 °C and at 600 °C are shown in Figures 4.8 and 4.9. Following calcination at both temperatures, the materials calcined using microwaves evidently exhibit significantly higher concentrations of basic sites than those calcined conventionally.

Equivalent plots for the LDH prepared with a lower level of copper, $Cu_{0.64}Mg_{5.8}Al_2(CO_3)(OH)_{16}.4H_2O$, are shown in Figures 4.10 and 4.11. The differences here between the basicity of materials calcined using microwaves and using conventional heating are less. This is a somewhat surprising results for which there is no obvious reason. The fact that both $Mg_{7.2}Al_2(CO_3)(OH)_{16}.4H_2O$ and the high copper LDH yield higher basicities on microwave calcination makes it difficult to understand why this intermediate material should behave differently.
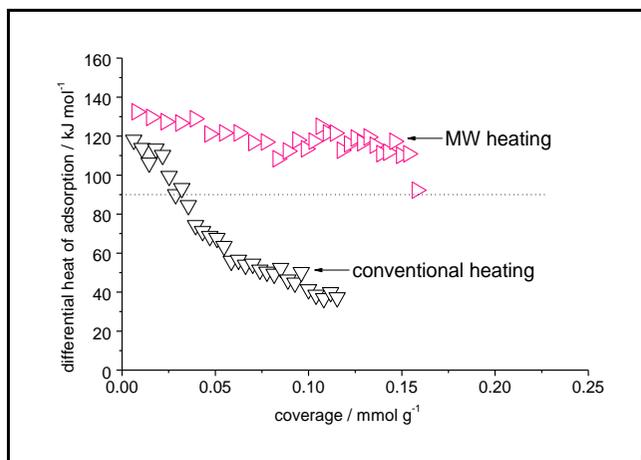
Figure 4.8 – Differential molar enthalpy of CO_2 adsorption against amount of CO_2 adsorbed for calcined $Cu_{1.32}Mg_{2.98}Al_2(CO_3)(OH)_{16}.4H_2O$ (heated at 2 ºC min^{-1} to 500 °C and held for four hours).
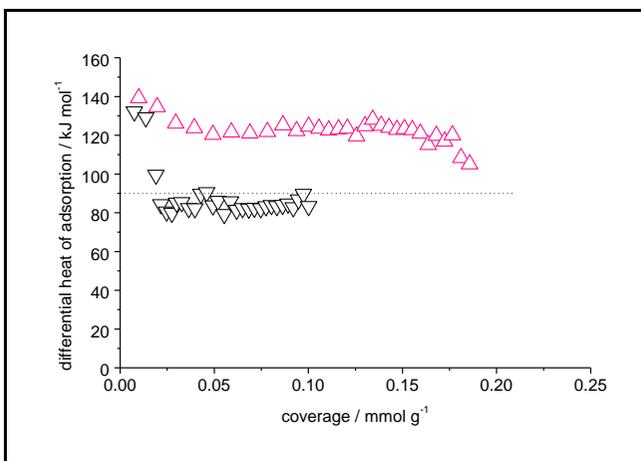
Figure 4.9 – Differential molar enthalpy of CO_2 adsorption against amount of CO_2 adsorbed for calcined ($\triangle$= microwave heating, $\triangle$= conventional heating) $Cu_{1.32}Mg_{2.98}Al_2(CO_3)(OH)_{16}.4H_2O$ (heated at 2 ºC min^{-1} to 600 °C and held for four hours).
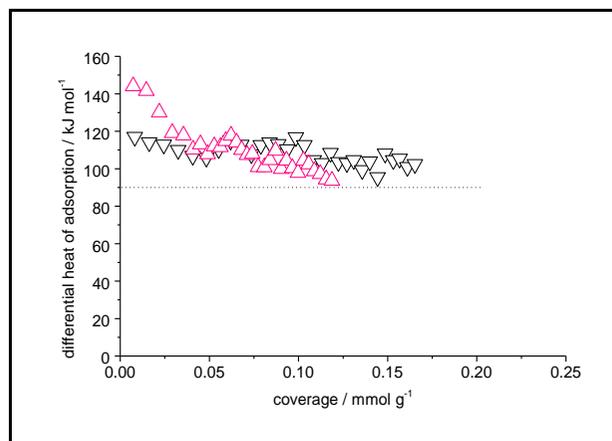
Figure 4.10 – Differential molar enthalpy of CO_2 adsorption against amount of CO_2 adsorbed for calcined (Δ= microwave heating, Δ= conventional heating) $Cu_{0.64}Mg_{5.8}Al_2(CO_3)(OH)_{16}.4H_2O$ (heated at 2 ºC min^{-1} to 500 °C and held for four hours)
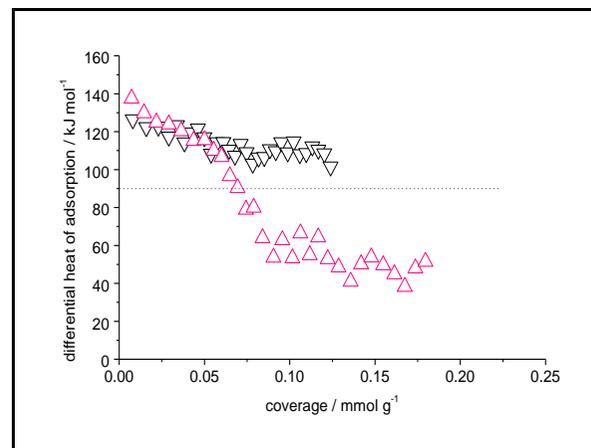
Figure 4.11– Differential molar enthalpy of CO_2 adsorption against amount of CO_2 adsorbed for calcined (Δ= microwave heating, Δ= conventional heating) $Cu_{0.64}Mg_{5.8}Al_2(CO_3)(OH)_{16}.4H_2O$ (heated at 2 ºC min^{-1} to 600 °C and held for four hours).

Calorimetric adsorption and surface area data (obtained from nitrogen adsorption measurements) for calcined Cu$_{1.32}$Mg$_{2.98}$Al$_2$(CO$_3$)(OH)$_{16}$.4H$_2$O are summarised in Table 4.2 and Table 4.3. The CO$_2$ calorimetry adsorption data is taken from the plots Figures 4.9 and 4.10 and expressed as a) the total amount of CO$_2$ adsorbed per gram of sample with ΔH^0_{ads} above 90 kJ mol^{-1}, as a measure of the concentration of basic sites on the sample and b) an averaged value of all the ΔH^0_{ads} measurements for pulses of CO$_2$ adsorbed on each sample with enthalpies greater than 90 kJ mol^{-1}. Cu$_{1.32}$Mg$_{2.98}$Al$_2$(CO$_3$)(OH)$_{16}$.4H$_2$O that has been calcined at 500 °C and 600 °C using microwaves is seen to exhibit strong basic sites, in the region of 130-140 kJ mol^{-1}. Table 4.3 shows data for conventionally calcined Cu$_{1.32}$Mg$_{2.98}$Al$_2$(CO$_3$)(OH)$_{16}$.4H$_2$O which are seen to exhibit medium strength sites in the region of 100-130 kJ mol^{-1}.

There are small differences in the way the specific surface areas of the calcined materials change with calcination temperature. The specific surface areas of calcined Cu$_{1.32}$Mg$_{2.98}$Al$_2$(CO$_3$)(OH)$_{16}$.4H$_2$O are higher than those of parent LDHs and it appears that they reach a maximum value at a temperature of 400-500 °C or below, decreasing as the calcination temperature is increased above this value. In general, the surface areas of materials calcined using microwaves are lower than for those calcined conventionally.

Calcination temperature / °C	^{a}CO$_2$ adsorbed / mmol g^{-1}	^{b}-ΔH^0_{ads} (CO$_2$) / kJ mol^{-1}	Surface area / m^2 g^{-1}
400	0.17	136	99
500	0.16	132	84
550	0.19	139	72

Table 4.2 - Surface basicity characteristics and surface areas of **microwave** calcined Cu$_{1.32}$Mg$_{2.98}$Al$_2$(CO$_3$)(OH)$_{16}$.4H$_2$O from flow CO$_2$ adsorption calorimetry. ^{a}Total amount irreversibly adsorbed, (above 90 kJ mol^{-1}). ^{b}Average ΔH^0_{ads} for all pulses above 90 kJ mol^{-1} (±4).

Calcination temperature / °C	^{a}CO$_2$ adsorbed / mmol g^{-1}	^{b}-ΔH^0_{ads} (CO$_2$) / kJ mol^{-1}	Surface area / m^2 g^{-1}
500	0.036	98	159
600	0.060	128	137
750	0.19	128	104
800	0.10	132	59

Table 4.3 - Surface basicity characteristics and surface areas of **conventionally** calcined Cu$_{1.32}$Mg$_{2.98}$Al$_2$(CO$_3$)(OH)$_{16}$.4H$_2$O from flow CO$_2$ adsorption calorimetry. ^{a}Total amount irreversibly adsorbed, (above 90 kJ mol^{-1}). ^{b}Average ΔH^0_{ads} for all pulses above 90 kJ mol^{-1} (±4).

The CO_2 adsorption calorimetry data for the microwave calcined LDHs at 400, 500 and 550 °C is combined and shown in Figures 4.12 and the data for conventionally calcined LDHs at 500 to 800 °C is shown in Figure 4.13. Initial enthalpies for all calcined catalysts are in good agreement with the literature for calcined LDHs [69,70] and range between 95 and 140 kJ mol⁻¹. It can be seen that there are higher concentrations of available basic sites and strengths for catalysts calcined using microwave. For comparison, the CO_2 adsorption calorimetry data for $Mg_{7.2}Al_2(CO_3)(OH)_{16}.4H_2O$ calcined at 500 °C under both microwave and conventional heating is shown in Figure 4.14. These show clearly that 1) copper containing LDHs are more basic than Mg/Al LDHs and 2) microwave calcination for the copper containing LDHs invariably generate higher surface basicity than conventional calcination.
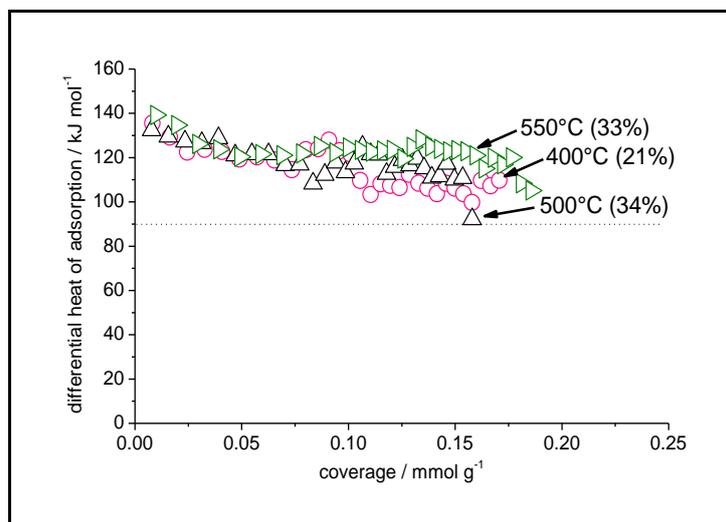
Figure 4.12 - Differential molar enthalpy of CO_2 adsorption against amount of CO_2 adsorbed for $Cu_{1.32}Mg_{2.98}Al_2(CO_3)(OH)_{16}.4H_2O$ calcined under microwave heating. (Conversion of tributyrin after 150 mins is displayed in brackets to allow comparisons of basicity with catalytic activities).
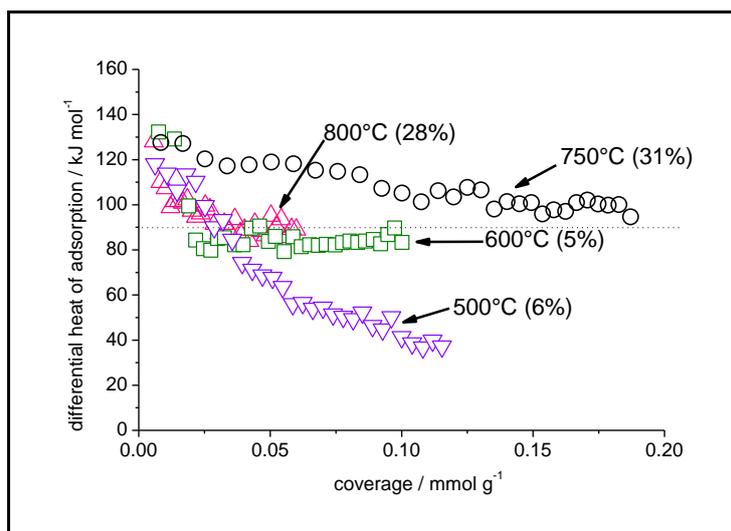
Figure 4.13 - Differential molar enthalpy of CO$_2$ adsorption against amount of CO$_2$ adsorbed for calcined Cu$_{1.32}$Mg$_{2.98}$Al$_2$(CO$_3$)(OH)$_{16}$.4H$_2$O calcined under conventional heating. Conversion of tributyrin after 150 mins is displayed in brackets.
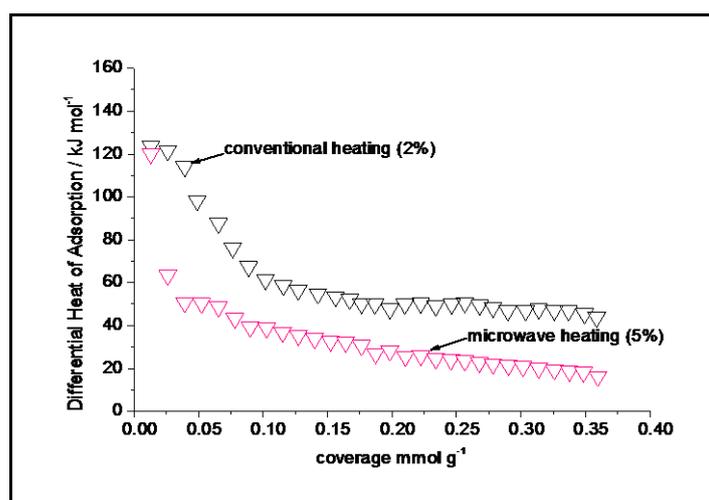
Figure 4.14 – Differential molar enthalpy of CO$_2$ adsorption against amount of CO$_2$ adsorbed for calcined Hydrotalcite Mg$_{7.2}$Al$_2$(CO$_3$)(OH)$_{16}$.4H$_2$O heated at 2 ^{0}C min^{-1} to 500 °C. Conversion of tributyrin after 150 mins is displayed in brackets.

The strength of basic sites on calcined Cu$_{1.5}$Mg$_{4.5}$Al$_2$(CO$_3$)(OH)$_{16}$.4H$_2$O is evidently enhanced by microwave calcination. It is possible that the basic sites are formed at surface defects and that the different mode of decomposition promoted by microwaves generates more of these defect sites than conventional heating. This is not easy to justify however, as the higher crystallinities generated by microwave

heating suggest that there might be fewer, not more, surface defects through this mode of heating. To understand this, it may be helpful to study hydrotalcites with other metals substituted for magnesium. The fact is that copper-containing hydrotalcites are generally thought to show lower basicities than hydrotalcites with many other substituent metals, including lanthanum and nickel [71].

The reaction of tributyrin with methanol was chosen to test the activity of the mixed oxide catalysts. The results of catalytic testing were mentioned briefly above, in which conversion of tributyrin after a defined period of time was compared with basicity. In this section, catalytic activities are considered in more detail. In all cases, the reaction was found to be pseudo-first order with respect to tributyrin in the initial period and rate constants were determined over the first 150 minutes from plots of ln(100-% conversion of tributyrin) vs. time. Kinetic data is presented as pseudo-first order rate constants.

$Cu_{1.32}Mg_{2.98}Al_2(CO_3)(OH)_{16}.4H_2O$ LDH was calcined conventionally up to 1000 °C and it can be seen in Table 4.4 that the most active catalyst arose from a conventional calcination temperature of 750 °C. Furthermore, when the material was calcined using microwaves at 500, 600 and 750 °C, the rate constant was significantly higher than for any calcination temperature using conventional heating.

It is interesting that, when calcined conventionally, there is a profound dependence of rate constant on calcination temperature, with a clear maximum at 700 °C. And in contrast, with microwave calcination, the rate constant is relatively insensitive to calcination temperature. At a calcination temperature of 500 °C, the difference between the activities of materials calcined in the two ways is very large, with the microwave prepared materials being almost eight times more active than the conventionally calcined precursor.

$Cu_{1.32}Mg_{2.98}Al_2(CO_3)(OH)_{16}.4H_2O$	Calcination temperature / °C	^ak /s^{-1}
Conventional	500	0.69
	600	0.57
	700	**3.42**
	750	**5.52**
	800	2.87
	900	0.53
	1000	0.52
Microwave	**400**	**2.91**
	500	**3.99**
	550	**3.92**
	600	**3.96**
	700	**4.99**

Table 4.4 – Rate constant (conversion of tributyrin) vs. calcination temperature for $Cu_{1.32}Mg_{2.98}Al_2(CO_3)(OH)_{16}.4H_2O$.

The rate of reaction, together with the amount of CO_2 adsorbed irreversibly (as a measure of the concentration of surface basic sites), is plotted against calcination temperature, for $Cu_{1.32}Mg_{2.98}Al_2(CO_3)(OH)_{16}.4H_2O$ for conventional heating (Figure 4.15). There is a strong correlation suggesting that catalytic activity is dependent on the concentration of basic sites on the catalyst.
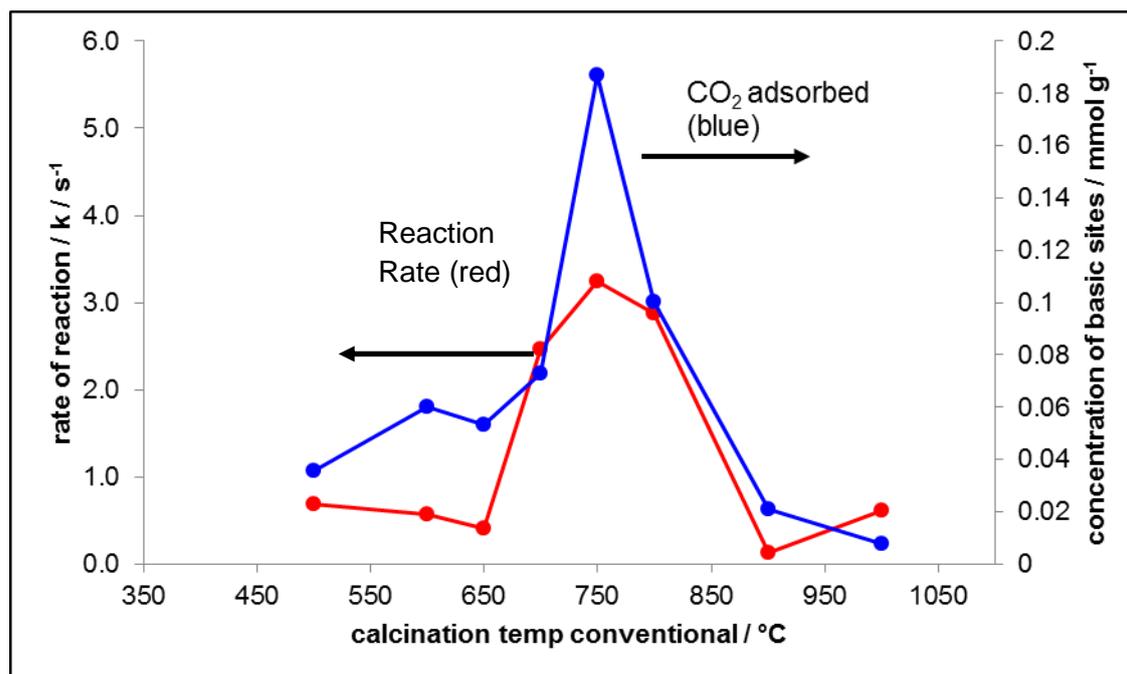
Figure 4.15 – Dependence of rate of tributyrin reaction and total CO_2 coverage for $Cu_{1.32}Mg_{2.98}Al_2(CO_3)(OH)_{16}.4H_2O$ calcined under conventional heating on calcination temperature.

Figure 4.16 shows data the reaction rate and the amount of irreversibly adsorbed CO_2 for $Cu_{1.32}Mg_{2.98}Al_2(CO_3)(OH)_{16}.4H_2O$ plotted against calcination temperature using temperature controlled microwave heating. Both the rate of reaction and the concentrations of basic sites can be seen to increase with the calcination temperature, again showing a reasonable correlation between concentration of basic sites and catalytic activity. A comparison between the data in Figure 4.15 and 4.16 shows clearly that, overall, the very much higher concentrations of basic sites generated by microwave calcination translate into much higher catalytic activities.
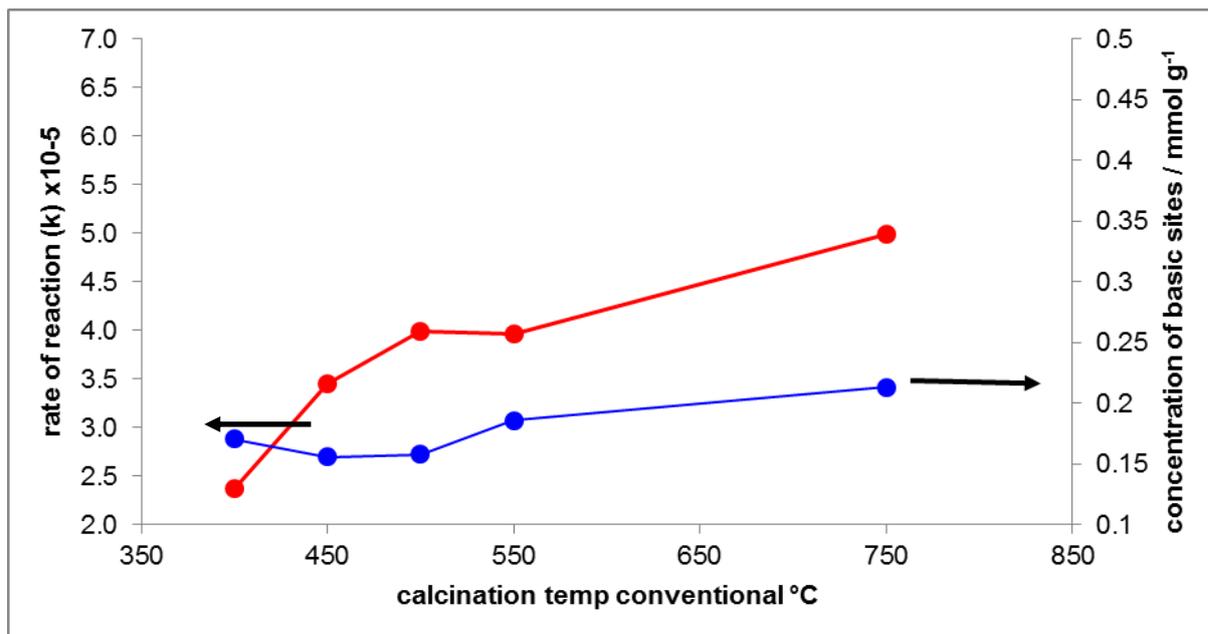
Figure 4.16 – Dependence of rate of tributyrin reaction and total CO$_2$ coverage for Cu$_{1.32}$Mg$_{2.98}$Al$_2$(CO$_3$)(OH)$_{16}$.4H$_2$O calcined under microwave heating on calcination temperature.

The low copper LDH, Cu$_{0.64}$Mg$_{1.58}$Al$_2$(CO$_3$)(OH)$_{16}$.4H$_2$O, was calcined conventionally up to 1000 °C and it can be seen in Table 4.5 that the most active catalyst arose from a calcination temperature of 500 °C or 600 °C, within experimental error. Above this calcination temperature, the rates of reaction were slightly lower. This is consistent with the CO$_2$ adsorption calorimetric results which showed that the basicity of this material was not significantly enhanced through the use of microwaves for calcination. It is not clear why microwave calcination is not advantageous with the low copper material. It is possible that the copper is crucial to interaction with microwaves and that the copper content is too low to result in significant interaction in the low copper LDH. If this is the case then an explanation for the slightly higher activity of the conventionally calcined LDHs might be that these materials have higher surface areas than the microwave-calcined materials. In other words, differences in specific surface areas between catalysts calcined in the two ways might override differences associated with the effects of microwave calcination. This is opposite to what happens with the high copper LDH, for which microwave calcination generates the higher basicity and higher activity, despite resulting in lower surface areas for the mixed oxides (Table 4.2 and 4.3).

$Cu_{0.64}Mg_{1.58}Al_2(CO_3)(OH)_{16}.4H_2O$	Calcination temperature / °C	[a]k / s^{-1}	Surface area / $m^2 g^{-1}$
Conventional	500	0.60	184
	600	0.56	156
	700	0.48	151
	800	0.44	61
	900	0.26	12
	1000	0.15	6
Microwave	400	0.32	148
	500	0.16	37
	600	0.22	20
	650	0.18	26

Table 4.5 – Initial rate constant k (conversion of tributyrin) vs. temperature of calcination of $Cu_{0.64}Mg_{5.8}Al_2(CO_3)(OH)_{16}.4H_2O$ using conventional and microwave heating. [a]Obtained for the first 20 minutes of the reaction. k values have associated confidence limits of ± 0.05.

4.4.4 – Single Metal Hydroxides

For comparison with the LDHs, the single pure oxides of aluminium, magnesium and copper were prepared by calcining the hydroxides of these metals. These hydroxides were prepared using the same methods used to prepare the LDHs, that is by precipitation from solutions of corresponding nitrates through addition of NaOH. These hydroxides were then calcined using both conventional and microwave heating.

The hydroxides were characterised by powder XRD. Figures 4.17 and 4.18 show the XRD pattern of magnesium hydroxide and aluminium hydroxide respectively. The copper (II) hydroxide spontaneously dehydrated to form the oxide (Figure 4.19). On calcination, the aluminium, magnesium and copper oxides were tested as catalysts in the tributyrin reaction. Under no calcination conditions was any activity detected for any of the three metal oxides, confirming that the higher base catalytically activity of the LDH-derived metal oxides is linked to the intimate mixing of the metal oxides that arises on their calcination.
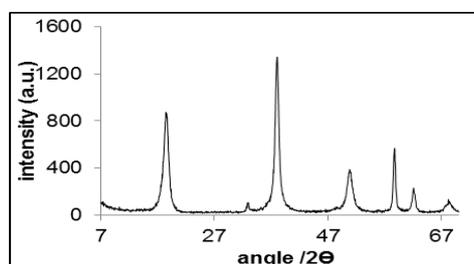
Figure 4.17– Powder XRD pattern of Mg(OH)$_2$, synthesised from magnesium nitrate
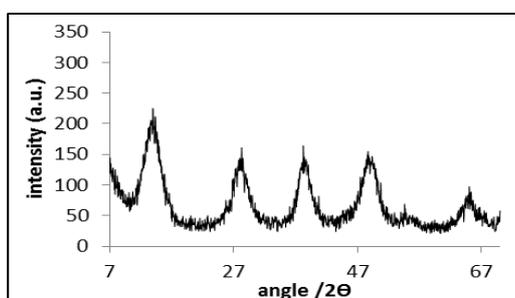
Figure 4.18 – Powder XRD pattern of Al(OH)$_3$, synthesised from aluminium nitrate
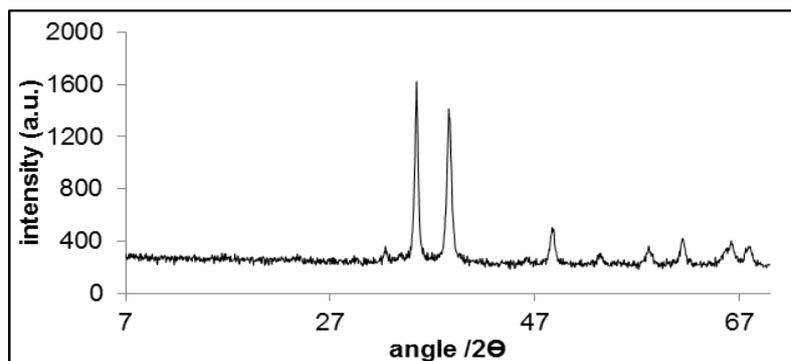
Figure 4.19 – Powder XRD pattern of as-synthesised CuO.

4.5 – Conclusions

The overall results, based on the two levels of copper containing LDH, show that there are major differences between the products of calcination under the two heating regimes. Conclusions here are based on the high-copper hydrotalcite, on the basis that the less conclusive results from the low-copper hydrotalcite are a direct consequence of the low copper concentration and the poor coupling of the salts with the microwave field.

Material prepared using microwaves are more crystalline, show higher basicity and higher base catalytic activity, as well as exhibiting a phase, Cu_2MgO_3, which is not detected under conventional heating at any temperature. This is despite the lower surface areas of the microwave calcined products. It is clear that the relative rates at which CuO and MgO are formed under microwave heating, and the subsequent conversions to spinel and to Cu_2MgO_3, are different under the two heating regimes. The general observation is that changes occur at nominally lower temperatures under microwave heating. It is possible that sample temperatures in the microwave cavity, which are necessarily taken at the surface of the solid, are not representative of the bulk temperatures, but the differences in products and relative product yields, together with the resultant differences in physical and chemical properties, suggest that there are mechanistic differences in how the two heating regimes bring about the solid state transformations in these layered hydroxide materials.

The differences in the way the products of calcination are formed under the two heating methods may be linked to the different temperature gradients developed in solid samples as they are heated in a microwave field, and the relative rates at which dehydration, dehydroxylation and decarbonation occur in the bulk and near the surface of the solid. It is not unreasonable to suppose that the structural disruption, and the different water vapour pressures and CO$_2$ partial pressures to which regions of the sample would be exposed, could affect the equilibria between one phase and another as the temperature is increased.

The selective formation of Cu$_2$MgO$_3$ under microwave heating is another possibly important difference between the effects of the two heating methods. A conceivable explanation is that microwaves induce transient hot spots where the local composition of the material is momentarily susceptible to particularly strong coupling with the microwave field. In this way, undetected temperatures very much higher than those detected by the pyrometer may exist, perhaps providing conditions favourable for the formation of this mixed oxide.

Another possible contributor may be associated with the exchangeable carbonate ions and that fact that, although most of the carbonate ion is decomposed below 400 ^{o}C, complete decarbonation normally requires much higher temperatures, up to 800 ^{o}C.[64]. There is infrared spectral evidence for a small proportion of the carbonate ion in the interlayer region becoming chemically grafted to the layered hydroxide, [65] and it is possible that it is these grafted carbonate ions that are thermally-resistant and responsible for the high temperature required to decompose them. Although speculative, it is not impossible that this last stage of decarbonation is promoted by microwave heating and that it is the complete removal of interlayer carbonate anions that then permits the crystallisation of mixed oxides that are not formed otherwise.

The results suggest that controlled microwave heating might be of value in calcining precursors to produce active catalysts. The feedback-controlled and process-controlled methods used here are essential for this and this work demonstrates that there may be useful applications of these methods in catalyst preparation.

References

[1]   A. Tschöpe, J. Markmann, P. Zimmer, R. Birringer, A.V. Chadwick, *Chem. Mater.*, 17 (2005) 3935–3943.

[2]   Thermochemical Processing of Biomass: Conversion into Fuels, Chemicals and Power (Hardback) Edited by R. C. Brown and C. V. Stevens, 104.

[3]   M. M. V. M. Souza, K. A. Ferreira, O. R. de Macedo Neto, N. F.P. Ribeiro, Martin Schmal, *Catal. Today.*, 133 (2008) 750-754.

[4]   E. M. Fuentes, A. Júnior, T. Silva, J. M. Assaf, M. C. Rangel, *Catal. Today.*, 171 (2011) 290-296.

[5]   H. Zeng, Z. Feng, X. Deng, Y. Li, *Fuel.*, 87 (2008) 3071-3076.

[6]   S. M. Auer, S. V. Gredig, R. A. Köppel, A. Baiker, *J. Mol. Catal.*, 141 (1999) 193-203.

[7]   O. Novelo-Peralta, G. González, G.A. Lara-Rodríguez, *Mater. Charact.*, 59 (2008) 773-780.

[8]   M. Crivello, C. Pérez, E. Herrero, G. Ghione, S. Casuscelli, E. Rodríguez-Castellón, *Catal. Today.*, 107-108, (2005) 215-222.

[9]   L. Zhang, J. Liu, W. Li, C. Guo, J. Zhang *J. Nat. Gas Chem.*, 18 (2009) 55-65.

[10]   M. Crivello, C. Pérez, J. Fernández, G. Eimer, E. Herrero, S. Casuscelli, E. Rodríguez-Castellón, *Appl. Catal. A-Gen.*, 317 (2007) 11-19.

[11]   D. Meloni, R. Monaci, V. Solinas, A. Auroux, E. Dumitriu, *Appl. Catal. A-Gen.*, 350 (2008) 86-95.

[12]   M. Crivello, C. Pérez, E. Herrero, G. Ghione, S. Casuscelli, E. Rodríguez-Castellón, *Catal. Today.*, 107-108 (2005) 215-222.

[13]   B. Monteiro, S. Gago, S. S. Balula, A. A. Valente, I. S. Gonçalves, M. Pillinger, *J. Mol. Catal.*, 312 (2009) 23-30.

[14]   S. Tanasoi, N. Tanchoux, A. Urdă, D. Tichit, I. Săndulescu, F. Fajula, I. Marcu *Appl. Catal. A-Gen.*, 363 (2009) 135-142.

[15]   Z. Zhu, Z. Liu, S. Liu, H. Niu, T. Hu, T. Liu, Y. Xie, *Appl. Catal. B.,* 26 (2000) 25-35.

[16]   R Nickolov, T Tsoncheva, D Mehandjiev, *Fuel.*, 81 (2002) 203-209.

[17]   Y. Sakata, N. Kouda, Y. Sakata, H. Imamura, *Stud. Surf. Sci. Catal.*, 143 (2000) 397-405.

[18]   C.M. Pradier, H. Vikström, J. Paul, *Stud. Surf. Sci. Catal.*, 96 (1995) 655-660.

[19]   A.M. Youssef, L.B. Khalil, A.A. Attia, Th. El-Nabarawy, *Mater. Lett.*, 24 (1995) 253-259.

[20]   H.Pan, Z. Li, Q. Xia, H. Xi, C. He *Catal. Comm.*, 10 (2009) 1166-1169.

[21]   R. Shannon, *Acta Crystallogr., Sect. A.*, 32 (1976) 751-767.

[22]   A. Vaccari, *Catal. Today.*, 41 (1998) 53-71.

[23]   J. S. Valente, J. Hernandez-Cortez, M. S. Cantu, G. Ferrat, E. López-Salinas, *Catal. Today.*, 150 (2010) 340-345.

[24]   L. Dussault, J.C. Dupin, E. Dumitriu, A. Auroux, C. Guimon, *Thermochim. Acta.*, 434 (2005) 93-99.

[25]   Hui-Fen Wu, Leo Brewer, *J. Alloys Compd.*, 247 (1997) 1-8.

[26]   K. Parida, T. Mishra, *J. Colloid Interface Sci.*, 179 (1996) 233-240*.*

[27]   Z. Zhao, Y. Yamada, A. Ueda, H. Sakurai, T. Kobayashi, *Catal. Today.*, 93-95 (2004) 163-171.

[28]   S. Casenave, H. Martinez, C. Guimon, A. Auroux, V. Hulea, A. Cordoneanu, E. Dumitriu, *Thermochim. Acta.*, 379 (2001) 85-93.

[29]   D. Meloni, R. Monaci, V. Solinas, A. Auroux, E. Dumitriu, *Appl. Catal. A-Gen.*, 350 (2008) 86-95.

[30]   A. Fási, I. Pálinkó, Á. Gömöry, I. Kiricsi, *J. Mol. Catal. A.,* 208 (2004) 307-311.

[31]   W. Cheng, W. Wang, Y. Zhao, L. Liu, J. Yang, M. He, *Appl. Clay Sci.*, 42 (2008) 111-115.

[32]   Z. Helwani, M.R. Othman, N. Aziz, J. Kim, W.J.N. Fernando, *Appl. Catal. A-Gen.*, 363 (2009) 1-10.

[33]   J.F. Puna, J.F. Gomes, M. Joana N. Correia, A.P. Soares Dias, J.C. Bordado, *Fuel*, 89 (2010) 3602-3606.

[34]   B. M. E. Russbueldt, W. F. Hoelderich, *J. Catal.*, 271 (2010) 290-304.

[35]   J.M. Encinar, J.F. González, A. Pardal, G. Martínez, *Fuel Process. Technol.*, 91 (2010) 1530-1536.

[36]   R. Chakraborty, S. Bepari, A. Banerjee, *Chem. Eng. J.*, 165 (2010) 798-805.

[37]   X. Yu, Z. Wen, H. Li, S.Tu, J. Yan, *Fuel.*, 90 (2011) 1868-1874.

[38]   M. J. Kim, S. M. Park, D. R. Chang, G. Seo, *Fuel Process. Technol.*, 91 (2010) 618-624.

[39]   J. Kansedo, K. T. Lee, S. Bhatia, *Biomass Bioenergy.*, 33 (2009) 271-276.

[40]   Y. Liu, E. Lotero, J. G. Goodwin Jr., X. Mo, *Appl. Catal. A-Gen.*, 331 (2007) 138-148.

[41]   K.G. Georgogianni, A.P. Katsoulidis, P.J. Pomonis, M.G. Kontominas, *Fuel Process. Technol.*, 90 (2009) 671-676.

[42]   I. Cota, E. Ramírez, F. Medina, G. Layrac, R. Chebout, D. Tichit, *Catal. Today.*, 152 (2010) 115-118.

[43]   V. Rives, M. A. Ulibarri, *Coord. Chem. Rev.*, 181 (1999) 61-120.

[44]   K. Rajkumar, S. Aravindan, *J. Mater. Process. Technol.*, 209 (2009) 5601-5605.

[45]   X. H. Liao, N. Y. Chen, S. Xu, S. B. Yang, J. J. Zhu, *J. Cryst. Growth.*, 252 (2003) 593-598.

[46]   S. Albertazzi, F. Basile, A. Vaccari, *Interface Sci. Technol.*, 1 (2004) 496-546.

[47]   G. Bond, R. B. Moyes, D. A. Whan, *Catal. Today.*, 17 (1993) 427-437.

[48]   K. Saitou, *Scr. Mater.*, 54 (2006) 875-879.

[49]   S.E. Hsu, J.Y. Wang, C.M. Li, T.W. Huang, K.L. Wang, *Physica C.,* 207 (1993) 159-166.

[50]   H.E. Cross, D.R. Brown, *Catal. Comm.*, 12 (2010) 243-245.

[51]   L. Dussault, J.C. Dupin, E. Dumitriu, A. Auroux, C. Guimon, *Thermochim. Acta.*, 434 (2005) 93-99.

[52]   A. K. Endalew, Y. Kiros, R. Zanzi, *Biomass Bioenergy.*, 35 (2011) 3787-3809.

[53]   A. Corma, S. Iborra, *Adv. Catal.*, 49 (2006) 239-302.

[54]   D. G. Cantrell, L. J. Gillie, A. F. Lee, K. Wilson, *Appl. Catal. A-Gen.*, 287 (2005) 183-190.

[55]   B. M. Choudary, M. Lakshmi Kantam, C. V.Reddy, S. Aranganathan, P. L. Santhi, F Figueras, *J. Mol. Catal. A.,* 159 (2000) 411-416.

[56]   C. García-Sancho, R. Moreno-Tost, J. M. Mérida-Robles, J. Santamaría-González, A. Jiménez-López, *Catal. Today.*, 167 (2011) 84-90.

[57]   C. Forano, *Interf. Sci. Technol.*, 1 (2004) 425-458.

[58]   Y. Wang, H. Gao *J. Colloid Interf. Sci.,* 301 (2006) 19-26.

[59]   F. Kovanda, T. Grygar, V. Dorničák, T. Rojka, P. Bezdička, K. Jirátová, *Appl. Clay Sci.*, 28 (2005) 121-136.

[60]   M. V. Veidis, G. H. Schreiber, T. E. Gough, G. J. Palenik. *J. Am. Chem. Soc.*, 91 (1969) 1859–1860.

[61]   O.D. Pavel, R. Zăvoianu, R. Bîrjega, E. Angelescu, *Catal. Commun.*, 12 (2011) 845-850.

[62]   T. Hibino, H. Ohya*, Appl. Clay Sci.*, 45, (2009) 123-132.

[63]   J. L. Shumaker, C. Crofcheck, S. A. Tackett, E. Santillan-Jimenez, T. Morgan, Y. Ji, M. Crocker, T. J. Toops, J. *Appl. Catal. B,* 82 (2008) 120-130.

[64]   H.G. El-Shobaky, J. Therm. Anal & Calor. 85 (2006) 32-327.

[65]   M. Leon, E. Diaz, S. Bennici, A. Vega, S. Ordonez, A. Auroux, *Ind. Eng. Chem. Res.*, 49 (2010) 3663-3671.

[66]   T. Stanimirova, I. Veriglov, G. Kirov, N. Petrova, *J. Mater. Sci.* , 34 (1999) 4153-4161.

[67]   P.F. Siril, A.D. Davison, J.K. Randhawa, D.R. Brown, *J. Mol. Catal. A.,* 267 (2007) 72-78.

[68]   L. Damjanovic, A. Auroux, *Handbook of Thermal Analysis and Calorimetry*, 5 (2008) 387-438.

[69]   H. A. Prescott, Z. Li, E. Kemnitz, A. Trunschke, J. Deutsch, H. Lieske, A. Auroux*, J. Catal.*, 234 (2005) 119-130.

[70]   R. Bouarab, O. Cherifi, A. Auroux, *Thermochim. Acta.*, 434 (2005) 69-73.

Chapter 5

Synthesis and Applications of LDHs containing Nickel, Cobalt and Iron

Chapter 5

5.1 – Objectives

The objectives of the work reported here are:

1. to incorporate transition metals into the conventional LDH, hydrotalcite,
2. to develop transition metal doped LDHs that possess catalytic activity and basicity superior to $Mg_{7.2}Al_2(CO_3)(OH)_{16}.4H_2O$ (hydrotalcite).

Calcination procedures that were applied in Chapters 3 and 4 using both microwaves and conventional heating were applied to transition metal LDHs in this chapter.

5.2 – Introduction

5.2.1 - Transition metal catalysts

Transition metals are frequently used as the basis of catalysts [1-5]. They have the ability to change oxidation states, and the very name of these types of metals is directly linked to catalysis, as a catalyst is defined as a substance that increases the rate of a reaction by lowering the activation energy or providing an alternative reaction route, via an alternative *transition* state [6]. The nature of a transition metal is that it conforms to the very principles of catalysis.

5.2.1.1 - Transition metals in Layered Double Hydroxides

As oxides, transition metals often exhibit catalytic properties, in part because of their variable oxidation states [7] but also because transition metal oxides often feature large numbers of surface defects and cationic and anionic vacancies which result in acidic, basic and acid-base paired catalytic sites. It is often through these properties that catalyst (or precursor) synthesis can be tuned to the reaction requiring catalysts, i.e. through the generation of strong/weak acid/base sites [8-14].

LDHs which incorporate transition metals upon calcination can produce transition metal-containing mixed oxides [16-20]. The transition metal oxide is likely to be highly dispersed in the overall solid lattice.

In this work nickel was chosen for building into an LDH because of its many uses in catalysis as a single oxide, being thermally stable and able to be formed by the calcination of its hydroxide [21-24]. Of importance to the synthesis of LDHs, nickel hydroxide is reliable in that nickel is stable in the +2 oxidation state and the hydroxide can be precipitated out of aqueous solution with NaOH. Nickel hydroxide cannot be precipitated from nickel nitrate with ammonia or by the hydrolysis of urea because it will form an ammine complex with ammonia and also the pH at which precipitation occurs is at about 9 [25].

Cobalt was chosen to be incorporated into the lattice of an LDH in part because cobalt oxide has been used successfully as a catalyst for biodiesel production [26-28]. Simple cobalt-containing LDHs do not exist in nature and the only naturally occurring cobalt-containing LDH compound is $Ni_6Co_2(CO_3)(OH)_{16} \cdot 4H_2O$ in which cobalt exists in oxidation state 3+ [29]. Cobalt is very stable in terms of oxidation state when in the form of Co^{2+}.

Iron has been incorporated in the Mg/Al lattice by many workers [30-31] and investigated in catalysis. If an iron (III) salt is used in the synthesis of an LDH, it is incorporated in the lattice in the +3 oxidation state, substituting for Al^{3+}. Fe^{2+} has been seen to exist in the lattice in addition to Fe^{3+} but in very small quantities [31].

5.2.1.1.1 - Transition metal oxides in the transesterification of tributyrin

The transesterification of tributyrin reaction can be catalysed by either acid or base. However, it is known that the rate of reaction using an acid is considerably lower than if a base is used [32]. However, as discussed in Chapter 1, waste vegetable oil can contain free fatty acids (FFAs) that should be esterified using an acid catalyst initially. The idea of using a single acid catalyst for both the pre-esterification and the transesterification steps will be considered in this chapter.

The transition metals used in this chapter were chosen in terms of the high activity anticipated when incorporated into the precursor LDH. As with the previous two chapters, the calcination process to achieve the active mixed oxide catalysts will be compared using both conventional and microwave heating. Previous work has involved many conventionally calcined transition metal LDHs for use as catalysts for the transesterification reaction, but the use of microwave heating for the calcination process has not been studied [33-41].

Incorporation of one or more transition metal into the hydrotalcite lattice is common in catalysis [42]. Mixed metal oxides formed from the calcination of $Mg_{7.2}Al_2(CO_3)(OH)_{16}.4H_2O$ exhibit basicity as seen in Chapter 3. In many reactions it has been noted that when hydrotalcite has transition metals incorporated, changes in basicity and acidity occur. Carlini et al [43] studied the incorporation of Pd, Rh, Ni and Cu into an LDH for use in the condensation reactions of methanol and n-propanol, to replace the non-environmentally friendly copper chromite. For comparison, the mixed metal oxides were simulated using physical mixtures of the pure oxides. Results showed that the catalytic activities were zero for the physical mixtures and all of the calcined LDHs showed similar activities and selectivities to copper chromite. These results suggest that the original layered structure enables configuration of the metal oxides to be significantly different to the single oxides mechanically mixed, as reported previously in this thesis for Mg/Cu/Al LDHs.

The transition metals used in this work are iron, cobalt and nickel (copper is reported in the previous chapter). There are existing reports of all four being successfully incorporated into the LDH lattice. Nickel and cobalt invariably exhibit the +2 oxidation states [44-46] but iron can be +2 or +3, or both in the same lattice [47]. Interestingly, in nature, LDHs exist with iron in the lattice but iron exists only in the +3 state in these compounds [30,31]. Examples are $Ni_6Fe_2(CO_3)(OH)_{16}.4H_2O$ (pyroaurite) and $Ni_6Fe_2(CO_3)(OH)_{16}.4H_2O$ (reevesite).

Cobalt has been incorporated in the LDH lattice previously and the Co^{2+} containing LDH has been used as a catalyst in the reaction of canola oil with ethanol to produce biodiesel [48]. It was found that cobalt played a major role in the increased activity achieved.

The full and partial isomorphic substitution of magnesium by nickel has been successfully achieved using standard methods of synthesis [49-52]. This relatively easy process is achieved because the ionic radius of nickel is very close to that of magnesium, (Table 5.1). It is interesting to note that there is a naturally occurring nickel LDH, takovite, in which nickel is the only divalent cation, $Ni_6Al_2(CO_3)(OH)_{16}.4H_2O$ [53].

For highly active catalysts a requirement is to have even dispersion of the transition metal and also a high surface area. Feng et al [40] looked at the morphology of nickel LDHs and reported high surface areas and enhanced metal dispersions, in addition to very well defined pore sizes. Evidently, all three aspects impacted on the catalytic activities of the corresponding mixed metal oxides formed from calcination.

Cation	Ionic radius (Å)
Mg^{2+}	0.72
Fe^{2+}	0.78
Co^{2+}	0.75
Ni^{2+}	0.69
Cu^{2+}	0.73
Fe^{3+}	0.65
Al^{3+}	0.54

Table 5.1 – Ionic radii of M^{2+} and M^{3+} cations [54].

5.2.2 – Summary

Several transition metal-doped hydrotalcites were synthesised and characterised relating their structure to activities of the mixed oxides produced after calcination. Transition metals that were incorporated were iron, cobalt and nickel. The corresponding mixed metal oxides formed from calcination of the LDHs were characterised using N_2 adsorption, powder XRD, SEM-EDS and adsorption

microcalorimetry using CO_2. Catalytic activity was tested using the transesterification reaction of tributyrin with methanol. Two different methods of calcination were studied, conventional and microwave heating.

5.3 – Experimental

5.3.1 – Synthesis of $Fe_xMg_{6-x}Al_2(CO_3)(OH)_{16}.4H_2O$, $Co_xMg_{6-x}Al_2(CO_3)(OH)_{16}.4H_2O$ and $Ni_xMg_{6-x}Al_2(CO_3)(OH)_{16}.4H_2O$

LDHs were prepared using the same method as in 4.3.1, the precipitation method (using $NaOH/Na_2CO_3$ as the precipitating agents). The molar ratio used in the synthesis of the transition metal doped LDHs was M^{2+}/M^{3+} = 3/1 (with Mg^{2+}/M_{TM}^{2+} = 1/1), e.g. target stoichiometries were $Co_3Mg_3Al_2(CO_3)(OH)_{16}.4H_2O$, $Ni_3Mg_3Al_2(CO_3)(OH)_{16}.4H_2O$. For iron the target stoichiometry (assuming Fe^{3+}) was $Mg_6Al_1Fe_1(CO_3)(OH)_{16}.4H_2O$.

The LDHs were prepared by slowing adding simultaneously a 250 ml solution of magnesium, aluminium and the corresponding transition metal nitrates (total of 1.0 mol dm^{-3}) (99.9 % Aldrich) and a 250 ml sodium carbonate solution (0.625 mol dm^{-3}) (99.9 % Aldrich) into a 1000 ml beaker. The pH of the solution was adjusted to 9.0 with sodium hydroxide (0.20 mol dm^{-3}) (99.9 % Aldrich) for precipitation of the metal hydroxides. Transition metal nitrates used were $Co(NO_3)_2.6H_2O$, $Ni(NO_3)_2.6H_2O$ and $Fe(NO_3)_3.9H_2O$ (99.9 % Aldrich). Care was taken to remove any residual sodium in the lattice with washing using hot deionised water and once the pH had stabilised the LDHs were filtered. LDHs were dried overnight in an oven at 100 °C and afterwards kept in a desiccator to minimise any contact with moisture from the air.

5.3.2 – Characterisation

Sodium contents of the transition metal oxides were determined by atomic absorption spectroscopy. Catalytic activities were measured in the transesterification of tributyrin with methanol, monitoring the conversion of tributyrin

(as described in 4.4.2). Powder X-ray diffraction (P-XRD) patterns were obtained. Elemental analysis was performed using SEM-EDS, to determine the relevant formula for each LDH. Surface areas were obtained using N_2 adsorption.

Catalytic activity was measured as in previous chapters in the transesterification reaction of tributyrin with methanol. Further details of the experimental conditions can be found in 2.12.1. Surface basicities were measured by CO_2 flow adsorption microcalorimetry and surface acidity by NH_3 flow adsorption calorimetry as described in Chapter 2. In a typical experiment, the catalyst (~50 mg) was activated under flowing helium, for one hour at 150 °C. The sample was then cooled to the adsorption temperature of 120 °C and small pulses of the probe gas were injected at regular intervals. Further details can be found in 2.13.1.

5.3.3 – Calcination

5.3.3.1 – Conventional heating

All LDHs were calcined in a conventional muffle furnace at 500 °C, 600 °C, 700 °C, 800 °C, 900 °C and 1000 °C for 4 hours in static air. The heating rate used was 2 °C min^{-1}. The mixed metal oxides were allowed to cool at the same rate and then transferred to a desiccator to prevent water re-adsorption by the oxide. It was important to do this as it is known that the mixed metal oxides can convert back to the LDHs in the presence of water.

5.3.3.2 – Microwave heating

Microwave calcination of the LDHs was carried out in air in a feedback-controlled manner to 500 °C, at a constant heating rate of 2 °C min^{-1}. The rate of heating was the same throughout all experiments using microwave and conventional heating to ensure comparative data. A more detailed description of this technique can be found in Chapter 2 (section 2.8).

5.4 – Results and discussion

5.4.1 – Elemental analysis

Elemental analysis of the transition metal LDHs was carried out using the EDS facility on a JEOL SEM. The data was interpreted in terms of the amount of Al, Mg and the transition metal in the LDH. The molar ratios of these metals were converted to stoichiometries and these can be seen in Table 5.2. Results indicate that the elemental composition of all the transition metal LDHs are close to the metal nitrate compositions employed in the synthesis step. For nomenclature purposes, the LDHs will be identified using simply the stoichiometric ratios of the metal ions in the materials.

With reference to $Mg_{5.82}Al_{1.12}Fe_{0.88}(CO_3)(OH)_{16}.4H_2O$, it was assumed that all the incorporated ion was in oxidation state +3. Many other workers have shown that Fe^{3+} does indeed become incorporated in this oxidation state [46-47].

Target composition	Measured stoichiometry
$Ni_3Mg_3Al_2(CO_3)(OH)_{16}.4H_2O$	$Ni_{4.4}Mg_{2.96}Al_2$
$Co_3Mg_3Al_2(CO_3)(OH)_{16}.4H_2O$	$Co_{2.24}Mg_{1.26}Al_2$
$Mg_6Al_1Fe_1(CO_3)(OH)_{16}.4H_2O$	$Mg_{5.82}Al_{1.12}Fe_{0.88}$

Table 5.2 – Elemental data of LDHs incorporated with various transition metals, determined by SEM-EDS. The numbers shown are relative molar abundances.

5.4.2 – Structural determination

5.4.2.1 – X-ray diffraction

Figure 5.1 shows the powder XRD pattern obtained for as-synthesised $Ni_{4.4}Mg_{2.96}Al_2(CO_3)(OH)_{16}.4H_2O$ and   conventional   hydrotalcite,

$Mg_{7.2}Al_2(CO_3)(OH)_{16}.4H_2O$.   The nickel/magnesium LDH exhibits broad peaks at values of 2θ characteristic of a layered double hydroxide structure. In general, the XRD pattern for $Ni_{4.4}Mg_{2.96}Al_2(CO_3)(OH)_{16}.4H_2O$ has slightly broader peaks than hydrotalcite, indicating smaller crystallites. The d_{110} spacings for both are about 3.04 Å, consistent with the similarly sized Ni^{2+} and Mg^{2+} ions.
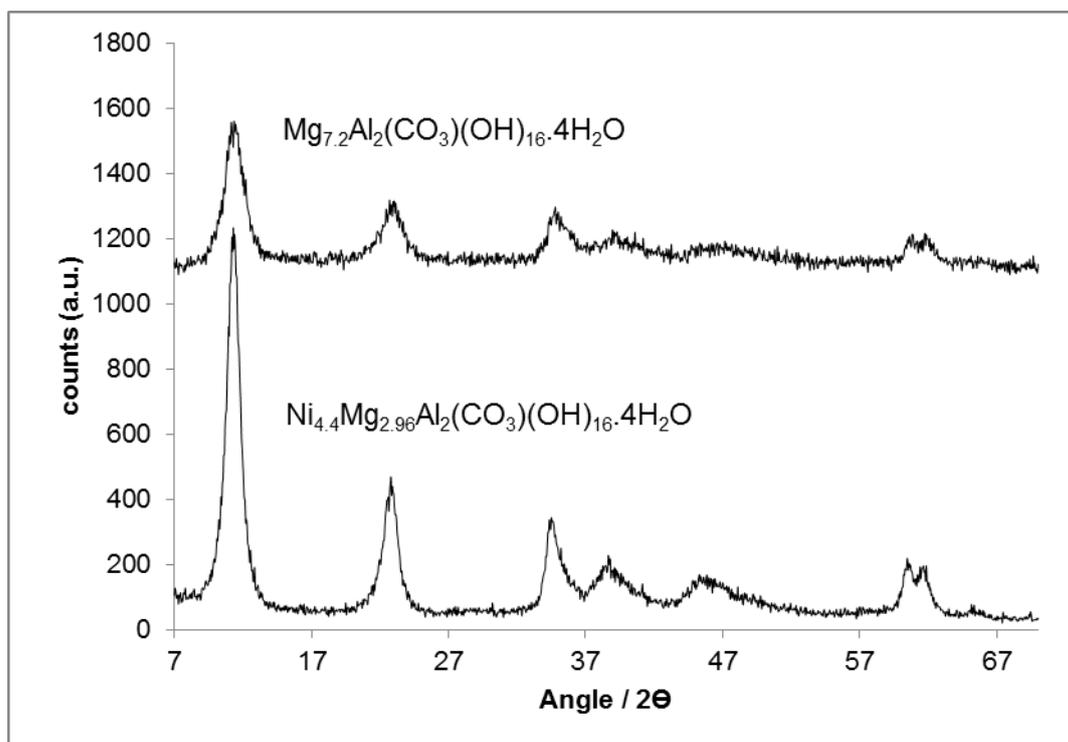
Figure 5.1 – Powder XRD diffraction pattern of as-synthesised
$Ni_{4.4}Mg_{2.96}Al_2(CO_3)(OH)_{16}.4H_2O$ and conventional hydrotalcite
$Mg_{7.2}Al_2(CO_3)(OH)_{16}.4H_2O$.

Figure 5.2 shows the XRD patterns of $Ni_{4.4}Mg_{2.96}Al_2(CO_3)(OH)_{16}.4H_2O$ through progressive conventional calcination. Reflections at 38 °, 43 ° and 62 ° attributed to either MgO or NiO (which have similar XRD patterns) have been assigned and can be seen up to 1000 °C, at which point a significant transformation into the $MgAl_2O_4$ spinel pattern is observed. As with LDHs discussed earlier this nickel/magnesium LDH seems to exhibit similar characteristics to hydrotalcite in that as the LDH is heated conventionally, the metal oxide reflections get narrower, suggesting that crystallite size increases with temperature and $MgAl_2O_4$ spinel is seen at higher temperature.
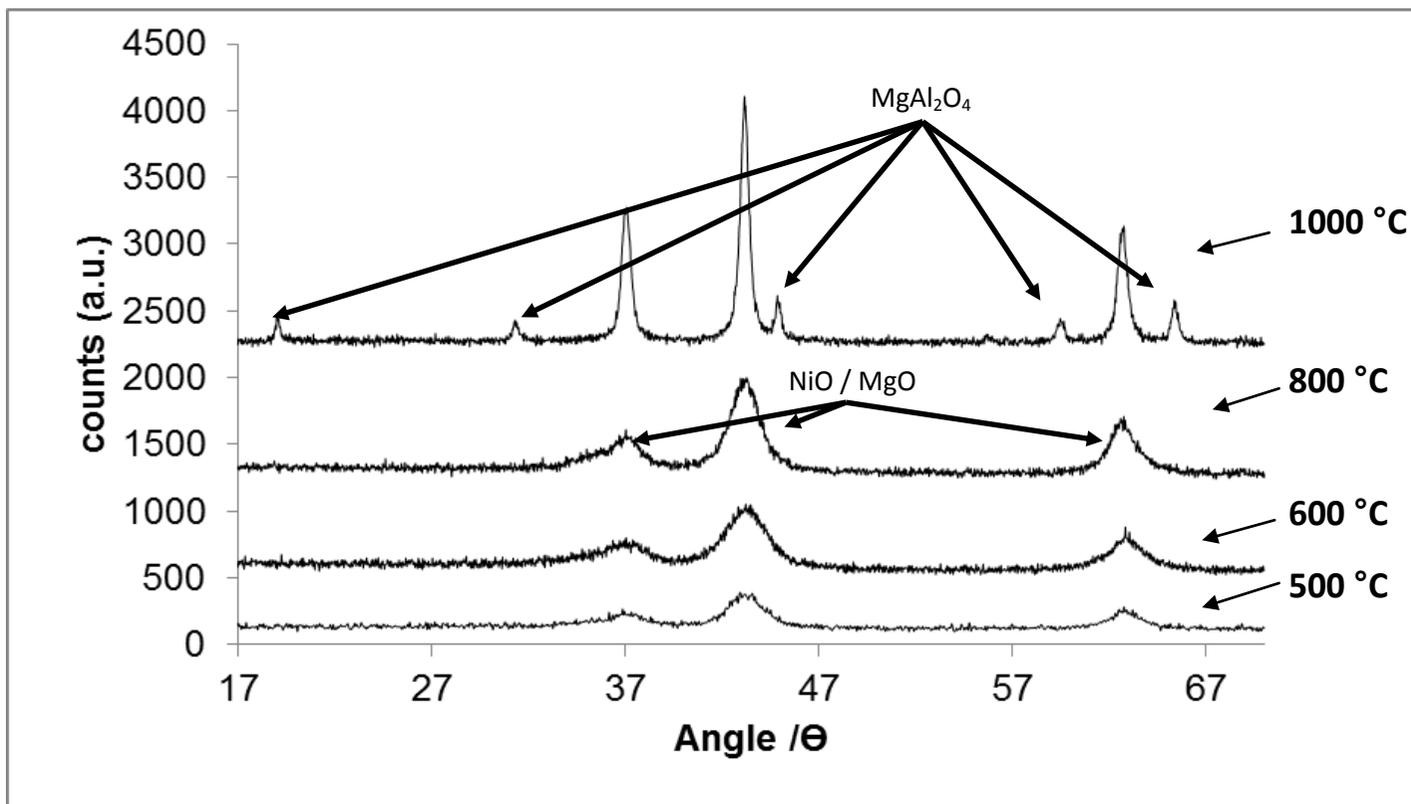
Figure 5.2 – Powder XRD pattern of $Ni_{4.4}Mg_{2.96}Al_2(CO_3)(OH)_{16}.4H_2O$, calcined for four hours under conventional heating.

Figure 5.3 shows the powder XRD pattern of the as-synthesised $Co_{2.24}Mg_{1.26}Al_2(CO_3)(OH)_{16}.4H_2O$. It is characteristic of the LDH structure and is compared to the $Mg_{7.2}Al_2(CO_3)(OH)_{16}.4H_2O$ diffraction pattern. The isomorphic substitution of cobalt for magnesium results in an increase in the d_{110} spacing. The spacing is calculated for $Co_{2.24}Mg_{1.26}Al_2(CO_3)(OH)_{16}.4H_2O$ to be 3.07 Å and for $Mg_{7.2}Al_2(CO_3)(OH)_{16}.4H_2O$ to be 3.04 Å. The spacing of the 110 planes is dependent on the size of the lattice cations and this increase in d_{110} reflects the fact that the ionic radius of Co^{2+} is 0.75 Å compared to Mg^{2+} which is 0.72 Å.
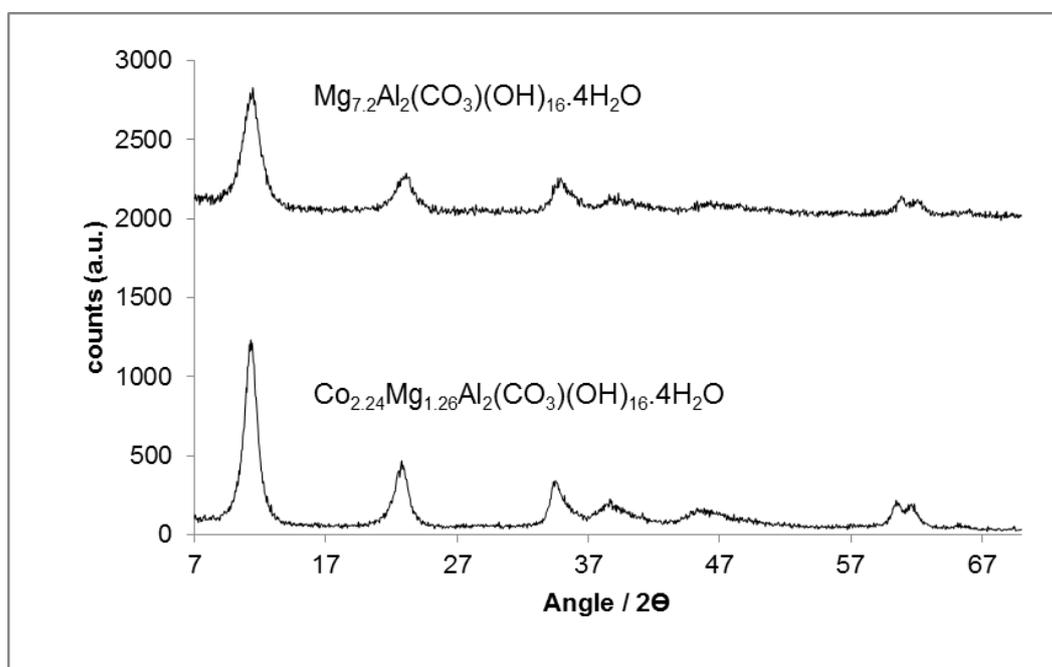
Figure 5.3 – Powder XRD diffraction pattern of as-synthesised $Co_{2.24}Mg_{1.26}Al_2(CO_3)(OH)_{16}.4H_2O$ and hydrotalcite, $Mg_{7.2}Al_2(CO_3)(OH)_{16}.4H_2O$.

Figure 5.4 shows the powder XRD patterns of CoMgAl LDH through progressive conventional heating to 1000 °C. The products of calcination are not the same as those seen for $Mg_{7.2}Al_2(CO_3)(OH)_{16}.4H_2O$, nor for similar materials containing nickel or copper. Firstly, the LDH reflections disappear by 500 °C (as with the others) but instead of being replaced by broad MgO reflections, (37 °, 43 °, and 62 °) quite narrow lines appear by 600 °C. MgO may be responsible for some of these, although the most intense line in the MgO pattern at 43 ° is absent. They may be

due to immediate formation of $MgAl_2O_4$ spinel phase, (19 °, 31 °, 37 °, 45 °, 59 ° and 65 °) or possibly they could be assigned to Co_3O_4. This is uncertain. One firm conclusion is that reflections from cobalt (II) oxide CoO are absent. At 1000 °C, the spinel or Co_3O_4 pattern persists. Sharp lines due to MgO persist too, and the reflection at 43 ° is now visible. Overall, the behaviour of this LDH on calcination is very different to that of the others studied.
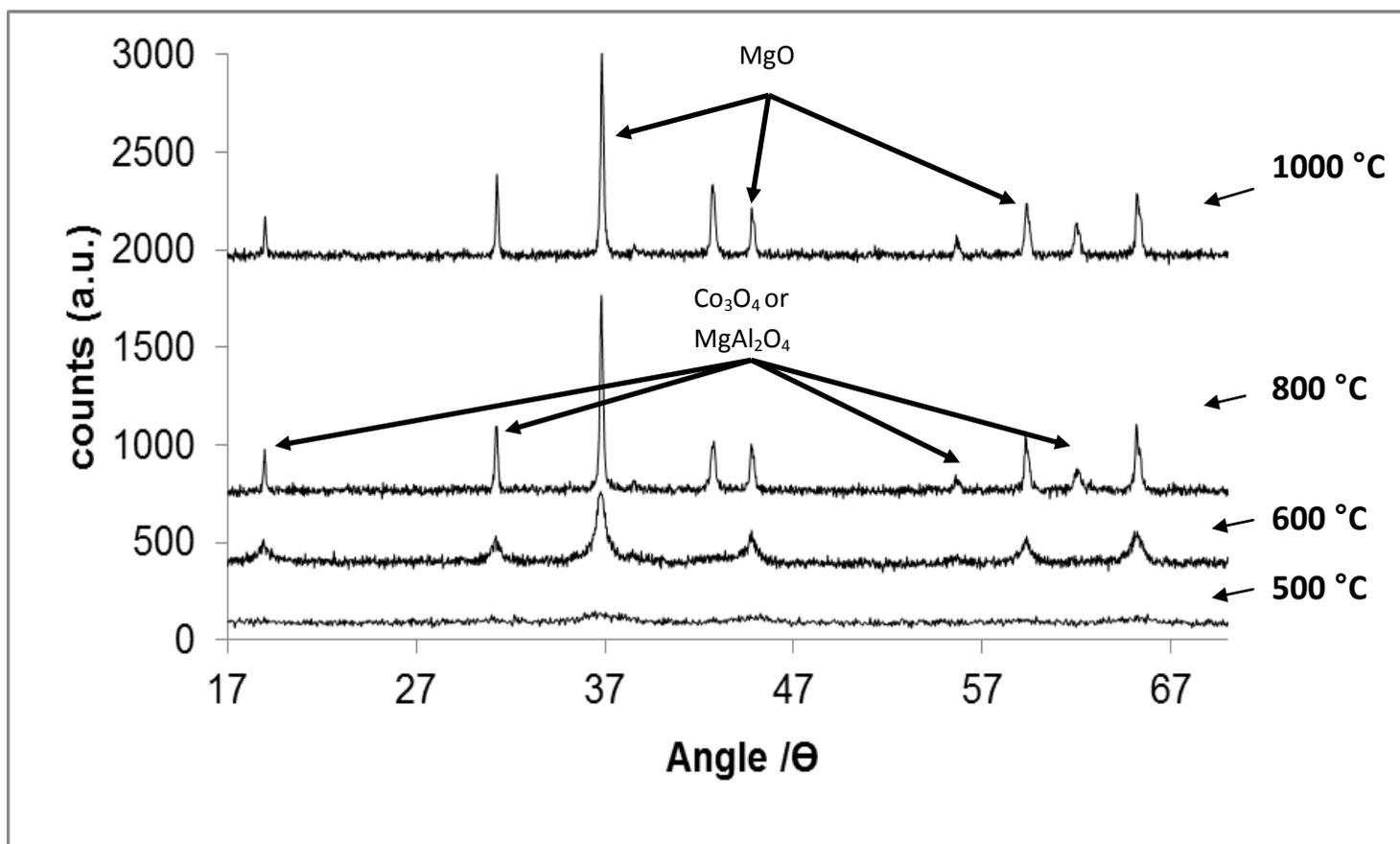
Figure 5.4 – Powder XRD pattern of $Co_{2.24}Mg_{1.26}Al_2(CO_3)(OH)_{16}.4H_2O$, calcined for four hours under conventional heating following a heating ramp of 2 °C min^{-1}.

Figure 5.5 shows powder XRD pattern for the as-synthesised $Mg_{5.82}Al_{1.12}Fe_{0.88}(CO_3)(OH)_{16}.4H_2O$. It is characteristic of the LDH structure and is compared to the hydrotalcite diffraction pattern. The iron/magnesium precursor exhibits broad peaks at values of 2θ characteristic to that of a layered double hydroxide structure. The d_{110} spacing for $Mg_{5.82}Al_{1.12}Fe_{0.88}(CO_3)(OH)_{16}.4H_2O$ is smaller than for conventional hydrotalcite. This is contrary to expectations if Fe^{3+} were simply replacing Al^{3+}. It might be explained however, by a lower $M^{2+}:M^{3+}$ ratio in the iron LDH than the conventional hydrotalcite because the M^{2+} ions are larger than the Mg^{2+} ions.
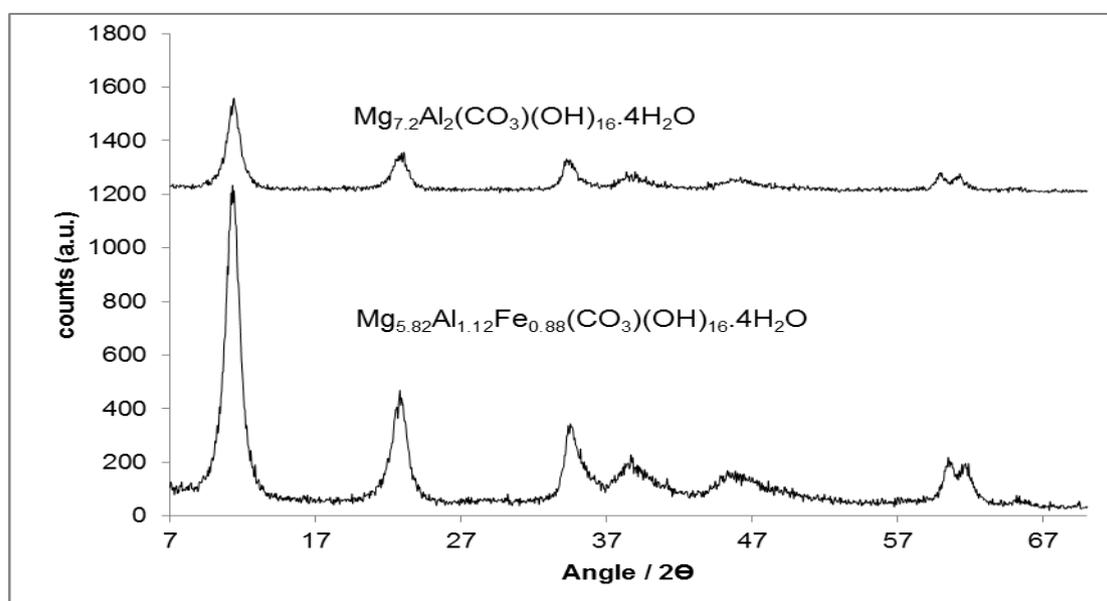
Figure 5.5 - Powder XRD diffraction pattern of as-synthesised
$Mg_{5.82}Al_{1.12}Fe_{0.88}(CO_3)(OH)_{16}.4H_2O$ and hydrotalcite, $Mg_{7.2}Al_2(CO_3)(OH)_{16}.4H_2O$.

Figure 5.6 shows the powder XRD pattern for $Mg_{5.82}Al_{1.12}Fe_{0.88}(CO_3)(OH)_{16}.4H_2O$ through progressive conventional heating. The results seen here are fairly typical of the calcination products of conventional LDH, hydrotalcite. Firstly at 500 °C, the LDH reflection disappears, to be replaced by broad reflections assigned to MgO suggesting the existence of poorly crystalline MgO. As the temperature is increased, the reflections narrow suggesting that crystallites are increasing in size. At 1000 °C reflections due to the spinel phase appear.
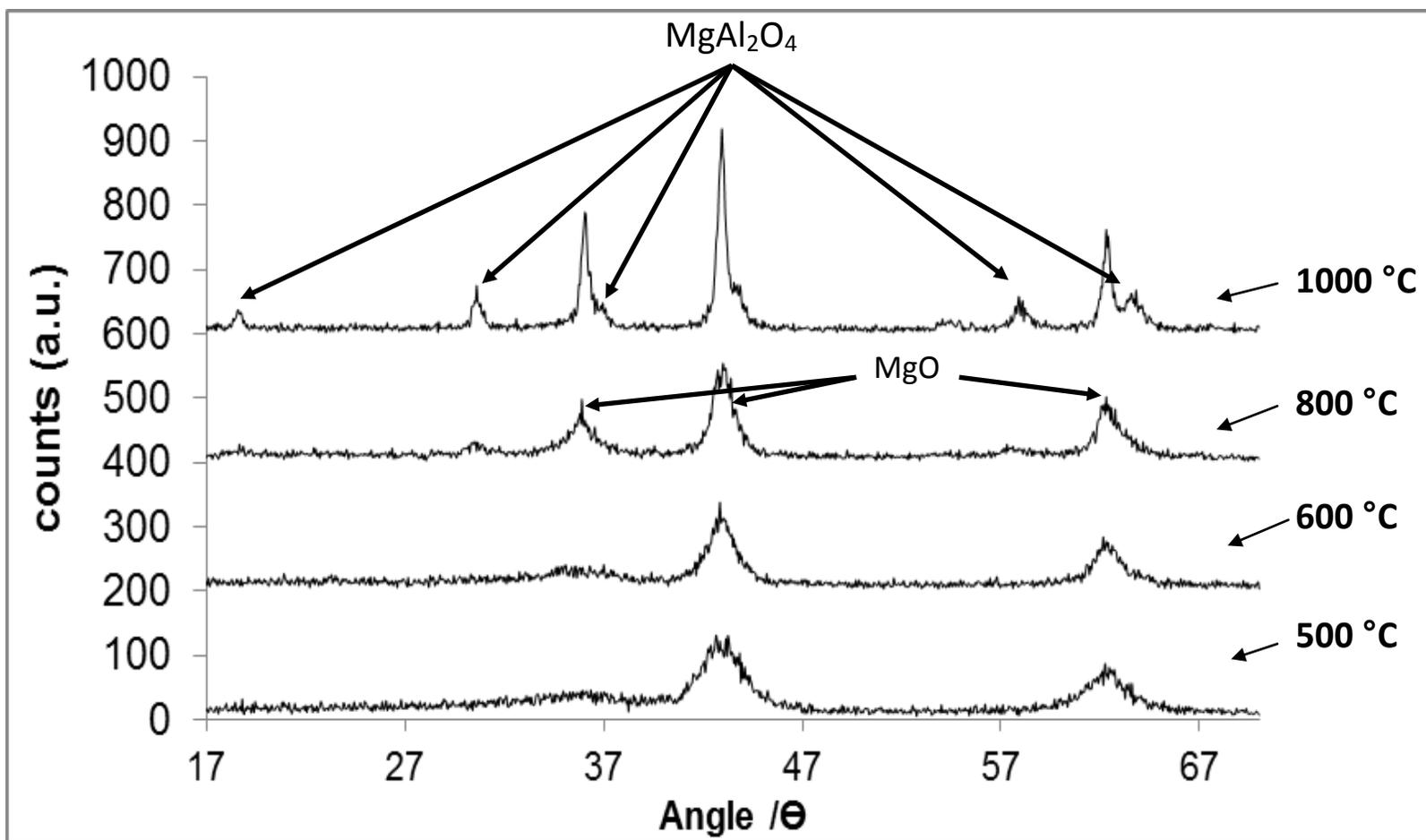
Figure 5.6 - Powder XRD pattern of $Mg_{5.82}Al_{1.12}Fe_{0.88}(CO_3)(OH)_{16}.4H_2O$, calcined for four hours under conventional heating.

The three LDHs containing Ni, Co and Fe were also subjected to microwave calcination. Comparisons of the results with those of conventional calcination is not straightforward however, because only one calcination temperature was studied using microwave heating, 500 °C because of instrumental limitations.

Figure 5.7 shows the powder XRD for all three transition metal LDHs under the feedback-controlled microwave technique, heated to 500 °C. We can see broad reflections assigned to MgO for all three calcined LDHs. The powder XRD patterns for $Ni_{4.4}Mg_{2.96}Al_2(CO_3)(OH)_{16}.4H_2O$ and $Mg_{5.82}Al_{1.12}Fe_{0.88}(CO_3)(OH)_{16}.4H_2O$ after 500 °C microwave calcination are broadly similar to the equivalent patterns after conventional calcination, exhibiting broad reflections from MgO. However, the equivalent pattern for $Co_{2.24}Mg_{1.26}Al_2(CO_3)(OH)_{16}.4H_2O$ differs dramatically as described above, showing reflections similar to those detected on conventional calcination at 600 °C (Figure 5.4). In the same way as the products of calcination when performed conventionally at 500/600 °C (i.e. MgO, $MgAl_2O_4/Co_3O_4$) were not expected, those same products formed on microwave calcination are similarly surprising.
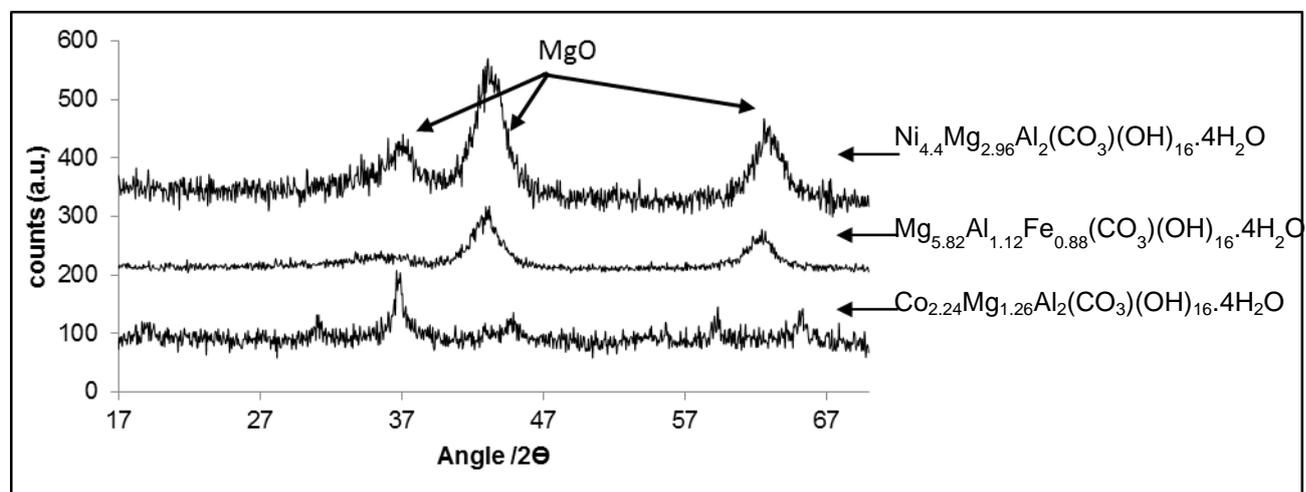
Figure 5.7 – Powder XRD pattern of transition metal doped hydrotalcites following microwave heating at 500 °C.

5.4.2.2 – XRD numerical data

Data representative of the structure of the LDHs prepared in this chapter was obtained using powder XRD. Table 5.3 shows lattice parameters calculated from the powder XRD results. Crystallite size (L) was determined from the width at half height on the d_{110} reflection, using the Scherrer equation. The unit cell parameters "c" and "a" were calculated from the d_{110} and d_{003} planes respectively. The ionic radii are also given for the corresponding transition metals (TM) used. The lattice parameter "a" includes the interlayer gap occupied by exchangeable anions. Crystallite sizes are larger for all the substituted LDHs than $Mg_{7.2}Al_2(CO_3)(OH)_{16}.4H_2O$. This is surprising as it might be expected that the conventional material would crystallise more easily. There is an expected relationship between crystallite size and surface area, with surface area decreasing as crystallite size increases.

The data for "c" (which is sensitive to the size of the cations in the lattice) shows very small differences between each LDH synthesised. $Ni_{4.4}Mg_{2.96}Al_2(CO_3)(OH)_{16}.4H_2O$ exhibits the smallest value of $2d_{110}$ consistent with the relatively small ionic radius of Ni^{2+}.

LDH	a (Å) 2d$_{110}$	c (Å) 3d$_{003}$	^{a}L$_{110}$ (Å)	Ionic radii^{TM} (Å)	Surface Area /m^{2}g^{-1}
Mg$_{7.2}$Al$_2$(CO$_3$)(OH)$_{16}$.4H$_2$O	3.04	23.28	44	0.72 (Mg^{2+}) 0.54 (Al^{3+})	110
Co$_{2.24}$Mg$_{1.26}$Al$_2$(CO$_3$)(OH)$_{16}$.4H$_2$O	3.07	23.05	68	0.72	69
Ni$_{4.4}$Mg$_{2.96}$Al$_2$(CO$_3$)(OH)$_{16}$.4H$_2$O	3.04	23.17	130	0.69	67
Mg$_{5.82}$Al$_{1.12}$Fe$_{0.88}$(CO$_3$)(OH)$_{16}$.4H$_2$O	3.09	23.32	150	0.65 (Fe^{3+}) 0.78 (Fe^{2+})	56

Table 5.3 - Powder XRD data for metal doped LDHs synthesised by three different preparative methods. ^{a}Calculated using the

Scherrer Equation.

5.4.3 – Calorimetry results

Conventionally and microwave calcined transition metal doped hydrotalcites were characterised using adsorption microcalorimetry for determining surface basicity and acidity. The extent of adsorption and the molar enthalpies of carbon dioxide and ammonia adsorption (ΔH°_{ads}) are interpreted in terms of the abundance and strength of the surface basic/acidic sites.

All adsorption experiments were carried out as before, producing profiles of enthalpies of adsorption vs. amount adsorbed. The data presented here is the average value of the amount of CO_2 or NH_3 adsorbed by each material and the average enthalpy of adsorption based on the assumption that only NH_3 that adsorbs with ΔH°_{ads} above 90 kJ mol^{-1} corresponds to adsorption on acid sites and only CO_2 that adsorbs with ΔH°_{ads} above 90 kJ mol^{-1} corresponds to adsorption on basic site.

These can be interpreted as a measure of the concentration of acidic and basic sites on the catalyst and an indication of the average strength of these sites, as described before.

Table 5.4 shows CO_2 adsorption data for $Co_{2.24}Mg_{1.26}Al_2(CO_3)(OH)_{16}.4H_2O$ that has been calcined using microwaves and conventional heating. By comparing the amount of CO_2 adsorbed, following calcination at 500 °C under microwave and under conventional heating it can be seen that microwave calcination results in both lower basic site concentration and lower base strength. The maximum amount of basic sites determined, in addition to the highest heat of adsorption, was for the LDH calcined conventionally at 500 °C. This mixed oxide also had the highest surface area.

Table 5.5 shows CO_2 adsorption data for $Ni_{4.4}Mg_{2.96}Al_2(CO_3)(OH)_{16}.4H_2O$ that has been calcined using microwaves and conventional heating. The concentration of basic sites was about the same for the two heating regimes at 500 °C. However, conventional heating provided a higher average strength of sites (111 kJ mol^{-1} vs. 98 kJ mol^{-1}). The surface areas of these samples calcined using microwaves and conventionally were similar.

Microwave heating				Conventional heating			
Calcination temperature / °C	[a]CO_2 adsorbed / mmol g^{-1}	[a]$-\Delta H^0_{ads}$ (CO_2) / kJ mol^{-1}	Surface area / m^2 g^{-1}	Calcination temperature / °C	[a]CO_2 adsorbed / mmol g^{-1}	[a]$-\Delta H^0_{ads}$ (CO_2) / kJ mol^{-1}	Surface area / m^2 g^{-1}
500	0.034	107	92	500	0.15	116	135
-	-	-	-	600	0.012	96	83
-	-	-	-	1000	No adsorption		

Table 5.4 - Surface basicity characteristics and surface areas of calcined $Co_{2.24}Mg_{1.26}Al_2(CO_3)(OH)_{16}.4H_2O$. [a]Total amount irreversibly adsorbed, (above 90 kJ mol^{-1} (±4)).

Microwave heating				Conventional heating			
Calcination temperature / °C	[a]CO_2 adsorbed / mmol g^{-1}	[a]$-\Delta H^0_{ads}$ (CO_2) / kJ mol^{-1}	Surface area / m^2 g^{-1}	Calcination temperature / °C	[a]CO_2 adsorbed / mmol g^{-1}	[a]$-\Delta H^0_{ads}$ (CO_2) / kJ mol^{-1}	Surface area / m^2 g^{-1}
500	0.16	98	141	500	0.16	111	135
-	-	-	-	600	0.069	94	127
-	-	-	-	1000	0.042	92	110

Table 5.5 - Surface basicity characteristics and surface areas of calcined $Ni_{4.4}Mg_{2.96}Al_2(CO_3)(OH)_{16}.4H_2O$. [a]Total amount irreversibly adsorbed, (above 90 kJ mol^{-1} (±4))

The summarised CO_2 adsorption data for microwave and conventionally calcined $Mg_{5.82}Al_{1.12}Fe_{0.88}(CO_3)(OH)_{16}.4H_2O$ is shown in Table 5.6. Materials calcined with both microwaves and with conventional heating show significant concentrations of basic sites based on CO_2 adsorption. In contrast to $Co_{2.24}Mg_{1.26}Al_2(CO_3)(OH)_{16}.4H_2O$ and $Ni_{4.4}Mg_{2.96}Al_2(CO_3)(OH)_{16}.4H_2O$, in this case microwave calcination appears to generate many more basic sites than conventional calcination. As with $Co_{2.24}Mg_{1.26}Al_2(CO_3)(OH)_{16}.4H_2O$ (but in contrast to the results for $Cu_{1.32}Mg_{2.98}Al_2(CO_3)(OH)_{16}.4H_2O$) the maximum concentration of basic sites is achieved at the relatively low calcination temperature of 500 °C. This is despite the fact that the surface area of the calcined LDH increases dramatically as the calcination temperature is increased to 1000 °C.

Figure 5.8 shows the CO_2 adsorption profiles for the three transition metal doped LDHs calcined conventionally at 500 °C. More detail can be obtained from these profiles compared to the simple averages given in the tables. An important indicator is the strongest sites, those measured by the first few CO_2 pulses. The data in Figure 5.8 reveals that calcined $Co_{2.24}Mg_{1.26}Al_2(CO_3)(OH)_{16}.4H_2O$ exhibits the strongest initial basic sites that react with CO_2 followed by $Ni_{4.4}Mg_{2.96}Al_2(CO_3)(OH)_{16}.4H_2O$ and $Mg_{5.82}Al_{1.12}Fe_{0.88}(CO_3)(OH)_{16}.4H_2O$.
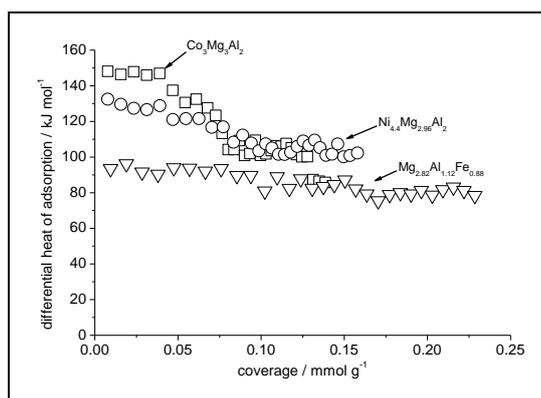
Figure 5.8 – Differential molar enthalpy of CO_2 against amount of CO_2 adsorbed for calcined transition metal doped hydrotalcites, calcined conventionally at 500 °C for four hours.

Microwave heating				Conventional heating			
Calcination temperature / °C	^{a}CO$_2$ adsorbed / mmol g^{-1}	^{a}-ΔH$^0_{ads}$ (CO$_2$) / kJ mol^{-1}	Surface area / m^2 g^{-1}	Calcination temperature / °C	^{a}CO$_2$ adsorbed / mmol g^{-1}	^{a}-ΔH$^0_{ads}$ (CO$_2$) / kJ mol^{-1}	Surface area / m^2 g^{-1}
500	0.18	101	104	500	0.081	95	50
-	-	-	-	600	0.066	91	171
-	-	-	-	1000	No adsorption		85

Table 5.6 - Surface basicity characteristics and surface areas of calcined Mg$_{5.82}$Al$_{1.12}$Fe$_{0.88}$(CO$_3$)(OH)$_{16}$.4H$_2$O. ^{a}Total amount irreversibly adsorbed, (above 90 kJ mol^{-1} (±4)).

$Co_{2.24}Mg_{1.26}Al_2(CO_3)(OH)_{16}.4H_2O$ calcined at 500 °C exhibits exceptionally high initial basic strength sites around 150 kJ mol^{-1}. Basic sites of this strength were seen previously for calcined (using microwaves at 500 °C) $Cu_{0.64}Mg_{5.8}Al_2(CO_3)(OH)_{16}.4H_2O$, referring back to data presented in Chapter 4. It is surprising that microwave calcination appears advantageous with the copper containing LDH but is inferior to conventional calcination with the other LDHs.

All the materials prepared in this work were also studied using ammonia adsorption calorimetry, to investigate surface acidity, if present. Calcined $Mg_{7.2}Al_2(CO_3)(OH)_{16}.4H_2O$, $Co_{2.24}Mg_{1.26}Al_2(CO_3)(OH)_{16}.4H_2O$ and $Ni_{4.4}Mg_{2.96}Al_2(CO_3)(OH)_{16}.4H_2O$ showed no ammonia adsorption so it can be concluded that they exhibited negligible surface acidity. Results can be used for determination of average acid strength and concentration of acid sites. The heats of adsorptions displayed in Table 5.7 are relatively high as is normal for NH_3 adsorption. Comparing directly iron LDHs calcined using microwaves and using conventional heating, we can see that the average heat of adsorption and amount adsorbed is higher when using conventional heating. As with basic sites and based on the results of conventional heating, it seems that calcination at 500 °C is optimum for generating acidic sites. And on calcination to 1000 °C, where the metal oxides have aggregated to relatively large crystals and/or spinel phases, acidity seems to be largely lost.

Microwave heating				Conventional heating			
Calcination temperature / °C	[a]NH_3 adsorbed / mmol g^{-1}	[a]$-\Delta H^0_{ads}$ (NH_3) / kJ mol^{-1}	Surface area / m^2 g^{-1}	Calcination temperature / °C	[a] NH_3 adsorbed / mmol g^{-1}	[a]$-\Delta H^0_{ads}$ (NH_3) / kJ mol^{-1}	Surface area / m^2 g^{-1}
500	0.18	142	104	500	0.22	156	50
-	-	-	-	600	0.16	132	171
-	-	-	-	1000	0.045	110	85

Table 5.7 - Surface acidity characteristics and surface areas of calcined $Mg_{5.82}Al_{1.12}Fe_{0.88}(CO_3)(OH)_{16}.4H_2O$ from flow NH_3 adsorption calorimetry. [a]Total amount irreversibly adsorbed, (above 90 kJ mol^{-1} (±4)).

5.4.4 – Catalytic Activity, Basicity and Acidity

As with previous chapters, the transesterification of tributyrin reaction was used as a measure of catalytic activity of the transition metal doped LDHs. The catalytic activities of the transition metal substituted LDHs are shown in Table 5.8.

Catalyst (LDH)	Calcination	Calcination temp / °C	^{a}k /s^{-1}
Mg_6/Al_2	Conventional	500	0.52
		600	0.52
		700	0.29
		800	0.025
		900	0.12
		1000	0.24
	Microwave	500	2.27
$Cu_{1.32}/Mg_{2.98}/Al_2$	Conventional	500	0.69
		600	0.57
		700	3.42
		800	2.87
		900	0.53
		1000	0.52
	Microwave	500	3.99
$Ni_{4.4}/Mg_{2.96}/Al_2$	Conventional	500	1.16
		600	1.42
		700	1.95
		800	0.61
		900	0.12
		1000	0.038
	Microwave	500	1.95
$Mg_{5.2}/Al_{1.12}/Fe_{0.88}$	Conventional	500	0.67
		600	0.35
		700	0.46
		800	0.09
		900	0.16
		1000	0.14
	Microwave	500	1.06
$Co_{2.24}/Mg_{1.26}/Al_2$	Conventional	500	2.99
		600	2.52
		700	2.34
		800	2.45
		900	0.45
		1000	0.033
	Microwave	500	1.76

Table 5.8 - Initial rate (conversion of tributyrin) vs. calcination temperature for all LDHs studied. ^{a}Obtained for the first 20 minutes of the reaction.

The data for $Ni_{4.4}Mg_{2.96}Al_2(CO_3)(OH)_{16}.4H_2O$, $Mg_{5.82}Al_{1.12}Fe_{0.88}(CO_3)(OH)_{16}.4H_2O$ and $Co_{2.24}Mg_{1.26}Al_2(CO_3)(OH)_{16}.4H_2O$ is shown alongside that for $Cu_{1.32}Mg_{2.98}Al_2(CO_3)(OH)_{16}.4H_2O$ previously given in Chapter 4, and the simple $Mg_{7.2}Al_2(CO_3)(OH)_{16}.4H_2O$ (hydrotalcite) LDH previously given in Chapter 3. Activities in the transesterification of tributyrin are expressed as the first order rate constant (pseudo-first order in tributyrin) taken over the first 20 minutes of the reaction. Details of the reaction conditions are given in the experimental section. Data is presented for catalysts calcined at from 500 °C to 1000 °C under conventional conditions, and at 500 °C under microwave heating. The data is plotted in Figure 5.9 to show the relationship between calcination temperature and catalytic activity for each of the catalysts.
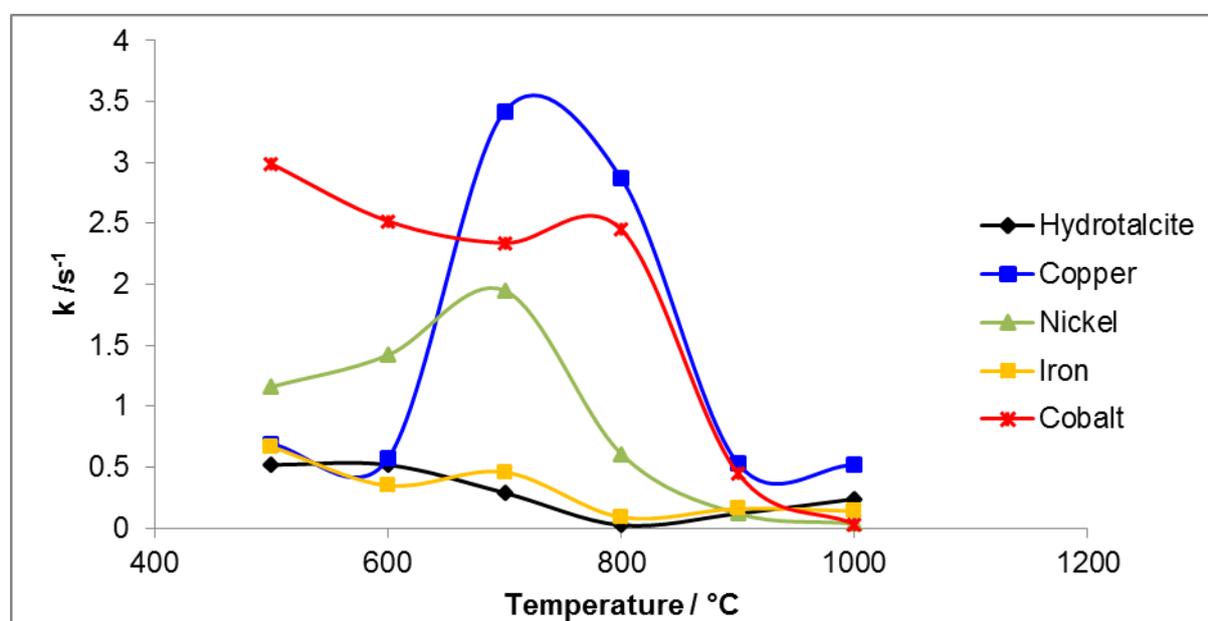
Figure 5.9 – Calcination temperature (conventional heating) vs. initial rate of reaction for all LDHs studied.

The first thing to note from this data is that the incorporation of transition metals into the hydrotalcite structure can increase the catalytic activity towards tributyrin transesterification. The most effective transition metal of those tested appears to be copper (II), although nickel (II) and cobalt (II) containing LDHs are also much more active than $Mg_{7.2}Al_2(CO_3)(OH)_{16}.4H_2O$. The iron (III) substituted LDH shows activities very similar to, or even lower than, $Mg_{7.2}Al_2(CO_3)(OH)_{16}.4H_2O$. The following additional conclusions can be drawn from the data in this chapter.

1.   In general, there is a reasonably good correlation between the measured basicity of the LDH-based catalysts and their catalytic activities in the transesterification for triglycerides. In comparing the profiles of CO_2 molar enthalpies of adsorption against the amount of CO_2 adsorbed, as indicators of basic strength distributions, the general trend is that high concentrations of basic sites tend to be associated with higher base strengths. This means that we cannot differentiate in this work between the importance of the concentration of basic sites compared to their strengths. If it were possible to determine the Arrhenius parameters for the reaction under the action of the various catalysts, then it might be possible to relate differences in activation energies to differences in basic site strengths (expressed in terms of CO_2 molar adsorption enthalpies).

2.   Based on the iron(III) containing LDH, which is the only material studied to exhibit surface acidity, this work does seem to confirm that the transesterification of triglycerides is not catalysed by acids very effectively. This is of course significant to those trying to develop single acid catalysts to catalyse both the esterification of free fatty acids (in low grade oils), which requires an acid catalyst, and the transesterification of triglycerides in a single step.   The data for the $Mg_{5.82}Al_{1.12}Fe_{0.88}(CO_3)(OH)_{16}.4H_2O$, combined with the data for surface acidity and surface basicity given in Tables 5.6 and 5.7 suggest that i) surface acidity is not a deciding factor in controlling activity in the reaction and ii) there may be a correlation between concentration/strength of surface base sites with activity but both surface basicity and catalytic activity are barely higher than those of $Mg_{7.2}Al_2(CO_3)(OH)_{16}.4H_2O$.   It can be seen that $Mg_{5.82}Al_{1.12}Fe_{0.88}(CO_3)(OH)_{16}.4H_2O$ shows reasonably consistent but relatively low activity on calcination at 500-700 °C and somewhat higher activity on microwave calcination at 500 °C. On conventional heating, calcination at 1000 °C reduces activity to a very low level and this correlates well with the observation that CO_2 adsorption is immeasurable after this treatment.

3.   The effect of microwave calcination on both the surface basicity and the activity or mixed metal oxide catalysts generated from LDH's containing transition metals, appears to be highly significant but somewhat variable and, based on this work, not easily predictable. LDH's containing high concentrations of copper (II) which is known to couple strongly with microwaves, do indeed generate oxides of high basicity. Lower copper levels result in much less profound effects. LDH's

containing nickel (II) and cobalt (II), do not seem to transform into more basic solids on microwave, compared to conventional calcination. It is reasonable to assume that microwave heating decomposes the hydroxides in a different manner to conventional heating, as discussed earlier, but more work is needed to investigate why this might yield more or stronger basic sites.

4.   Both nickel (II) and cobalt (II) are very readily incorporated into the LDH structure, especially nickel (II). On calcination, nickel-containing LDH appears to behave in a conventional way, and the products of calcination are the same under the two forms of heating. But for cobalt-containing LDH, the products of calcination seem to be different to those normally seen. They are described earlier in the chapter, but there is evidence for either the formation of an easily-observed spinel phase, or a Co_3O_4 phase at relatively low temperature. Microwave heating does not affect this very much and surface basicity and catalytic activity are similar to those of the nickel-containing materials. Again, however, this unusual behaviour is worthy of further work.

Those transition metal substituted LDHs that do show higher activities than $Mg_{7.2}Al_2(CO_3)(OH)_{16}.4H_2O$,   that   is $Cu_{1.32}Mg_{2.98}Al_2(CO_3)(OH)_{16}.4H_2O$, $Ni_{4.4}Mg_{2.96}Al_2(CO_3)(OH)_{16}.4H_2O$ and $Co_{2.24}Mg_{1.26}Al_2(CO_3)(OH)_{16}.4H_2O$ LDHs, do not show very consistent behaviour in terms of the effects of calcination temperature and the   effect   of   microwave   versus   conventional   calcination. $Cu_{1.32}Mg_{2.98}Al_2(CO_3)(OH)_{16}.4H_2O$, as described in Chapter 4, exhibits maximum activity when heated conventionally on calcination at 700 °C. It shows much higher activity after microwave calcination, even at 500 °C.   Surface basic site concentrations and strengths correlate reasonably well with these trends as described before and, interestingly, there is no correlation between the specific surface areas of the catalysts and their activities. $Ni_{4.4}Mg_{2.96}Al_2(CO_3)(OH)_{16}.4H_2O$ shows broadly similar trends, with maximum activity detected on calcination at 700 °C and relatively high activity detected for the microwave calcined material. But in this case, the correlation with surface basicity, as measured by CO_2 adsorption, is relatively poor. The adsorption studies do show that basicity falls off as the calcination temperature is increased to 1000 °C however, and this is consistent with the low activity of material calcined at this temperature.

$Co_{2.24}Mg_{1.26}Al_2(CO_3)(OH)_{16}.4H_2O$ shows relatively high activity on calcination conventionally at the relatively low calcination temperatures (conventional heating) of 500 °C and 600 °C. At higher calcination temperatures activity falls off and on microwave calcination activity is relatively low in comparison. There is an excellent correlation between these high activities at the lower calcination temperatures and the concentration/strength of basic sites, and the plot in Figure 5.11 shows that $Co_{2.24}Mg_{1.26}Al_2(CO_3)(OH)_{16}.4H_2O$ exhibits some very strong basic sites even on calcination at 500 °C. The importance of this is that the powder XRD data shows that this LDH behaves quite differently to the others at the lower calcination temperatures, with sharp reflections appearing at these temperatures representing either Co_3O_4 or $MgAl_2O_4$ formation. Crystallites are clearly larger than are formed at 500 °C for the other LDHs.

Why spinel formation should occur with such facility in $Co_{2.24}Mg_{1.26}Al_2(CO_3)(OH)_{16}.4H_2O$, or why Co_3O_4 should be so clearly formed so early in the calcination process is not clear. It does seem however, that there is something fundamentally different about the behaviour of this LDH on calcination than the others, and this leads to high surface basicity and high base catalytic activity.

Overall the results suggest that catalytic activity is not particularly dependent on the specific surface areas of the catalysts, but does depend on the surface basicities. Basicity appears to be enhanced by the presence of copper (II) and by cobalt (II) particularly. Whether this is because of the presence of these ions on the catalyst surface and their behaviour as Lewis bases, or whether their presence leads to surface defect sites that show electron donating abilities, is not clear. It is certainly not obvious why these ions in themselves should show significant basicity so it seems more likely that they promote the formation of defect sites that are the catalytic centres.

The effect of microwaves seems to be variable and not always as pronounced as it is with $Cu_{1.32}Mg_{2.98}Al_2(CO_3)(OH)_{16}.4H_2O$. It seems likely that the extent to which microwaves are effective depends on their capacity to couple with the microwave field and the fact that this varies between metals perhaps explains why the different LDHs show different behaviours.

The results discussed in this thesis show clear differences in the properties of transition metal doped hydrotalcite both in terms of structural properties and catalytic activity. Further work could be to look at the selectivity of these transition metal catalysts in different reactions as the work shown in this chapter shows that they possess acid/base sites.

Finally, in the first chapter of this thesis it was implied that hydrotalcite and hydrotalcite-type materials may be suitable for use as adsorbants. One of the most popular fields is CO_2 capture. Although calorimetric measurements in this thesis have shown that the potential of these materials in the field of heterogeneous catalysis in terms of relative strengths of acid/base sites, they have also shown the possibility or potential of CO_2 storage. Calcination of all LDHs studied in this thesis showed potential of irreversible CO_2 adsorption (capture) to be in the region of up to 1.0 mmol g^{-1}. This amount of adsorption of CO_2 is relatively small for CO_2 capture and storage but as shown in this thesis very applicable for use in the field of catalysis.

References

[1]   P. P. Pescarmona, J. V. Noyen, P. A. Jacobs., *J. Catal.*, 251 (2007) 307-314.

[2]   D. A. Peña, B. S. Uphade, P. G. Smirniotis *J. Catal.,* 221 (2004) 421-431.

[3]   A. T. Bell, *J. Mol. Catal. A. Chem.,* 100 (1995) 1-11.

[4]   D. Tang, W. Zhang, Y. Zhang, Z. Qiao, Y. Liu, Q. Huo., *J. Colloid Interface Sci.*, 356 (2011) 262-266.

[5]   F. Lena, K. Matyjaszewski *Prog. Polym. Sci.*, 35 (2010) 959-1021.

[6]   A. Cimino, F. S. Stone, *Adv. Catal.*, 47, (2002) 141-306.

[7]   C. Ettarh, A. K. Galwey.*Thermochim. Acta.*, 261 (1995) 125-139.

[8]   A. Maltha, S.C. van Wermeskerken, B. Brunet, V. Ponec, *J. Mol. Catal.*, 93 (1994) 305-316.

[9]   L. Chmielarz, P. Kuśtrowski, A. Rafalska-Łasocha, R. Dziembaj, *Appl. Catal. B.,* 58 (2005) 235-244.

[10]   K. Bourikas, C. Fountzoula, *Appl. Catal. B.,* 52 (2004) 145-153.

[11]   Z. Wu, B. Jiang, Yue Liu, *Appl. Catal. B.,* 79 (2008) 347-355.

[12]   W. Suprun, M. Lutecki, R. Gläser, H. Papp, *J. Mol. Catal. A.,* 342 (2011) 91-100.

[13]   A. Clark, *Ind. Eng. Chem.,* *45* (195) 1476–1480.

[14]   W. C. Sheets, E. Mugnier, A. Barnabé, T. J. Marks, K. R. Poeppelmeier, *Chem. Mater.,* *18* (2006) 7–20.

[15]   S. Balakrishnan, A. Launikonis, P. Osvath, G. F. Swiegers, A. P. Douvalis, G. J. Wilson, *Mater. Chem. Phys.,* 120 (2010) 649-655.

[16]   X. Xiang, L. Zhang, H. I. Hima, F. Li, D. G. Evans, *Appl. Clay Sci.,* 42 (2009) 405-40.

[17]   A. Tsyganok, A. Sayari*, J. Solid State Chem.,* 179 (2006) 1830-184.

[18]   H. Morioka, Y. Shimizu, M. Sukenobu, K. Ito, E. Tanabe, T. Shishido, K. Takehira *Appl. Catal. A*, 215 (2001) 11-19.

[19]   J. C. Villegas, O. H. Giraldo, K. Laubernds, S. L. Suib, *Inorg. Chem.,* 42 (2003) 5621–5631.

[20]   J. Wang, G. Fan, H. Wang, F. Li, *Ind. Eng. Chem. Res.,* 50 (2011) 13717–13726.

[21]   A.J. Vizcaíno, M. Lindo, A. Carrero, J.A. Calles, *Int. J. Hydrogen Energy.,* 37 (2012) 1985-1992.

[22]   S. Skurnik, M. Steinberg, *Ind. Eng. Chem. Fund.,* 6 (1967) 459–460.

[23]   M. C. Boswell, R. K. Iler. *J. Am. Chem. Soc.,* 58 (1936) 924–928.

[24]   F. Chang, T. Hsiao, J. Shih, *Ind. Eng. Chem. Res.,* 37 (1998) 3838–3845.

[25]   P. Oustadakis, S. Agatzini-Leonardou, P.E. Tsakiridis, *Miner. Eng.*, 19 (2006) 1204-1211.

[26]   N. A. A. Rahman, M. A. Olutoye, B.H. Hameed, *Bioresour. Technol.*, 102, (2011) 9749-9754.

[27]   E. B. Pereira, P. R. Piscina, N. Homs, *Bioresour. Technol.*, 102 (2011) 3419-3423.

[28]   G. Marbán, A. López, I. López, T. Valdés-Solís, *Appl. Catal. B.,* 99 (2010) 257-264.

[29]   C. Forano, T. Hibino, F. Leroux, C. Taviot-Guého, *Dev. Clay Sci.*, 1 (2006) 1021-1095.

[30]   H. C. B. Hansen, C. B. Koch, *Appl. Clay Sci.*, 10 (1995) 5-19.

[31]   C. Ruby, M. Usman, S. Naille, K. Hanna, C. Carteret, M. Mullet, M. François, M. Abdelmoula, *Appl. Clay Sci.,* 48 (2010) 195-202.

[32]   S. Jain, M.P. Sharma, S. Rajvanshi, *Fuel Processing Technology*, 92 (2011) 32-38.

[33]   G. Mitran, T. Cacciaguerra, S. Loridant, D. Tichit, I. Marcu, *Appl. Catal. A. Gen.,* 417 (2012) 153-162.

[34]   M. Gabrovska, R. Edreva-Kardjieva, K. Tenchev, P. Tzvetkov, A. Spojakina, L. Petrov, *Appl.Catal. A.* Gen., 399 (2011) 242-251.

[35]   L. Huang, Q. Liu, R. Chen, A. T. Hsu, *Appl. Catal. A.* Gen.*,* 393 (2011) 302-308.

[36]   G.Carja, R. Nakamura, H. Niiyama, *Appl. Catal. A.* Gen.*,* 236 (2002) 91-102.

[37]   G. S. Machado, F. Wypych, S. Nakagaki, *Appl. Catal. A.* Gen.*,* 413 (2012) 94-102.

[38]   Y. Ohishi, T. Kawabata, T. Shishido, K. Takaki, Q. Zhang, Y. Wang, K. Nomura, K. Takehira, *Appl. Catal. A.* Gen.*,* 288 (2005) 220-231.

[39]   Y.Zhao, Q. Jiao, C. Li, J. Liang, *Carbon.*, 45 (2007) 2159-2163.

[40]   A. I. Tsyganok, T. Tsunoda, S. Hamakawa, K. Suzuki, K. Takehira, T.Hayakawa*, J. Catal.,* 213 (2003) 191-203.

[41]   H. Morioka, Y. Shimizu, M. Sukenobu, K. Ito, E. Tanabe, T. Shishido, K. Takehira*, Appl. Catal. A.* Gen.*,* 215 (2001) 11-19.

[42]   J. Feng, Y.Lin, D. G. Evans, X. Duan, D. Li, *J. Catal.*, 266 (2009) 351-358.

[43]   C. Carlini, P. Patrono, A.M. Raspolli Galletti, G. Sbrana, *Appl. Catal. A: Gen.* 275 (2004) 111.

[44]   F. Kovanda, K. Jirátová, *Appl. Clay Sci.*, 53 (2011), 305-316.

[45]   P. Selvam, S.K. Mohapatra, *J. Catal.*, 233 (2005) 276-287.

[46]   F. Kovanda, T. Grygar, V. Dorničák, *Solid State Sci.*, 5 (2003) 1019-1026.

[47]   M. Hadnadjev, T. Vulic, R. Marinkovic-Neducin, Y. Suchorski, H. Weiss, *Appl.Surf. Sci.*, 254 (2008) 4297-4302.

[48]   E. Li, Z. P. Xu, V. Rudolph, *Appl. Catal. B.*, 88 (2009) 42-49.

[49]   M. E. Pérez-Bernal, R. J. Ruano-Casero, F. Benito, V. Rives, *J. Solid State Chem.*, 182 (2009) 1593-1601.

[50]   H. Abdolmohammad-Zadeh, S. Kohansal, G.H. Sadeghi, *Talanta.*, 84 (2011) 368-373.

[51]   F. B. D. Saiah, B. Su, N. Bettahar, *J. Hazard. Mater.*, 165 (2009) 206-217.

[52]   P. Benito, F.M. Labajos, V. Rives, *J. Solid State Chem.*, 179 (2006) 3784-3797.

[53]   L. J. Michot, J. Ghanbaja, V. Tirtaatmadja, P. J. Scales, *Langmuir*, 17 (2001) 2100–2105.

[54]   R. Shannon, *Acta. Crystallogr. Sect. A.*, 32 (1976) 751-767.

[55]   J.S. Valente, J. Hernandez-Cortez, M.S. Cantu, G. Ferrat, E. Lopez-Salinas, *Catal. Today.,* 150 (2010) 340-345.

Chapter 6

Conclusions and Further Work

Conclusions and Further Work

The main objective of the work reported here was to relate the structure of several LDHs to their function as catalysts in the transesterification of tributyrin.

The first conclusion concerns the method used to synthesise the LDHs. The most widely used, easiest and probably economically most advantageous, method involves the use of sodium hydroxide and sodium carbonate solutions. The work in this thesis has shown how difficult it is to remove the last traces of sodium salts from the LDH, and hence from the oxides produced when they are calcined, and how much residual entrained sodium can affect the catalytic properties of the mixed oxides. Importantly, the impact on catalytic activity seems almost certain to be due to leaching of the sodium salts to the reaction mixture and, in the case of biodiesel synthesis, this is extremely undesirable. The work has shown that extensive washing of the LDH can remove residual sodium and that washing the precipitate with hot water is an absolute necessity if synthesis is carried out using sodium salts. The work has also shown that alternative methods, using ammonia solution and using urea, while allowing better control of pH, do not make a significant difference to the degree of crystallinity or surface area of the LDH. The properties of the resultant mixed oxides following calcination are largely unaffected by the method of synthesis.

The incorporation of copper (II) in the LDH structure has been studied. Results demonstrate that copper (II) can indeed be successfully substituted for magnesium in the hydrotalcite structure and that, on calcination, mixed oxides containing aluminium, magnesium and copper are formed. These mixed oxides exhibit very much higher basicity than the calcined hydrotalcite and this results in very much higher catalytic activity in the base-catalysed transesterification reaction. It seems clear that the copper (II) is responsible for this enhancement. Evidently the extent to which copper (II) can be substituted for magnesium is limited. In this work, copper (II) was successfully substituted for about half of the magnesium but attempts to add higher concentrations were not successful. It is significant that the catalytic properties of the mixed oxides of copper, magnesium and aluminium formed from calcination of the LDHs, could not be duplicated by physically mixing the pure oxides of the three metals, no matter how finely the oxides were ground and blended.

Clearly, the basicity and activity of the calcined LDH are linked to interactions between the metal oxide structures at a very fine scale. The powder X-ray diffraction data for the calcined LDHs shows that the individual oxides exist as distinct entities but it is possible that there are small amounts of some mixed oxides, possibly mixed at an atomic level, and it is conceivable that it is these genuine double, or triple oxides that give rise to the important catalytic properties.

Other transition metals, nickel (II), cobalt (II) and iron (III) have also been incorporated in the LDH structure. Nickel (II) and cobalt (II) appear to be favourably substituted for magnesium with the resultant LDHs containing disproportionately more of these ions than are used in the synthesis mixtures. They too seem to enhance basicity and base catalytic activity, but not to the same extent as copper (II).

Iron (III) was incorporated readily and it was assumed it substituted for aluminium. In contrast to the other metals, iron (III) imparted some acidity to the calcined LDH, as might be expected given the acidity of salts of this metal ion. However, these oxides showed very little catalytic activity in the transesterification reaction, largely confirming the known fact that these reactions are very much more effectively catalysed by bases than by acids.

All the LDHs studied here were calcined at a range of temperatures and their properties were characterised as a function of calcination temperature. In general, they all showed that at 500 °C the oxides start to form, exhibiting broad reflections. At higher temperatures, sintering of the oxides occurs and the reflections become narrower. At higher temperatures still, some evidence for mixed oxides in the spinel structure appears. The calcined materials do not exhibit exceptionally high surface areas. The concentration and strength of basic sites tend to be at their maximum values after calcination at 600-700 °C, corresponding to almost complete formation of the oxides from the hydroxides but before extensive sintering takes place. One of the LDHs shows behaviour rather different to this, the cobalt (II) containing LDH. This material exhibits well resolved reflections from the oxides, including either a cobalt oxide (Co_3O_4) or a spinel material, at somewhat lower temperatures than the others. Base site formation and catalytic activity is largely in line with the behaviour

of the other LDHs. This system is clearly a potentially interesting subject for further work.

The effect of microwave calcination, which was performed in this work under feedback-control to ensure that sample temperature control was maintained through solid state transformations,   was investigated in the calcination of LDH's and compared with conventional calcination using a muffle furnace.   The first conclusion was that microwave calcination does appear to yield different products to conventional calcination. This is not surprising in the case of LDH decomposition where one would expect the product of dehydroxylation (water vapour) to have a profound effect on the final catalyst depending on whether it is produced first from the outside of the LDH particles and only afterwards in the bulk of the crystals, or whether it is produced more evenly across the LDH particles. Particularly in the case of copper-containing LDHs, microwave calcination significantly increases surface basicity and catalytic activity. It also results in the formation of a mixed copper (II), magnesium (II) oxide phase that is undetected on conventional calcination. Whether the relatively strong effect of microwaves on copper LDHs is linked to the strength with which copper (II) couples with microwave fields is uncertain. It is important to say however, that in other cases the effects of microwaves are somewhat unpredictable and variable. It seems that there may well be potential for enhancing catalytic properties using microwave calcination, using feedback control, but that is largely the limit of the conclusions that can be drawn here.   This is an area for extensive further work.

One additional objective of the work was to evaluate the ability of adsorption calorimetry to predict catalytic activities in the test reaction used here. The work has been limited to using CO_2 adsorption data for predicting surface basicity.   The technique provides a value for the concentration of basic sites, an average value for the strength of the sites (based on the enthalpy of CO_2 adsorption) and, by looking at the adsorption enthalpy associated with CO_2 on the strongest sites, some indication of the strength of the strongest (and possibly most active) base sites.   In general, the strength of sites in these substituted LDHs tends to follow the concentration of sites so the term "basicity" can be used to refer to both. The strongest sites follow the same trends. In terms of how well the data correlates with catalytic activity, there is a strong relationship between basicity measured using the technique and catalytic

activity. In fact it would have been easy to explain an absence of such a strong correlation because it is not obvious that the adsorption of CO_2 on a surface base site in the absence of a solvent or other reactants should be constrained by the same factors as control the adsorption of methanol, the de-protonation of the methanol, and the reaction with the methoxide ion with the triglyceride. The fact that the relationship is strong strengthens the case for adsorption calorimetry as a reliable method for predicting base catalytic activity. It is difficult to draw conclusions about the reliability of the technique for predicting surface acidity and acid catalytic activity as this was only measured for one material, the iron-containing LDH, which shows negligible activity in the transesterification reaction.

Overall, the work has demonstrated the potential of transition metal-substituted LDH's as precursors for solid base catalysts. It has also demonstrated that microwave calcination has the potential to influence the catalytic activities of calcined materials. It is particularly in this last regard that further work would be of value.

Appendix

1. **Spread sheet for treating adsorption calorimetry data**

2. **AAS sodium absorption calibration graph**

3. **Publications by H E Griffiths (née Cross)**

Calculations for flow adsorption calorimetry measurements

Adsn Temperature		120		Activation temp		500 @20	injection vol	1 mL	
Sample weight		20.8 (24.9)		Date		05.02.2009			
Flow rate		5 mlmin							
Date ref		04.02.2009		Pressure	3.1 E-07		m/z -15		

Obs. Area	Ref area	Net area	% adsorbed	No. of moles	dH/J	dH/kJ mol-1	coverage	cumulative coverage	cumulative coverage (mmol g^{-1})
0.00E+00	5.81E-08	5.81E-08	100	4.13E-07	0.0617	149.3946731	1.98558E-05	0.0000099	0.0099
0.00E+00		5.81E-08	100	4.13E-07	0.0573	138.7409201	1.98558E-05	0.0000298	0.0298
0.00E+00		5.81E-08	100	4.13E-07	0.0554	134.1404358	1.98558E-05	0.0000496	0.0496
0.00E+00		5.81E-08	100	4.13E-07	0.0534	129.2978208	1.98558E-05	0.0000099	0.0099
0.00E+00		5.81E-08	100	4.13E-07	0.0516	124.9394673	1.98558E-05	0.0000298	0.0298
1.67E-09		5.64E-08	97.1268503	4.0113E-07	0.0503	125.3945405	1.92853E-05	0.0000491	0.0491
5.80E-09		5.23E-08	90.0181756	3.7178E-07	0.0481	129.3793063	1.78738E-05	0.0000669	0.0669
1.67E-09		5.64E-08	97.1259036	4.0113E-07	0.0485	120.9084391	1.92851E-05	0.0000862	0.0862
3.07E-09		5.50E-08	94.7181756	3.9119E-07	0.0491	125.5157184	1.8807E-05	0.0001050	0.1050
3.77E-09		5.43E-08	93.5184509	3.8623E-07	0.0481	124.5368052	1.85688E-05	0.0001236	0.1236
2.84E-09		5.53E-08	95.110241	3.9281E-07	0.0464	118.1246805	1.88849E-05	0.0001425	0.1425
2.94E-09		5.52E-08	94.9388124	3.921E-07	0.0458	116.8077428	1.88508E-05	0.0001613	0.1613
6.20E-09		5.19E-08	89.3207573	3.6889E-07	0.0424	114.9379398	1.77353E-05	0.0001791	0.1791
3.85E-09		5.43E-08	93.3761274	3.8564E-07	0.0416	107.8716746	1.85405E-05	0.0001976	0.1976
9.28E-09		4.88E-08	84.0202926	3.47E-07	0.0392	112.9670599	1.66829E-05	0.0002143	0.2143
9.67E-09		4.84E-08	83.3619277	3.4428E-07	0.0388	112.6974073	1.65522E-05	0.0002309	0.2309
3.93E-09		5.42E-08	93.2385886	3.8508E-07	0.03749	97.36405601	1.85132E-05	0.0002494	0.2494
5.58E-09		5.25E-08	90.3933219	3.7332E-07	0.03619	96.92642145	1.79483E-05	0.0002673	0.2673
7.55E-09		5.05E-08	87.0004819	3.5931E-07	0.03488	97.06745373	1.72746E-05	0.0002846	0.2846
5.42E-09		5.27E-08	90.6762306	3.7449E-07	0.03357	89.64123498	1.80045E-05	0.0003026	0.3026
1.08E-08		4.73E-08	81.4769363	3.365E-07	0.03226	95.87674371	1.61779E-05	0.0003188	0.3188
8.30E-09		4.98E-08	85.7066954	3.5397E-07	0.03096	87.451247	1.70177E-05	0.0003358	0.3358
1.13E-08		4.68E-08	80.5944923	3.3286E-07	0.02965	89.0702482	1.60027E-05	0.0003518	0.3518
4.89E-09		5.32E-08	91.578537	3.7822E-07	0.02834	74.93006218	1.81836E-05	0.0003700	0.3700
8.34E-09		4.98E-08	85.6418589	3.537E-07	0.02703	76.42757412	1.70048E-05	0.0003870	0.3870
3.74E-09		5.44E-08	93.5617384	3.8641E-07	0.02573	66.57436755	1.85774E-05	0.0004056	0.4056
4.42E-09		5.37E-08	92.3890706	3.8157E-07	0.02442	63.99271653	1.83446E-05	0.0004239	0.4239

Calibration graph for sodium analysis using AAS

$y = 824227x + 344140$
$R^2 = 0.997$